Studies on the replication and pathogenic mechanisms of tick-borne encephalitis virus in neuron

ダニ媒介性脳炎ウイルスの神経細胞における複製および病原性発現機序の研究

Minato Hirano

Laboratory of Public Health,
Graduate School of Veterinary Medicine,
Hokkaido University

Contents

Abbreviations

AOI: Area of interest

BDNF: Brain-derived neurotrophic factor

BHK-21: Baby hamster kidney-21

C: Capsid

CaMKIIa: Ca^{2+}/Calmodulin-dependent protein kinase IIa

CDS: Coding sequence

CMV: Cytomegalovirus

CNS: Central nervous system

DAPI: 4′, 6-diamidino-2-phenylindole

DENV1-4: Dengue virus serotype1-4

DIG: Digoxigenin

d.p.i.: Days post infection

dsRNA: Double-stranded RNA

E: Envelope

EDTA: Ethylenediaminetetraacetic acid

FISH: Fluorescent *in-situ* hybridization

ER: Endoplasmic reticulum

FBS: Fatal bovine serum

FMRP: Fragile X mental retardation syndrome protein

GFAP: Glial fibrillary acidic protein

GFP: Green fluorescent protein

HDV: Hepatitis delta virus

HEK293T: Human embryonic kidney 293T

h.p.i.: Hours post infection

IFA: Indirect immunofluorescence assays

JEV: Japanese encephalitis virus

LANV: Langat virus

LMS: Laminal membrane structure

M: Membrane

MAP2: Microtubule-associated protein2

MEM: Minimum essential medium

MOI: Multiplicity of infection

NS: Non-structural

nt: Nucleotide

OHFV: Omsk hemorrhagic fever virus

PBS: Phosphate-buffered serine

PCR: Polymerase chain reaction

PFU: Plaque-forming unit

prM: Premembrane

RBP: RNA-binding protein

RC: Replication complex

RdRp: RNA-dependent RNA-polymerase

RNAi: RNA interference

RNG105: RNA granule protein 105

RPMI: Roswell Park Memorial Institute

RT-PCR: Reverse transcription-PCR

SEM: Standard error mean

SL: Stem-loop

TBEV: Tick-borne encephalitis virus

TEM: Transmission electron microscopy

UTR: Untranslated region

VLPs: Virus-like particles

WNV: West Nile virus

YFV: Yellow fever virus

ZIKV: Zika virus

Preface

Flavivirus is a genus in the family *Flaviviridae*, and consists of positive-polarity single-strand RNA viruses [1–3]. The genus *Flavivirus* contains over 70 members, many of which are arthropod-borne human pathogens [2–5]. Many outbreaks have been reported, and flaviviruses are attracting global attention as emerging or re-emerging infectious diseases [6–11].

The flavivirus virions are 40-50 nm in diameter, spherical in shape, and contain a nucleocapsid and an envelope [3,12] (Fig.1A). The flavivirus genome encodes three structural proteins: the capsid (C), premembrane (prM), and envelope (E), and seven non-structural (NS) proteins: NS1, NS2A, NS2B, NS3, NS4A, NS4B and NS5, within a single long coding sequences (CDS) [13] (Fig. 1B).

The 5′ and 3′ un-translated regions (UTRs) are involved in stability and replication efficiency of genomic RNA. 5′ end of the genomic RNA contains a type 1 cap (m^7GpppAmG) modification which is important for RNA stability and protein translation [3,14]. The NS5 protein is thought to be recruited to the 5′ UTR during genome replication [15]. The flavivirus genomic RNA lacks poly-A tail unlike cellular mRNAs, but the 3′ UTR has an activity to bind poly-A binding protein during protein translation [3,16].The 5′ and 3′ UTRs have complemental sequences for cyclization of the genomic RNA, required for genome replication [3,17,18]. In addition, recent studies showed that the 3′ UTR produces viral non-coding RNAs, sub-genomic flaviviral RNA, for immune evasion and virulence [19–21]. The E proteins (supported by prM) form a homodimer, and the 90 dimers are tightly packed in an unusual herringbone pattern of icosahedral symmetry on the viral envelope membrane. The E protein is the principal target of neutralizing antibodies and triggers membrane fusion with cellular membrane of endocytotic vesicle [22]. The prM protein has chaperon-like activity aiding folding and maturation of the E protein [23]. During the

maturation of the virion, the M protein is produced from the prM protein by the cleavage of a host protease, furin, in Trans-Golgi network [24]. The C protein binds to viral genomic RNA and forms icosahedral nucleocapsid inside the envelope [25]. The transcribed NS proteins form replication complex (RC) on host intracellular membranes of endoplasmic reticulum (ER) and reconstitute the membrane structure, during the replication of viral genomic RNA [26–28] (Fig. 1C). NS3 and NS5 are well characterized, large multifunctional protein; The NS3 protein has serine protease and RNA helicase activity [29], and the NS5 works as a methyltransferase [30] and an RNA-dependent RNA-polymerase (RdRp) [31].

Figure 2A shows a schematic of the flavivirus replication cycle [3]. Flavivirus are considered to enter cells by endocytosis via cellular receptors for viral envelope proteins, but there is no consensus on what is the receptor molecule. The low pH of the endocytotic pathway induces fusion of the virion envelope with cellular membranes [22]. Following uncoating of the nucleocapsid, the RNA genome is released into the cytoplasm. The released genomic RNA is translated to the viral proteins by host ribosome. The RC replicates viral genomic RNA on the ER-derived host membrane [26–28] (Fig. 2B). Progeny virions are thought to assemble by budding into the ER and to be matured and transported through the host secretory pathway [24]. The infectious virions are released by exocytosis [32].

Flaviviruses are divided into four distinct evolutionary lineages closely related to their arthropod-vectors: mosquito-borne, tick-borne, no-known vector, and insect flaviviruses [33–35] (Table 1). Mosquitoes of *Aedes* and *Culex* families are the major vector of mosquito-borne flaviviruses, including yellow fever virus (YFV), dengue virus serotype1-4 (DENV1-4), West Nile virus (WNV), Japanese encephalitis virus (JEV) and Zika virus (ZIKV) [2]. *Ixodiae* ticks carry tick-borne flaviviruses, including tick-borne encephalitis virus (TBEV) and Langat virus (LANV) [36]. The majority of flaviviruses is transmitted by arthropod blood-sucking and maintained in the

meta-zoonotic transmission cycles between vector and mammals (or birds) [3]. For example, the principal reservoirs of TBEV are small rodents and ticks, and TBEV can chronically infect ticks in their life via transstadial and transovarial transmission [36]. WNV and JEV are maintained between mosquitoes of *Culex* family and wild birds or pigs, respectively [4]. These meta-zoonotic transmission cycles make them difficult to prevent and eliminate the infections. DENV is classified into stage four zoonosis (undergoes long sequences of secondary transmission between humans without the involvement of animal hosts) and is circulating between human and *Aedes* mosquitos continuously [37].

Flaviviruses are widely distributed all over the world [2,3] (Table 1). In the tropical and temperate areas, mosquito-borne flaviviruses are problematic, such as JEV in Eastern and Southern Asia, YFV in Africa and South America, and DENV1-4 in the equatorial region throughout the world. As for tick-borne flaviviruses, TBEV is endemic in wide areas of Eurasia (from Middle Eastern Europe to Russia and East Asia). Recent climate change and advancements of transportation have changed and expanded the flavivirus geographical distribution of flaviviruses [38,39]. The WNV migration to the United States is one of the most typical cases of an emerging spread of pathogen in modern history. Until early 1990s, the WNV was localized geographically in Africa, Europe and Middle East. However in 1999, West Nile encephalitis suddenly appeared in New York City for the first time in North America, and rapidly spread to North and South American Continent [2,11,40,41].

Flaviviruses are also endemic in Japan. Hundreds of Japanese encephalitis cases were reported annually in 1960s. Recent advances in disease-control, such as vaccination program and mosquito control, drastically reduced incidences of Japanese encephalitis, but JEV is still circulated between mosquito and pigs in Japan, and several human cases are reported annually [42]. One hundred and sixty-two cases of domestic infection of DENV1 were reported in Tokyo area in

2014, but domestic outbreak has not been reported since then [43]. Cases of other mosquito-borne flaviviruses are limited in imported cases. As for tick-borne flaviviruses, no confirmed case of tick-borne encephalitis had been reported for many years. However, in October 1993, a human case of tick-borne encephalitis was reported in Kamiiso, Hokkaido [44]. From 2016, three additional cases were reported in Hakodate and Sapporo cities, Hokkaido [45,46]. Epidemiological studies showed high seropositive rate in wild animals, indicating that virus circulates in wild animals in Hokkaido continuously [47,48].

Flavivirus causes various manifestations in humans, such as hemorrhage, encephalitis, biphasic fever, flaccid paralysis and jaundice [2]. Among these, encephalitis following to central nervous system (CNS) infection is severe and associated with high mortality. In particular, the far eastern subtype of TBEV causes the most severe encephalitis with a mortality rate of 5–30% [36]. All encephalitic flaviviruses (JEV, WNV and TBEV) target neuron during the replication in CNS. However, the pathogenic mechanisms, such as how viral replication in neuron contributes to the development of neurological disease, are still unclear. In this study, I tried to investigate the mechanism of viral replication and pathogenicity of encephalitic flaviviruses, especially those of TBEV.

In chapter I, the neuronal replication of encephalitic flaviviruses was analyzed by using a primary culture of mouse neuronal cells. It was shown that the TBEV replicated in dendrites locally and caused membrane alteration of the infected neurons. In chapter II, it was investigated that the molecular mechanism of the viral genome transport of the TBEV in neuron, involved in the local viral replication in dendrites. It was revealed that TBEV hijacked a host RNA transport machinery during the replication in neurons. These studies will improve further understanding of the molecular mechanisms of viral replication and the pathogenicity of TBEV and other neurotropic viruses.

Table 1. Epidemiology of representative flaviviruses.

Viruses	Lineages	Human disease type	Geographical distribution
Dengue (DEN)	Mosquito-borne	Hemorrhagic	Tropical areas of Asia, Australia, Oceania, Africa, America
Japanese encephalitis (JE)		Neurologic	Far eastern Russia and Southeastern Asia, East Asia including Japan
St. Louis encephalitis virus		Neurologic	America
West Nile (WN)		Neurologic	Africa, Europe, America, Australia
Yellow fever virus (YF)		Hemorrhagic	Africa, South America
Zika (ZIK)		Unconfirmed	Africa, Southeastern Asia, America
Omsk hemorrhagic fever (OHF)	Tick-borne	Hemorrhagic	Siberia
Tick-borne encephalitis (TBE)		Neurologic	Central and eastern Europe, Russia, East Asia including Japan
Langat (LAN)		Neurologic	Southeastern Asia
Louping ill		Neurologic	British Isles, Ireland
Apoi	No-known vector	No report	America
Rio Bravo		No report	America
Aedes flavivirus	Insect	No report	Unconfirmed
Culex flavivirus		No report	Unconfirmed
Kamiti River		No report	Africa

This table data is based in previous reports
(mosquito –borne and no-known vector flaviviruses [3], tick-borne flaviviruses [36], and insect flavivirus [35]).

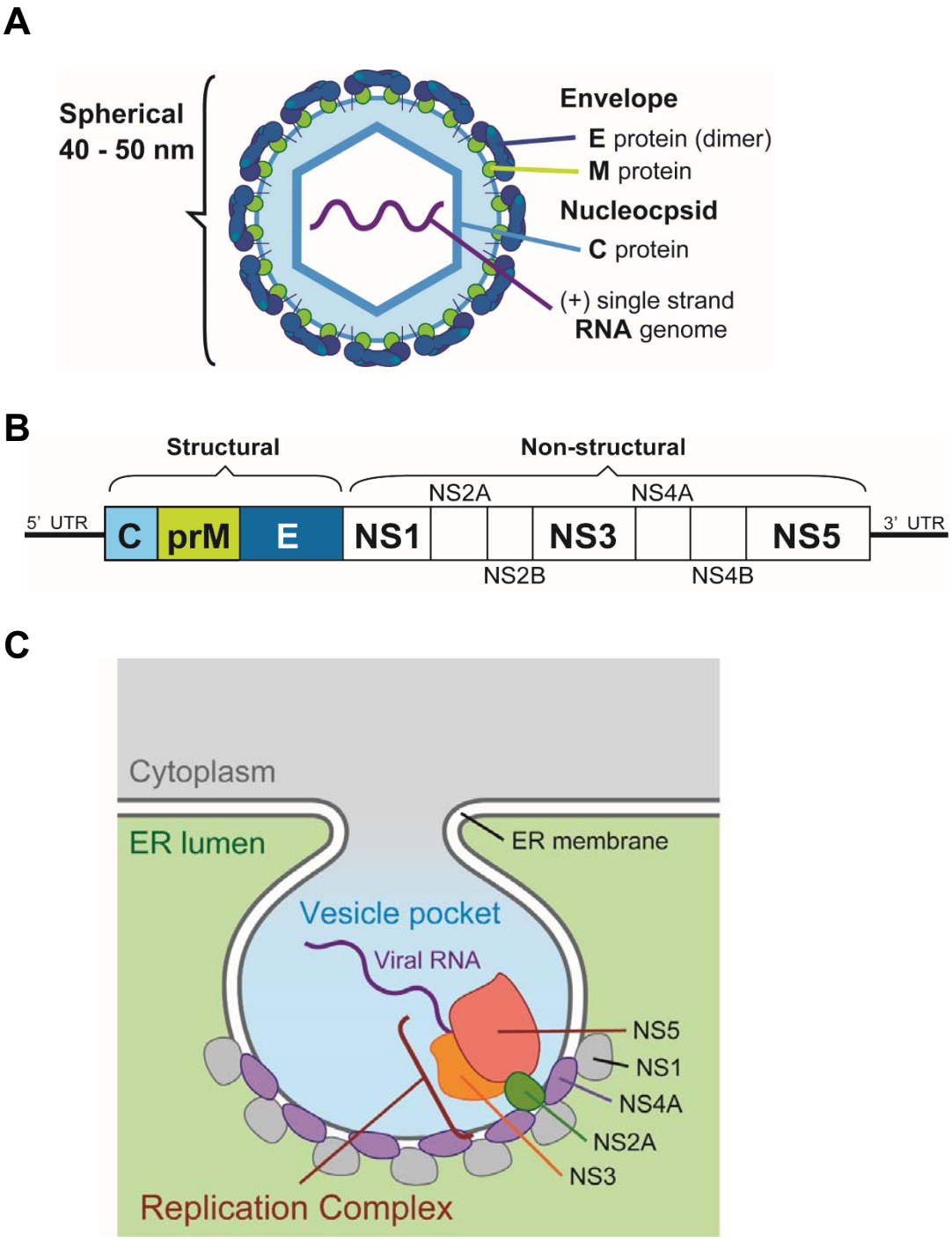

Fig. 1. Structure of flavivirus.

(A) Schematic of flavivirus virion. The flavivirus virions are 40-50 nm in diameter, spherical in shape, and contain a nucleocapsid (formed by C protein and gneomic RNA) and an envelope (formed by E and M proteins, and lipid bilayer). **(B)** Schematic of flavivirus genome. The flavivirus genome encodes three structural proteins: the C, prM and E, and seven NS proteins: NS1, NS2A, NS2B, NS3, NS4A, NS4B,and NS5, within a single long open reading frame. (**C)** Schematic model of flavivirus replication complex. Several NS proteins of flavivirus form the replication complex on the vesicle pocket membrane (reconstituted structure of ER).

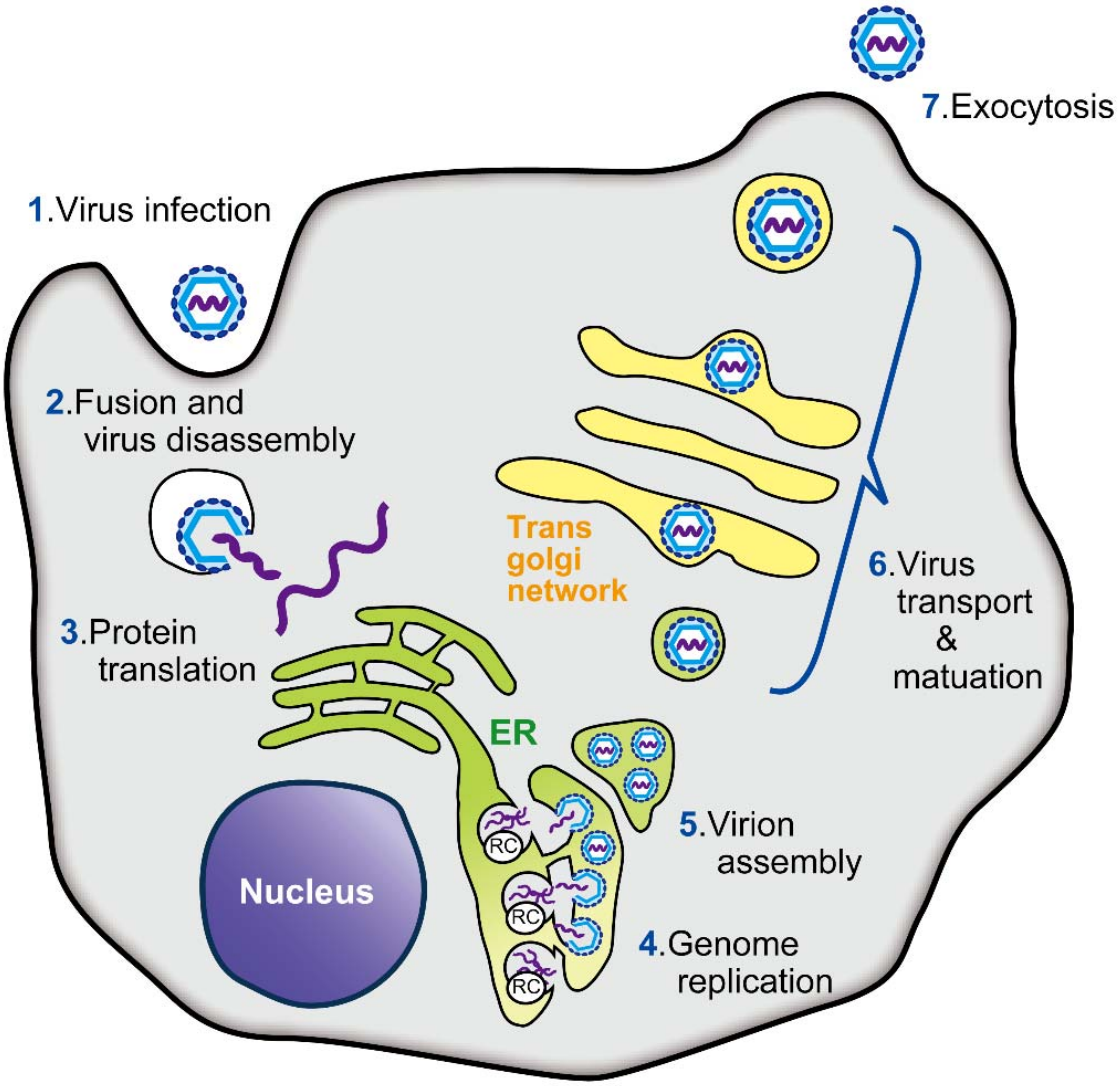

Fig. 2. Flavivirus replication cycle.

Schematic of flavivirus replication cycle. Flaviviruses replicate in cells via following steps: 1. Virus Infection, 2. Fusion and virus disassenmbly, 3. Protien translation, 4. Genome replication, 5. Virion assenmbly, 6. Virus transport and Matuation, 7. Exocytosis.

Chapter I:

Tick-borne flaviviruses alter membrane structure and replicate in dendrite of primary mouse neuronal cultures.

Summary

Neurological diseases caused by encephalitic flaviviruses are severe and associated with high levels of mortality. However, detailed mechanisms of viral replication in CNS and features of viral pathogenesis remain poorly understood. I carried out a comparative analysis of replication of encephalitic flaviviruses, WNV, JEV and TBEV, in primary cultures of neurons from mouse brains. The distribution of viral-specific antigen in the neurons varied: TBEV infection induced accumulation of viral antigen in the neuronal dendrites to a greater extent than infection with other viruses. Viral structural proteins, NS proteins and double-stranded RNA (dsRNA) were detected in regions in which viral antigens accumulated in dendrites after TBEV replication. Replication of a TBEV replicon after infection with virus-like particles of TBEV also induced antigen accumulation, indicating that accumulated viral antigen was the result of viral RNA replication. Furthermore, electron microscopy confirmed that TBEV replication induced characteristic ultrastructural membrane alterations in the neurites: newly formed laminal membrane structures containing virion-like structures. This is the first report describing viral replication in and ultrastructural alterations of neuronal dendrites, which may cause neuronal dysfunction.

Introduction

Encephalitis, a neurological manifestation of disease, is particularly problematic among the symptoms caused by infection of flaviviruses. This condition is associated with high-level mortality and severe sequelae. All of WNV, JEV and TBEV are neurotropic and cause encephalitic diseases in humans. Common symptoms are headache, vomiting, ataxia and paralysis. In addition, differences in neurologic symptoms have been reported in the infection of each virus. WNV infection generally triggers development of systemic symptoms, and neurologic manifestations are rare [49,50]. JEV infection triggers acute spasm and development of a dull pathognomonic Parkinsonian syndrome [51,52]. Cognitive function is characteristically compromised upon TBEV infection; patients develop photophobia, irritability and sleep disorders [53–55]. On histopathological examinations, all these viruses mentioned above induce typical nonsuppurative encephalitis, including neuronal death (associated with shrunken perikarya), perivascular infiltration of mononuclear cells, and neuronophagia [2,56]. The distribution of viral antigens in the cerebellum differs, but viral antigens are seen in several brain regions among encephalitic flaviviruses, including the brainstem, the cerebral cortex, and the cervical spinal cord [56–58]. However, it remains unclear how viral replication and pathogenicity contribute to the neurologic manifestations.

Primary culture has been developed for maintaining brain cells [59], and such cultures can be used to investigate detailed intracellular activities of neurons [60,61]. This approach has been used to explore not only physiological functions, but also neuronal response affected by virus invasion, including lyssavirus [62], herpesvirus [63], and flaviviruses [64,65]. Primary cultured neurons could provide detailed information about flavivirus replication in neurons.

In this chapter, primary neuronal cultures of mouse brain was used to explore replicative and neuropathogenic features of encephalitic flaviviruses. It was revealed that the replicative properties of mosquito and tick-borne flaviviruses differed.

Materials and methods

Cell culture

Baby hamster kidney-21 (BHK-21) cells were cultivated at 37°C in minimum essential medium (MEM) (Life Technologies Co., Carlsbad, CA) supplemented with 8% (v/v) fetal bovine serum (FBS) and penicillin/streptomycin. Human embryonic kidney 293T (HEK293T) cells were cultured at 37°C in Dulbecco's modified Eagle's medium (Life Technologies), containing 10% (v/v) FBS and penicillin/streptomycin.

Pregnant Slc: ICR mice were purchased from Japan SLC Inc. (Shizuoka, Japan), and hippocampal, cerebral cortical, and cerebellar neuronal cultures were established from brain cells of the embryos. Neurons for primary culture were prepared from mouse embryos at embryonic day 17−18 as described previously [66,67]. Briefly, the hippocampus, cerebral cortex, and cerebellum were dissected from embryonic brains into dissection medium: HBSS (Life Technologies) supplemented with 10 mM HEPES (Life Technologies) and 1 mM sodium pyruvate (Life Technologies). Tissues were treated with 0.0125% (w/v) trypsin (Becton Dickinson, Co., Franklin Lakes, NJ) for 5 min at 37°C, and gently dissociated via trituration in neuronal medium: neurobasal medium (Life Technologies) supplemented with 6 mM Glutamax (Life Technologies) and 1× B27 supplement (Life Technologies). Dissociated cells were seeded into eight-well glass chamber slide (Matsunami Glass Ind., Osaka, Japan) coated with cell matrix type IC (Nitta Gelatin Inc., Osaka, Japan). The cells propagated at 37°C and were used after 6−7 days of culture. All animal experiments were approved by the President of Hokkaido University after review by the Animal Care and Use Committee of Hokkaido University (Approval No. 13025).

Viruses

The TBEV Oshima 5-10 strain was isolated from a dog in Hokuto City (Japan) in 1995 (AB062063.2) [44]. The Sofjin-HO strain of TBEV was isolated from the brain of a human patient in Khabarovsk (Russia) in 1937 (AB062064.1) [68]. The Guriev strain of Omsk hemorrhagic fever virus (OHFV) was isolated from human blood (AB507800). The recombinant viruses of these strains were recovered from infectious cDNA clones as previously described [69–71]. The WNV 6-LP strain was plaque-purified from a New York City isolate, NY99-6922 (AB185914.2). The JEV Sw/Mie40/2004 strain was isolated from a pig (AB241118.1). The Hochosterwitz strain of TBEV was isolated from an *Ixodes* tick in Carinthia (Austria) in 1971 [72]. The LANV TP21 strain was isolated from an *Ixodes* tick (AF253419.1). Working stocks of the all viruses were propagated once in BHK-21 cells, and stored at −80 °C. All viral infections were conducted in the BioSafety Level 3 conditions, in a dedicated laboratory located in the Graduate school of Veterinary Medicine of Hokkaido University.

Antibodies

Polyclonal mouse anti-LANV (cross-reactive among the tick-borne flaviviruses), anti-WNV, and anti-JEV, antibodies were prepared from ascites of mice repeatedly immunized with LANV TP21, WNV 6-LP, and JEV Ja-Gar01, respectively. Rabbit polyclonal antibodies were prepared by immunization with recombinant E and NS3 proteins derived from *Escherichia coli* as described previously [73]. The J2 mouse monoclonal antibody was used to detect the dsRNA, product of viral genome replication (English and Scientific Consulting, Szirak, Hungary) [74]. Chicken anti-microtubule-associated protein2 (MAP2), rabbit anti-grial fibrillary acidic protein (GFAP), anti-β3 tubulin, and anti-synaptophysin polyclonal antibodies were the products of Abcam plc. (Cambridge, UK). The secondary antibodies, including anti-mouse IgG, anti-rabbit IgG, and anti-chicken IgG conjugated with AlexaFluor488 or AlexaFluor555, were purchased from Life Technologies.

Construction of virus-like particles (VLPs) of TBEV

The plasmids, Oshima REP [75] and pTBECME [76], were used to construct VLPs of TBEV. The TBEV replicon was transcribed from the Oshima REP plasmid using a mMESSAGE mMACHINE SP6 kit (Life Technologies), and transfected into HEK293T cells with a Trans IT mRNA transfection kit (Mirus Biology, Co., Madison, WI). After 5-6 h of culture, the cells were transfected with the pTBECME plasmid, which expresses the structural proteins of TBEV, with a TransIT-LT1 reagent (Mirus Biology). The supernatant was harvested at 48 h post-transfection and cleared by centrifugation at 1,700 xg for 5 min. VLPs in the supernatant were precipitated by 10% (w/v) PEG 8000 and 1.9% (w/v) NaCl followed by incubation for 2 h at 4°C, and centrifugation at 16,000 xg for 30 min. Pellets were resuspended in neurobasal medium and stored at −80°C.

Infection of primary neuronal cultures

Primary neuronal cultures were infected at an multiplicity of infection (MOI) of 0.1. After viral adsorption for 1 h, half of the culture medium was replaced. The medium was harvested at 12 h, 24 h, 48 h, 72 h post-infection (h.p.i.), and stored at −80°C. Cells were fixed and were subjected to following experiments. Unless otherwise stated, TBEV Oshima 5-10 strain was used for TBEV infection.

Viral titration

Monolayers of BHK-21 cells, prepared in multi-well plates, were incubated with serial dilutions of viruses for 1 h, and next overlaid with MEM containing 2% (v/v) FBS and 1.5% (w/v) carboxymethyl cellulose. After 3−5 days of incubation, cells were fixed and stained with a solution of 0.25% (w/v) crystal violet in 10% (v/v) buffered formalin. Plaques were counted and viral titers expressed as plaque-forming unit (PFU)/ml.

Indirect immunofluorescence assay (IFA)

At 12−72 h.p.i., infected primary neuronal cultures were fixed in 4% (w/v) paraformaldehyde for 20 min at 37°C, and next washed with 0.1 M glycine in phosphate-buffered serine (PBS). Fixed cells were permeabilized by incubation in 0.1% (v/v) Triton X-100 for 5 min at room temperature, and next blocked with 2% (w/v) bovine serum albumin. The cells were incubated at room temperature for 1 h with primary antibodies. After extensive washing, cells were incubated with secondary antibodies bearing fluorescent tags. The cells were enclosed with a solution of the Slowfade Gold antifade reagent with DAPI (Life Technologies), and observed via BZ-9000 (Keyence, Osaka, Japan) or LSM 700 confocal laser scanning microscopy (Carl Zeiss Microscopy Co., Ltd., Jena, Germany). Images were processed using the BZ-2 Analyser (Keyence) or ZEN 2009 (Zeiss) software.

Cytoskeletal perturbation

After viral adsorption for 1 h, half of the culture medium was exchanged, and nocodazole (final concentration 10 μM) was added to the medium. The cells were fixed 48 h later, and effect of cytoskeletal perturbation was assessed using IFA.

Transmission electron microscopy (TEM)

Infected and mock-infected primary neuronal cultures growing in eight well-chambered slides were directly pre-fixed overnight with a solution of 2.5% (w/v) glutaraldehyde and 2% (w/v) paraformaldehyde in 0.1 M phosphate buffer at 4°C. After washing with 0.1 M phosphate buffer, cells were post-fixed in 1% (w/v) osmium tetroxide and dehydrated in a graded series of alcohol. Cells were next embedded in a Quetol 812, DDSA, and MNA mixture (Nisshin EM, Tokyo, Japan). Ultrathin sections were stained with uranyl acetate and lead citrate, and then visualized via JEM-1400plus (JEOL Ltd., Tokyo, Japan).

Statistical analysis

Data are expressed as mean ± the standard deviation. Following a one-way analysis of variance test, the Tukey−Kramer test was used to determine the statistical significance of differences in the viral titer and the number of antigen accumulations (Fig. 3A, 3B & 6B) The statistical analysis was performed with SAS University Edition software (SAS Institute Inc., Cary, NC).

Results

Replication of neurotropic flaviviruses in primary neuronal cultures

Prior to experiments using infectious viruses, cell components of primary cultured brain cells were examined. Primary neuronal cultures were prepared from hippocampi, cerebral cortexes, and cerebella, and stained for a neuronal marker (MAP2), astroglial marker (GFAP), and 4′, 6-diamidino-2-phylindole (DAPI). The primary cultures of cerebral cortexes contained principally neurons (70−80%) and astroglial cells (20%), and lacked microglial cells.

To compare growth kinetics of encephalitic flaviviruses, primary cultures from each region were infected with TBEV, WNV, or JEV at an MOI of 0.1, and viral titers in the culture supernatant were measured at various time points. Figure 3A and 3B show that viral titers did not differ among primary cultures from different brain regions. The viral titer of TBEV at 48 h.p.i. was slightly higher than that attained by the other viruses, but the difference was not statistically significant. Viral growth kinetics was similar all studied primary cultures. Thus, cerebral cortex cells were used in all subsequent experiments. Apart from slight degeneration of the neurites in TBEV-infected neurons, no obvious morphological change was evident upon light microscopy (data not shown).

The distribution of viral antigens in primary neuronal cultures was examined via IFA (Fig. 3C). At 48 h.p.i., infected cells stained with antibodies against MAP2 (a marker of neuronal cell body and dendrites, green), virus-specific antibodies (red), and DAPI (blue). In the cell bodies, distributions of viral antigens were similar in neurons infected with each virus studied. However, distributions in the dendrites were differed among the viruses. Viral antigens were sparsely distributed in dendrites of cells infected with WNV or JEV. On the other hand, antigen accumulations were observed in dendrites infected with TBEV (Fig. 3C, white arrows). This form of antigen-accumulation was also observed in neurons infected with the tick-borne flaviviruses,

Far Eastern and European subtypes of TBEV, OHFV and LANV (Fig. 4).

Detailed images of accumulated viral antigens are shown in Figure 5. Antigen accumulations varied in diameter, being 5−10 μm on the major and 3−5 μm on the minor axis and were surrounded by MAP2 in structures that appeared to be swollen (Fig. 5A). In some large swellings, Z-stack images showed an unstained (hollow) region within the accumulation of viral antigen (Fig. 5B).

Changes over time in viral antigen distribution are shown in Figure 6. In the early stages of TBEV infection, viral antigens were detected in the cell body principally, thus minimally in the dendrites (Fig. 6A). From 48−72 h.p.i., viral antigen accumulated in the dendrites (Fig. 6A & B). However, viral antigen in WNV- or JEV- infected cells was located principally in the cell body at all examined timepoints (Fig. 6A & B). WNV antigen accumulated in dendrites of several neurons by 72 h.p.i., but such accumulations were fewer compared with neurons infected with TBEV.

In a previous study, TBEV infection triggered microtubule re-arrangement in neuroblastoma cells [77], possibly associated with the viral antigen accumulations in dendrites. As shown in Figure 7, neurons uninfected or infected with TBEV were co-stained with the anti-TBEV and anti-MAP2, anti-β3-tublin, or anti-synaptophysin antibodies. However, no re-arrangement of microtubules distribution was observed in infected primary neuronal cultures (Fig. 7). Accumulated viral antigens in TBEV-infected cells were localized with the calreticulin, a marker of ER, but were not with synaptophysin, a marker of synaptic vesicles (Fig. 7). Thus, the virus antigens accumulate on the ER in the dendrites, but it was not directly associated with rearrangement of microtubules and synaptic vesicles.

Cytoskeleton-mediated transport of neurotropic viruses, such as lyssavirus [78,79], herpes virus [80,81], and influenza virus [82], proteins has been reported previously. The viral protein accumulation of TBEV could be related to the microtubule transportation and stagnation. Nocodazole (which disrupts microtubules) was used to observe the effect of perturbation of microtubule on the distribution. Addition of nocodazole induced dendrite loss (Fig. 8), and TBEV or WNV antigens were present in the neural cell body only. Thus, the viral antigen accumulations were affected by microtubule.

Viral constituent of the protein accumulations in dendrites

Viral constituents in accumulations were investigated. Staining of TBEV-infected neurons with specific antibodies detecting structural (E) and non-structural (NS3) proteins showed that both proteins were present in the antigen accumulations (Fig. 9A, white arrows). In addition, dsRNA (reflecting viral genome replication) was also detected (Fig. 9B). These results suggest that viral genome replication occurred in the regions of viral protein accumulations in dendrites.

To investigate the viral constituents required for the formation of the accumulated viral antigens, we next infected primary cultures with VLPs of TBEV ("single-round" infectious particles containing replicon RNA as a genome) [83–85]. VLPs were constructed as described followed. Briefly, after the induction and replication of replicon RNA in HEK293T cells, viral structural proteins were supplemented in trans. Structural proteins package the replicon RNA automatically, and triggers secretion of VLPs. The replicon RNA lacks the most of the cording region for viral structural proteins. The VLPs can enter cells, and replicate within, but cannot produce a progeny virus. Viral antigen also accumulated in dendrites after infection of the TBEV-VLPs (Fig. 9C, white arrows). The viral protein accumulations did not require expression of viral structural proteins.

The ultrastructure of flavivirus infected primary cultured neuron

To observe the membrane structure of infected neurites, infected primary neuronal cultures were examined by TEM (Fig. 10). In the cell body of mock-infected neurons, large nuclei, ER, mitochondria, and Golgi apparatus were observed readily (Fig. 10A−C). However, virus-infected neurons exhibited cytoplasmic condensation with granular structures, and reactive lysosomes were evident (Fig. 10D). Apoptotic cells (identified by nuclear distortion or the presence of apoptotic bodies) were rare in the ultrastructural observation. The spherical virions coated with lipid bilayer were observed in infected neurons (Fig. 10E). The cell bodies of neurons infected with TBEV or WNV were similar in appearance (data not shown). In the dendrites of mock-infected neurons, organized microtubules were observed (Fig. 10F). After infection of WNV, degenerated membrane and granular structures were appeared in neurites (Fig. 10G). In contrast, TBEV infection caused neurite swelling and appearance of elliptical structures (Fig. 10H & I). These structures were surrounded by laminal membranes and adjacent to microtubules, and mitochondria were observed in the one side the structures unevenly (Fig. 10I). Virions coated with lipid bilayers were observed both inside and outside of these structures (Fig. 10J-L). TBEV infection caused a characteristic ultrastructural change of membrane in the neurites: a laminal membrane structure (LMS) besides the microtubules. WNV infection was not associated with LMS formation.

Discussion

Despite the importance of neuro-pathogenicity of flavivirus, the detailed feature of the replication mechanism in the neural cells is still unknown. Primary cultures of brain cells was used to examine the replication of several flaviviruses comparatively. Viral antigen distribution in infected primary neuronal cultures differed when such cells were infected with mosquito and tick-borne flaviviruses (Figs. 3 & 4). IFA and TEM studies revealed that dendritic replication of tick-borne flaviviruses caused abnormal swelling of neurites and development of a specific structure, LMS (Figs. 5-10).

Each studied flavivirus multiplied effectively in primary neuronal cultures from several brain regions, indicating that use of such cells is appropriate when investigating flavivirus infection. However, the flaviviruses showed similar growth kinetics in primary cultures from several brain regions (Fig. 3A & B). Encephalitic flaviviruses have been reported to exhibit differences in distribution and multiplication among the various parts of the brain. WNV infections spare granule cell neurons of the cerebellum compare to other neuronal populations [86]. In contrast, JEV replicated well in granule cell neurons [87], and TBEV replicated throughout the cerebellum, including granule cells [57,88]. Two possible reasons may be suggested to explain the difference in the *in vivo* and *in vitro* results. First, lack of glial cell maturation may influence viral replication. Mammalian neurons interact with glial cells soon after birth; the neurons mature and become myelinated [89]. Some reports have emphasized that the presence of glial cells affect flavivirus replication in the brain [64,65,90]. It is possible that the difference of glial cell-condition affect the viral growth. Second, incomplete maturation of the innate immune response of neurons may affect the susceptibility of such cells to flavivirus infection. The granule cells of the cerebellum have been reported that to mount an effective innate immune response against viral infection [91]. Embryonic neurons used in this study may lack a well-developed innate immune

system. Thus, the susceptibility of primary embryonic neuronal cultures to viral infection may differ from that of adult brains *in vivo*. Interferon treatment of primary neuronal cultures may render viral replication patterns similar to those observed *in vivo*.

Infection with tick-borne flaviviruses was associated with accumulations of viral antigens in the dendrites of infected neurons, but this was not true of mosquito-borne flaviviruses. The accumulations contained structural proteins, NS proteins, and dsRNA (Fig. 9A & B). Accumulations were also evident upon the replication of replicon RNA after infection with VLPs of TBEV (Fig. 9C). Flavivirus replicates at ER membranes, and buds into the ER lumen [3,26–28,32]. Dendrites are known to contain free ribosomes and satellite secretory pathways to secure synaptic plasticity [92–95]. Together, the data suggest that tick-borne flaviviral replication in dendrites induced viral protein accumulation. The previous reports described that infection with rabies virus [96], influenza virus [82] and other viruses similarly accumulated viral antigens in the dendrites. Such accumulation has been considered to reflect inhibition of viral protein transportation (mainly structural proteins of virion) in dendrites in which cytoskeleton has been disrupted. However, we found that the mechanism of antigen accumulations during TBEV infection were quite different. This is the first report to show the viral replication in dendrites.

TBEV infection caused a characteristic ultrastructural change in neurite membranes of infected neuron. An LMS, lying parallel to microtubules, was developed, and virions were observed both inside and outside of this structure (Fig. 10H-L). LMS-like membranes were previously observed in glioblastoma cells infected with TBEV [77]. Flavivirus infection induces typical alterations in ER membranes. The membranes assume vesicle pockets and convoluted structure, forming a platform on which viral genome replication and virion assembly proceed [3,26–28,97]. It is possible that LMS is formed via membrane reconstitution triggered by the viral replication, and serves as the platform for dendritic viral replication and virion assembly. The

unstained hollow regions evident when the accumulations of viral proteins were examined by IFA may be attributable to the fact that degenerated membranes are poorly permeable to antibodies.

A proposed model of LMS formation is shown in Figure 11. Viral proteins are synthesized in dendrites (Fig. 11A). Membrane structures are reconstituted to form the LMS after such synthesis (Fig. 11B), and the LMS becomes multilayered and grows to compress the microtubules (Fig. 11C).

Time-course experiments revealed that viral proteins were synthesized principally in the neuronal cell bodies during the early stages of infection, becoming distributed in dendrites only later (Fig. 6). Thus, TBEV genomic RNA (with or without viral proteins) was transported principally from cell bodies to dendrites. And, experiment using VLPs showed that the RNA transport did not require expression of viral structural proteins. Viral genomic RNA bound to membrane-associated RC (formed by viral NS proteins) may be transported along dendritic membrane. Another important transport mechanism involves formation of RNA granules. Recently, mRNA transportation to the dendrites, and local translational control therein, have been described in neuron [98–100]. Specific mRNAs form RNA granules containing several different RNA binding proteins are transported along microtubules to dendrites in a kinesin-dependent manner [101,102]. It is possible that viral genomic RNAs may hijack or mimic this transport mechanism. Microtubule-dependent formation of viral antigen accumulations in dendrites may support this hypothesis (Fig. 8).

All tick-borne flaviviruses used in the present thesis, Far Eastern and European subtype of TBEV, OHFV, and LANV, accumulated viral antigens in dendrites (Fig. 4). However, WNV and JEV formed smaller accumulations. Some previous studies used the primary brain cultures to investigate replication of mosquito-borne flaviviruses, but no mention was made of the viral

antigen accumulation in dendrites [64,65]. Such differences may reflect viral adaptive evolution to arthropod vector; tick-borne flaviviruses spend most of their life-cycle in ticks.

Alteration in membrane structure and accumulation of viral proteins in dendrites may cause the neuronal dysfunction and degeneration *in vivo*. LMS formation and viral protein accumulation induced ultrastructural changes in neurites, including compression of the microtubules, the obstruction of trafficking pathways, and reconstitution of membrane structure (Fig. 10). Such changes may affect synaptic function and induce neurite degeneration leading to development of neurological disease. Synaptic connections are dynamically regulated via intracellular trafficking pathways, protein modifications, and local protein synthesis in the dendrites [98–100]. Such connections play important roles in CNS, being in recognition, memory, and behavioral regulation. Dendritic degeneration occurs in some diseases associated with loss of cognitive function, including Alzheimer's disease [103], fragile-X syndrome [104], and Rett syndrome [105]. Especially, fragile-X syndrome is caused by disruption of local protein synthesis in dendrites [106]. In addition, viral protein accumulations in dendrites may affect neural function via the interaction of such proteins with host factors. In a previous study, TBEV replication arrested the neurite outgrowth in a cell line derived from a phenochromocytoma of the rat adrenal medulla. Such arrest was caused by interaction between TBEV NS5 protein and host proteins-Rac1 and Scribble [107]. The latter proteins are involved in maintaining cell polarity, regulation of synaptic plasticity, and synaptic vesicle dynamics [108]. It is possible that the accumulated viral proteins affect the distribution and functionality of host proteins with which the viral proteins interact, in turn causing neural dysfunction and cell-degeneration.

In this chapter I, I showed that mosquito and tick-borne flaviviruses replicated differently in primary neuronal cultures. Tick-borne flaviviruses induced ultrastructural membrane alterations and replication thereof was associated with accumulation of viral proteins

in dendrites; this was not true of mosquito-borne flaviviruses. It was also shown that tick-borne flaviviruses replicate in the neural dendrites for the first time.

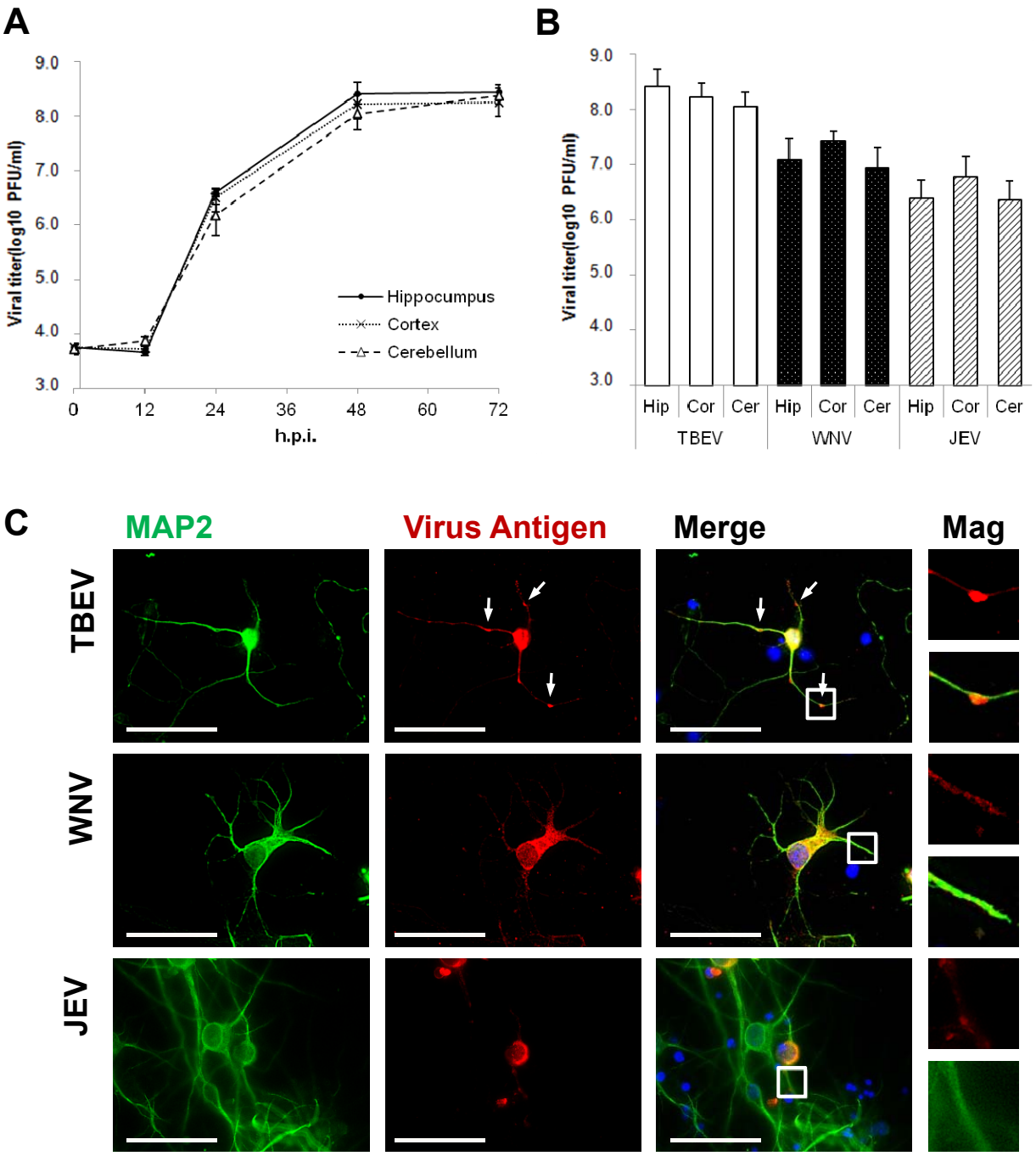

Fig. 3. Replication of encephalitic flaviviruses in primary neuronal culture.

(A) TBEV growth kinetics in primary cell cultures. Hippocamal (closed circles), cerebral cortex (crosses), and cerebellal (open triangles) cells were infected with TBEV at an MOI of 0.1 and, at the indicated time poins, the media were harvested, and virus titers were determined by plaque forming assay. Error bars: standard deviations. **(B)** Virus production levels in primary cultures of cells from various brain regions. Cells from the hippocampus (Hip), cerebral cortex (Cor), and cerebellum (Cer) were infected with TBEV, WNV, or JEV at an MOI of 0.1. Virus titers in supernatants at 48 h.p.i. were measured. **(C)** Viral antigen distribution at 48 h.p.i.. Cultured cerebral cortex cells were infected with TBEV, WNV, or JEV, at an MOI of 0.1. The infected cells were fixed at 48 h.p.i., and stained with antibodies against MAP2 (green), antisera against each virus (red), and DAPI (blue). Right panels show magnifications of dendrites from the indicated regions of the merged images. Scale bars indicate 50 μm in length.

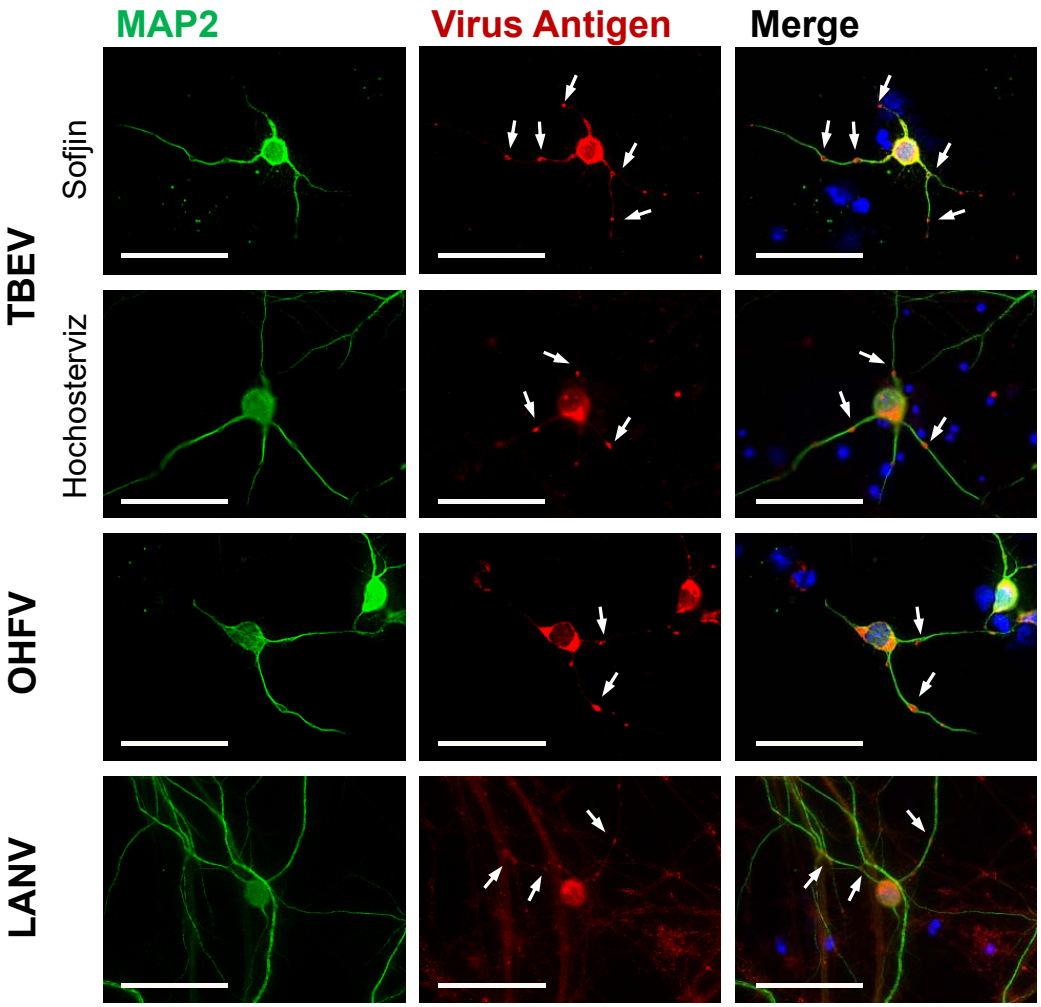

Fig. 4. Viral antigen distribution of tick-borne flaviviruses in primary neuronal cultures.

Cultured cerebral cortex cells were infected with TBEV Sofjin strain, TBEV Hochostervitz strain, OHFV, or LANV. The infected cells were fixed at 48 h.p.i., and stained with antibodies against MAP2 (green), antisera against tick-borne flavivirus (red), and DAPI (blue). Viral antigen accumulations in dendrites are indicated by white arrows. Scale bars indicate 50 μm in length.

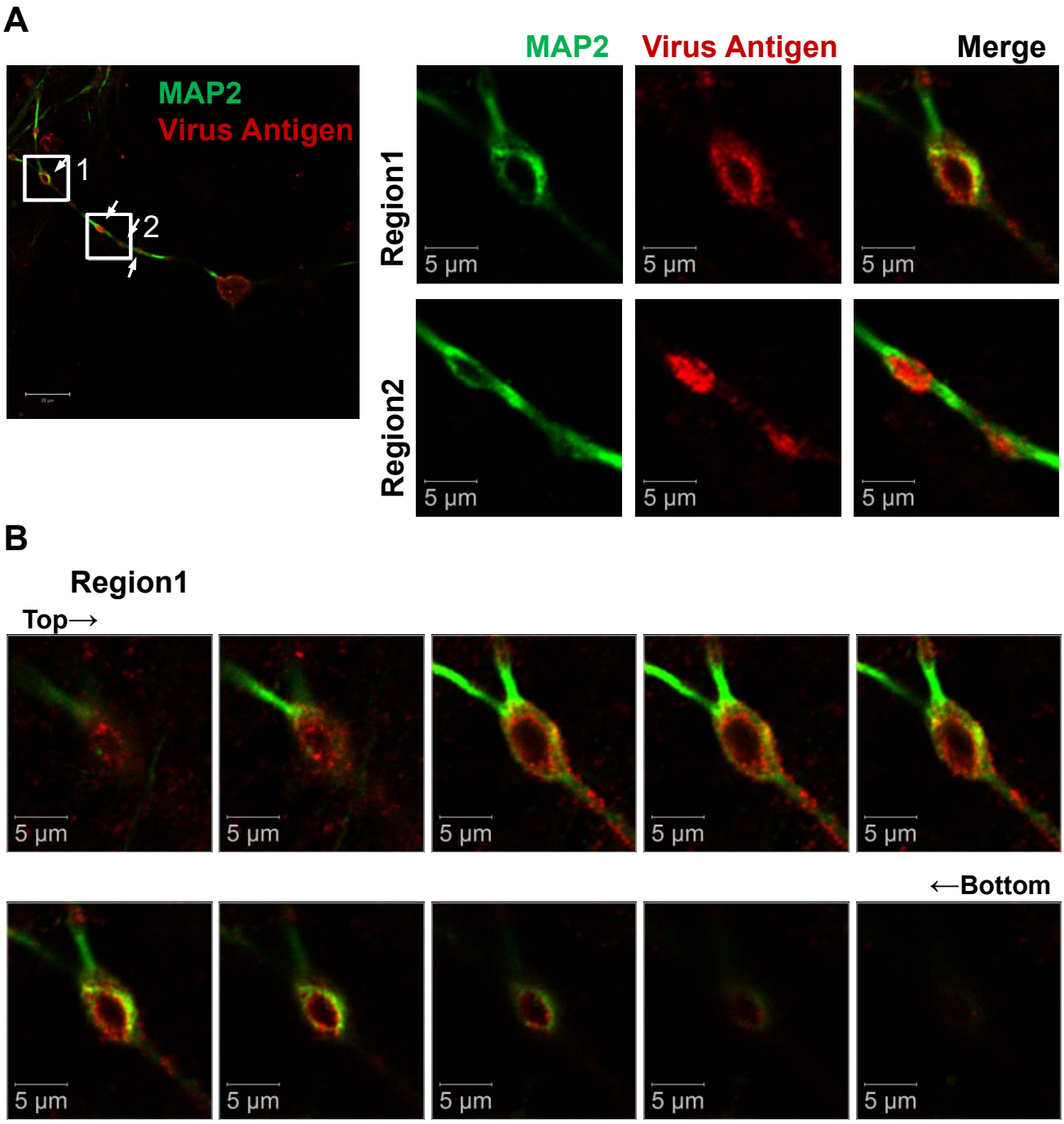

Fig. 5. Detailed images of the antigen accumulations in the neuronal dendrite.

(A) Viral protein accumulations in TBEV-infected dendrites. Infected cells were fixed at 48 h.p.i. and stained with antibodies against MAP2 (green) and an antiserum against a tick-borne flavivirus (red). The images were collected with a confocal microscope. Panels (termed Region1 and Region2) show magnifications of dendrites in the indicated region of right panel. Accumulations of viral antigens in dendrites are indicated by white arrows. **(B)** Z stack images of viral protien accumulation in a TBEV-infected dendrite. The slice images of the accumulation (shown in the region 1above) were collected with an interval of 0.65 μm in depth.

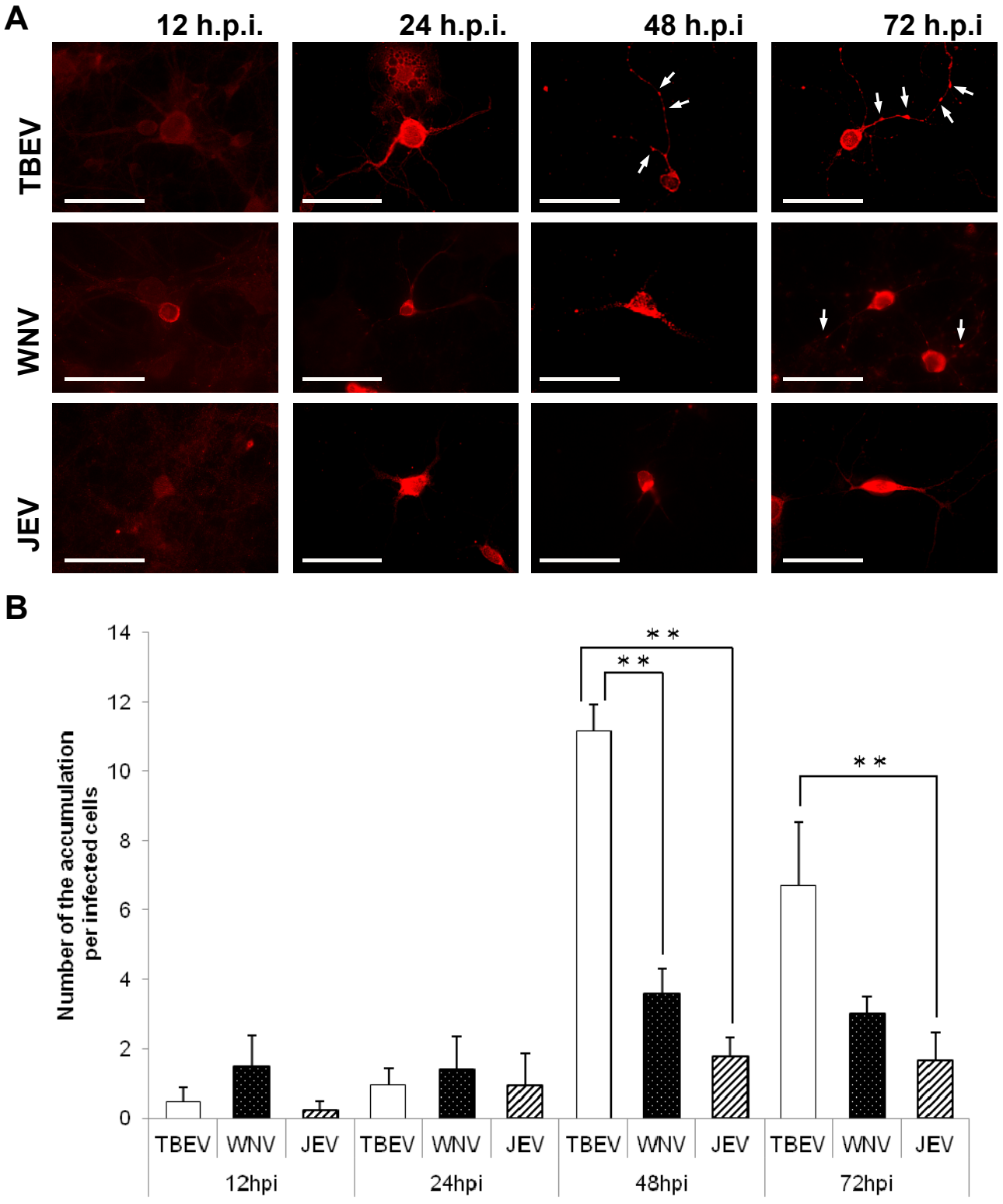

Fig. 6. Time-course changes in viral antigen distribution.

(A) IFA images showing the changes over time in viral antigen distributions in primary neuronal cultures. Cultured cerebral cortex cells were infected with TBEV, WNV, or JEV at an MOI of 0.1. The infected cells were fixed at the indicated time points (12, 24, 48, and 72 h.p.i.), and stained with antisera against each virus (red). Accumulations of viral antigens are indicated by white arrows. Scale bars: 50 μm. **(B)** The extent of viral antigen accumulations in infected cells. Cultured cerebral cortex cells were infected with TBEV, WNV, or JEV at an MOI of 0.1., fixed the indicated timepoints (12, 24, 48, and 72 h.p.i.), and stained with antisera against each virus and DAPI. The numbers of infected cells and antigen accumulationsins in such cells were counted in four different microscopic fields. Error bars: standard deviation. **: $P<0.01$ by Tukey's test.

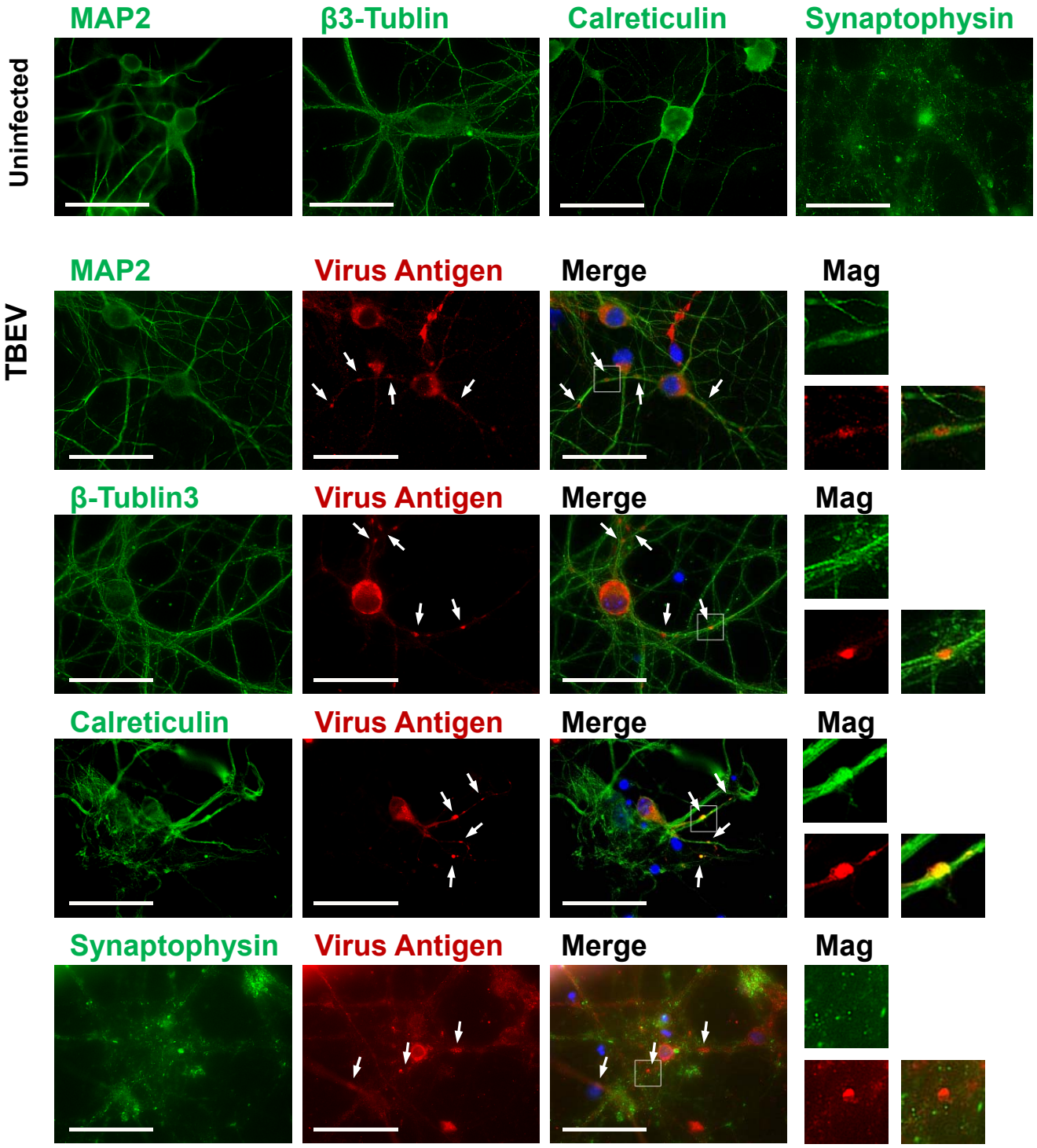

Fig. 7. Co-staining of TBEV-antigen and cellular organelles.

Neuronal cells were uninfected or infected with TBEV at an MOI of 0.1, and fixed at 48 h.p.i.. The cells were stained with antibodies against organelle markers (green), an antiserum against tick-borne flaviviruses (red), and DAPI (blue). Antibodies against MAP2, β3-tublin, Calreticulin, and synaptophysin were used as organelle markers. Right panels show magnifications of antigen accumulations from the indicated regions by white rectangles of the merged images. Accumulations of viral antigens are indicated by white arrows. Scale bars indicate 50 μm in length.

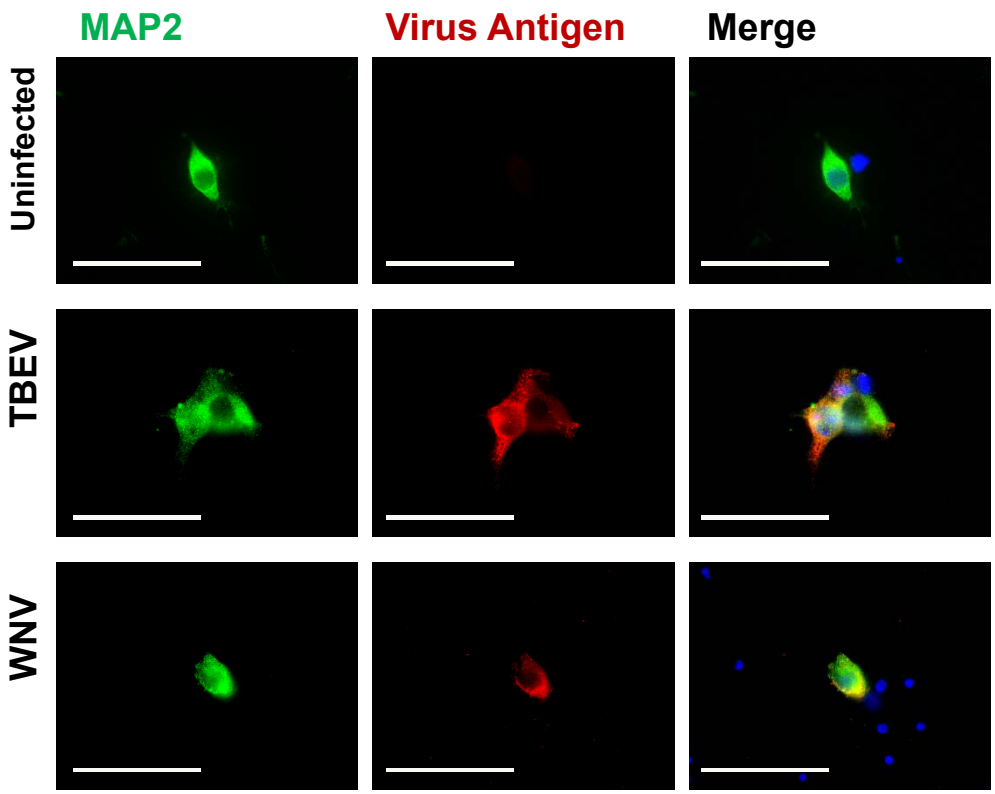

Fig. 8. Effect of microtubule perturbation on viral antigen distribution.

Cells were uninfected or infected with TBEV or WNV at an MOI of 0.1, and treated with nocodazole. The infected cells were fixed at 48 h.p.i. and stained with antibodies against MAP2 (green), antisera against each virus (red), and DAPI (blue). Scale bars indicate 20 μm in length.

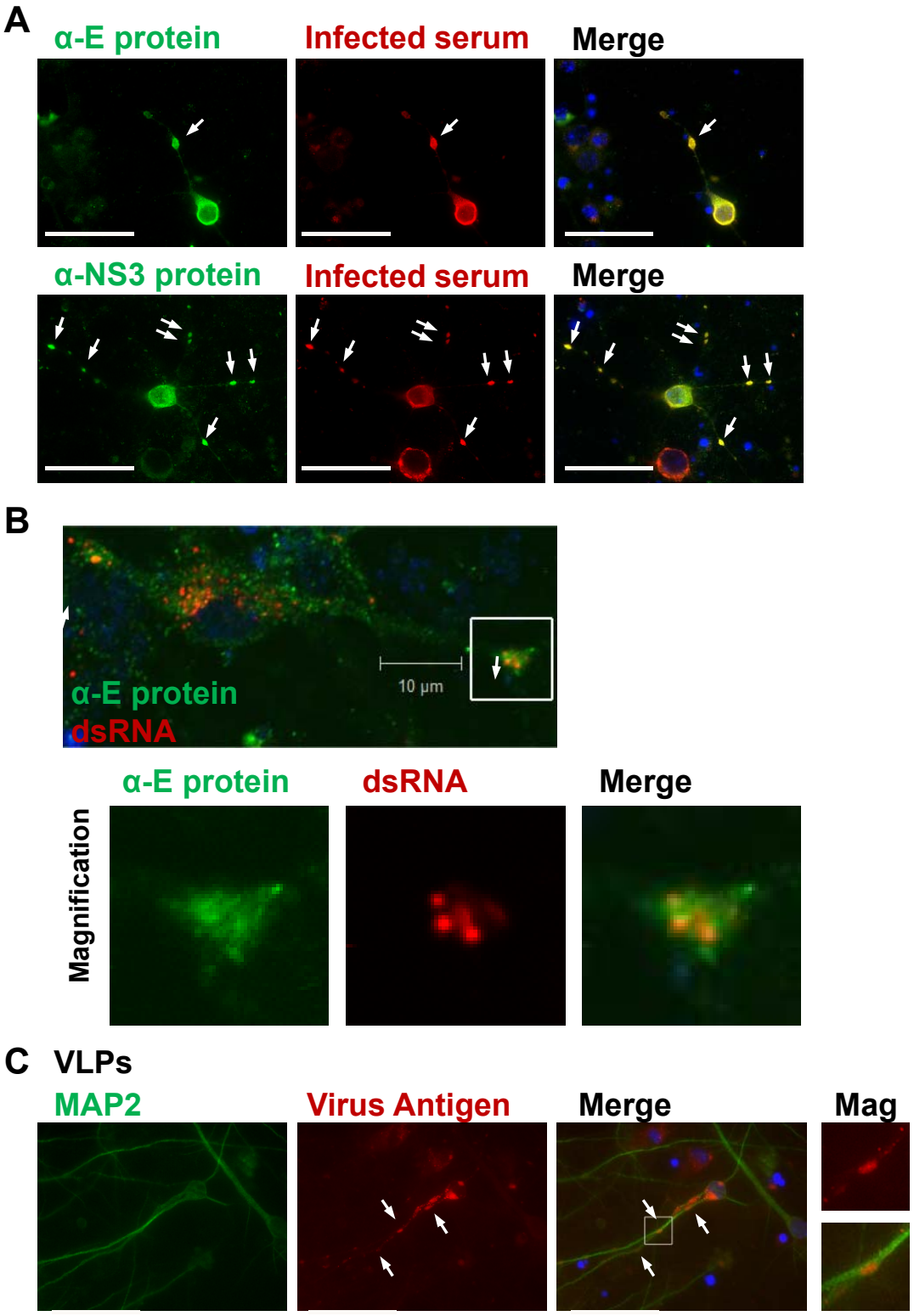

Fig. 9. Viral constituents present in antigen accumulations in dendrites.

(A) Cells were infected with TBEV at an MOI of 0.1, and fixed at 72 h.p.i.. The fixed cells were stained with antibodies against viral proteins (green), an antiserum against a tick-borne flavivirus (red), and DAPI (blue). To detect viral proteins, antibodies targeting E protein and NS3 were used. Scale bars: 50 µm. **(B)** Cells were infected with TBEV at an MOI of 0.1, and fixed at 48 h.p.i. The fixed cells were stained with antibodies against the TBEV E protein (green), an antibody against dsRNA (red), and DAPI (blue). The viral antigen is magnified in magnification panels. Accumulations of viral antigens are indicated by white arrows. **(C)** Cells were infected with VLPs of TBEV and fixed at 48 h.p.i.. Neurons were stained with an antibody against MAP2 (green), an antiserum against a tick-borne flavivirus (red), and DAPI (blue). Right panels show magnifications of antigen accumulations from the indicated regions of the merged images. Scale Bars indicate 50 µm in length. Accumulations of viral antigens are indicated by white arrows.

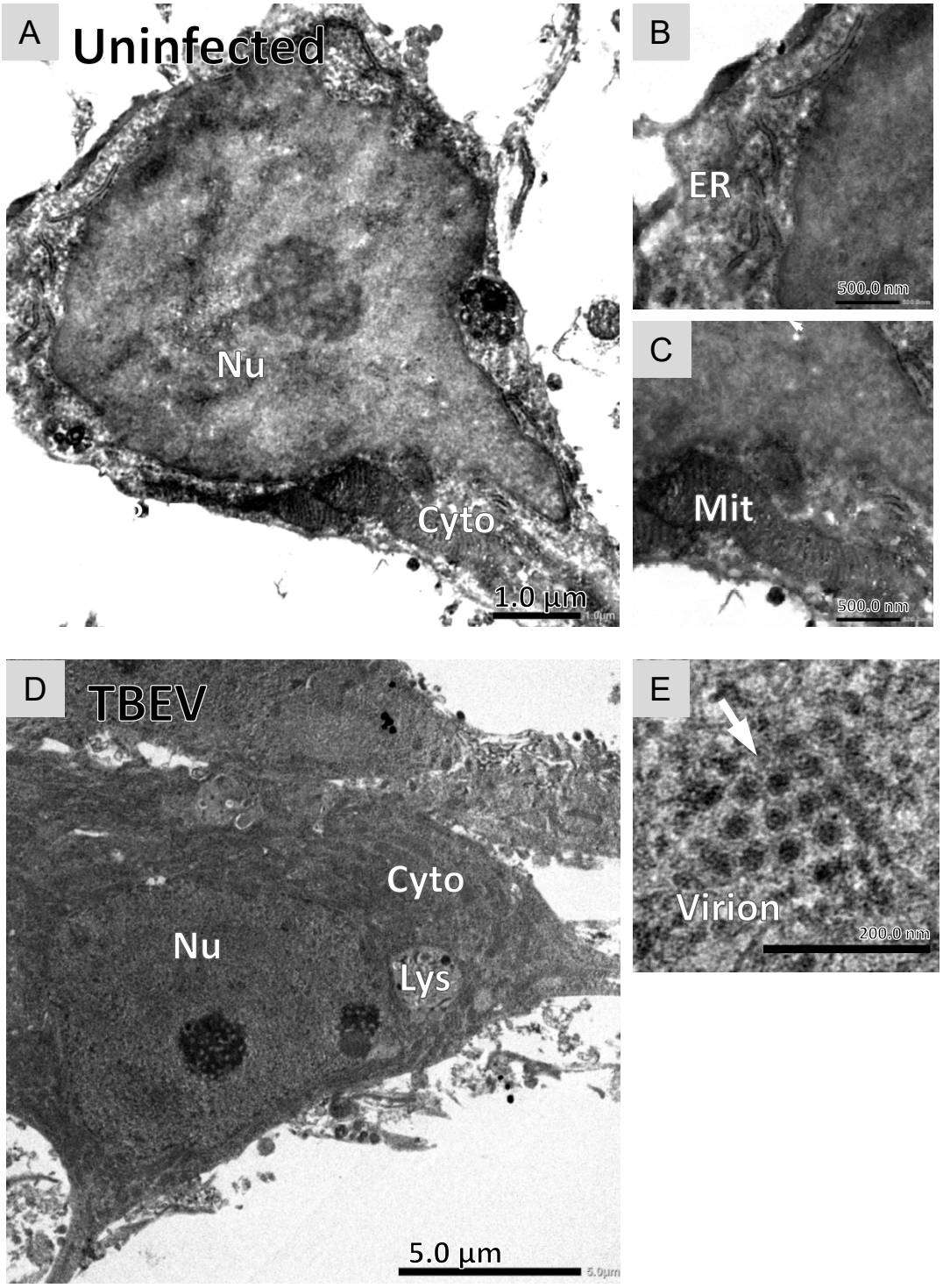

Fig. 10. Ultrastructural changes in primary neuronal cultures upon flaviviral infection.

Primary neuronal cultures were examined by TEM at 54 h.p.i.; these included uninfected cells (A−C, and F), cells infected with TBEV (D, E, and H−L), and cells infected with WNV (G). **(A−C)** Mock-infected neurons contained structurally intact organelles (Nu: Nucleus, Cyto: Cytosol, ER: endoplasmic reticulum, and Mit: Mitochondria). **(D)** TBEV infected neurons exhibited cytoplasmic condensation, and reactive lysosomes were also observed (Lys: Lysosome). **(E)** Virions coated with lipid bilayers were evident (white arrows). **(F)** Normal microtubule structure was observed in mock-infected neurites. **(G)** WNV-triggered degeneration of membrane structure (white arrowhead) and the appearance of granular aggregates in the neurites. **(H)** TBEV infection triggered swelling of and development of elliptical membrane-encased structures in neurites. **(I)** A laminal membrane structure was observed adjacent to microtubules. Mitochondria were unevenly distributed in one side of neurites with the structures. **(J−L)** Representative images of the regions (surrounding those shown in H, and I). Virion-like structures coated with lipid bilayers were observed both inside and outside the observed structures(white arrows).

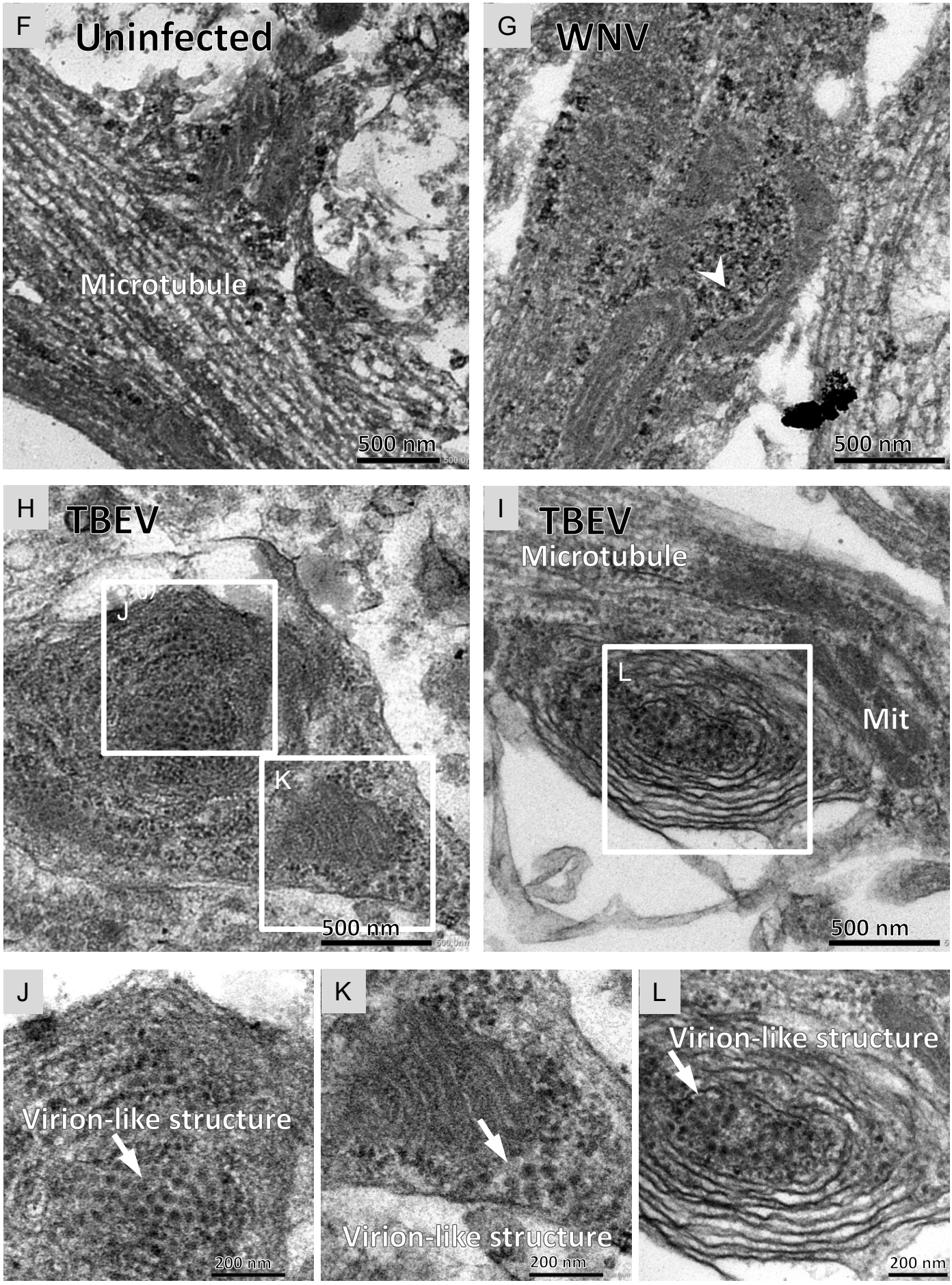
F
Uninfected
Microtubule
500 nm
G
WNV
500 nm
H
TBEV
J
K
500 nm
I
TBEV
Microtubule
L
Mit
500 nm
J
Virion-like structure
200 nm
K
Virion-like structure
200 nm
L
Virion-like structure
200 nm

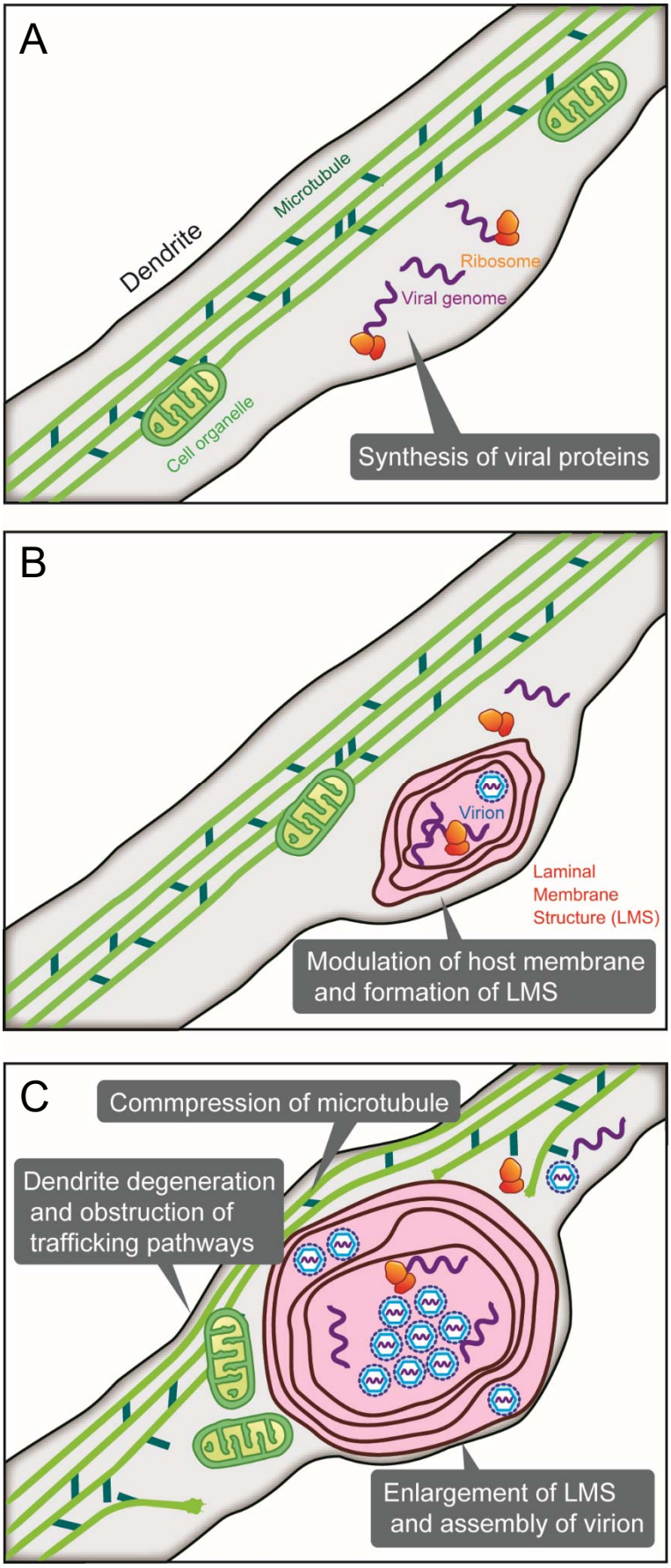

Fig. 11. Schematic of LMS formation and the contribution to neuro-pathogenicity.

(A) Viral proteins are synthesized by free ribosomes in the dendrites. **(B)** Synthesized proteins form the LMS by modulating the structure of host-membranes. **(C)** The LMS becomes enlarged and compromises microtubule linearity, thus obstructing trafficking pathways.

Chapter II:

Dendritic transport of tick-borne flavivirus RNA by neuronal granule affects development of the neurological disease.

Summary

Neurological diseases caused by encephalitic flaviviruses are severe and associated with high levels of mortality. However, little is known about the detailed mechanisms of viral replication and pathogenicity in CNS. In chapter I, it was shown that the genomic RNA of TBEV, a member of genus *Flavivirus*, is transported and replicated in the dendrites of neurons. In this chapter II, I analyzed the transport mechanism of the viral genome to dendrites. Specific sequences of the 5′ UTR of TBEV genomic RNA was identified as a *cis*-acting element for RNA transport. Mutated TBEV with impaired RNA transport in dendrites caused a reduction in neurological symptoms in infected mice. It was shown that neuronal granules, which regulate the transport and local translation of dendritic mRNAs, are involved in TBEV genomic RNA transport. TBEV genomic RNA bound a RNA-binding protein of neuronal granules and disturbed the transport of dendritic mRNAs. This is the first report of a neuropathogenic virus hijacking the neuronal granule system for the transport of viral genomic RNA in dendrites, resulting in severe neurological disease.

Introduction

Some of the pathogenic flaviviruses, such as JEV, WNV, and TBEV, are neurotropic and cause encephalitic disease [2–5]. The encephalitic flaviviruses histologically induce typical nonsuppurative encephalitis [2,56,58]. However, differences in neurological symptoms were observed in the flaviviruses, and neurologic manifestations such as photophobia, irritability, and sleep disorders are characteristically observed following TBEV infection [53–55]. These differences in the symptoms have suggested that the pathogenic mechanism in neurons may differ in the encephalitic flaviviruses. In chapter I, it was shown that the TBEV replicated locally in dendrites in primary cultures of mouse neurons [109]. To replicate within dendrite locally, viral genomic RNA must be transported from cell body to dendrites. Genomic RNA transport and local replication are thought to be important in the pathogenesis of neurological diseases that are result of TBEV infection, although their detailed mechanism are not well understood.

It has been reported that mRNAs are transported and locally translated in neuronal dendrites [98,99]. Specific mRNAs form a complex, called a neuronal granule, with several RNA-binding proteins (RBPs), and are transported along microtubules to dendrites in a kinesin-dependent manner. Transport of the mRNA and local translation in neuronal dendrites have been shown to be important for neurogenesis and the plasticity of the synaptic communication [110,111]. Furthermore, disruption of the neuronal granule system has been shown to be involved in mental retardation and neurodegenerative diseases, such as fragile X syndrome [106,112], autism spectrum disorder [113], and Alzheimer's disease [103]. It was hypothesized that the genomic RNA of TBEV is also transported by neuronal granules, resulting in the severe neurological symptoms caused by TBEV infection.

In this chapter II, I investigated the mechanism of the transport of TBEV genomic RNA to the dendrites in neurons. A *cis*-acting element in the viral genomic RNA important for transport was identified. Genomic RNA transport contributed to the development of neurological symptoms following TBEV infection. TBEV genomic RNA interacted with an RBP of neuronal granules and disturbed the transport dendritic mRNAs using neuronal granules for dendritic transport.

Materials and Methods

Cell culture

PC12 cells were purchased from DS Pharma Biomedical Co., Ltd. (Osaka, Japan) and were grown at 37°C in Roswell Park Memorial Institute (RPMI) 1640 medium (Wako Pure Chemical Industries, Ltd., Osaka, Japan) containing 10% (v/v) horse serum, 5% (v/v) FBS, and penicillin/streptomycin.

Viruses

To construct the TBEV stem-loop (SL)-2 loop C-U mutant, a C-to-T mutation was introduced into the Oshima-IC at nt position 120 by polymerase chain reaction (PCR) and subcloning in a stepwise manner. Working stocks of the viruses were propagated once in BHK-21 cells, and stored at −80 °C. Experiments using live TBEV were conducted in Biosafety Level 3 or Animal Biosafety Level 3 facilities located at the Graduate School of Veterinary Medicine at Hokkaido University.

Plasmids

The pCMV-TBEV REP plasmid was constructed from the pCMV-TBEV REP-GFP plasmid (kindly provided by Dr. Igarashi, Kyoto University) by deleting the inserted *Green fluorescent protein (GFP)* gene. Under the control of a cytomegalovirus (CMV) promotor, this plasmid was designed to transcribe a replicon RNA of the TBEV Oshima 5-10 strain in which most of the CDS for the viral structural proteins (nucleotide (nt) 239−2291) had been deleted. The hepatitis delta virus (HDV) ribozyme sequence and a poly-A signal were inserted after the replicon sequence. For construction of the other RNA-expressing plasmids, PCR fragments were synthesized by standard fusion-PCR and subcloned into pCMV-TBEV REP. The pCMV-TBEV REP dGDD and pCMV-TBEV REP dATG plasmids were constructed by introducing a mutation in the RdRp motif of the NS5 protein (GAT-to-GTC: nt 9654−56) and in the first translation

initiation codon of the CDS (ATG-to-AGG: nt 132−134), respectively.

To construct pCMV-Luc, the *luciferase* gene of pGL4.0 (Promega, Madison, WI) was inserted between the CMV promoter and the HDV ribozyme sequence. Partial CDS of the TBEV Oshima 5-10 strain (nt 132−244; partial CDS for capsid protein, and 2292−4304; from NS1 to NS2A, nt 4206−7007; from NS2B to NS4A or nt 6909−1037; from NS4B to NS5) was inserted into pCMV-Luc to construct plasmids expressing TBEV CDS with *luciferase* sequence. The plasmids expressing flavivirus UTRs with the *luciferase* gene were constructed by inserting the 5′ and 3′ UTRs of the TBEV Oshima 5-10 strain or the WNV 6-LP strain (AB185914.2) into the pCMV-Luc plasmid. The sequences of stem-loop (SL) -1 (nt 4−103) and SL−2 (nt 107−128) were deleted from the pCMV-Luc (5′ TBEV/3′ TBEV) plasmid to construct the pCMV-Luc (5′ TBEV dSL-1/3′ TBEV) and (5′ TBEV dSL-2/3′ TBEV) plasmids, respectively. G-to-T mutations at nt positions 114, 115, and 117 were introduced into pCMV-Luc (5′ TBEV/3′ TBEV) to construct pCMV-Luc (5′ TBEV SL-2 loop G-U/3′ TBEV) plasmid. The pCMV-Luc (5′ TBEV SL-2 loop C-U/3′ TBEV) plasmid was constructed by introducing a C-to-T mutation (120 nt) in pCMV-Luc (5′ TBEV/3′ TBEV). Four mutations (G109U, C110A, G125A, and C126U) were introduced in the pCMV-Luc (5′ TBEV/3′ TBEV) to construct the pCMV-Luc (5′ TBEV SL-2 stem/3′ TBEV) plasmid.

To construct pCXSN-Flag-fragile X mental retardation syndrome protein (FMRP), CDS of the *FMR-1* gene from HEK293T cells was cloned into the pCXSN-Flag plasmid [114]. To construct pCXSN-Flag-FMRP (I304N), a T-to-A mutation at nt position 911 was introduced by site-directed mutagenesis.

Infection and transfection

For neuronal differentiation, 1.0×10^4 PC12 cells/well were seeded on eight-well glass chamber slides with RPMI 1640 medium containing 0.5% (v/v) horse serum, 0.25% (v/v) FBS and penicillin/streptomycin. Following overnight incubation, the medium was changed with medium supplemented with 50 ng/mL of 2.5s Neuronal growth factor (COSMO BIO co. ltd., Tokyo, Japan) and the cells were incubated for 6−7 days until neurites developed. The differentiated PC12 cells were infected with TBEV at a MOI of 0.1 or transfected with the plasmids by using X-treameGENE HP Transfection Reagent (Hoffmann-La Roche Ltd., Basel, Switzerland).

Primary neuronal cultures were infected with TBEV at an MOI of 0.1. Following viral adsorption for 1 h, half of the culture medium was replaced. The medium was harvested at 24, 48, and 72 h.p.i. and stored at −80°C.

Antibodies

Rabbit anti- RNA granule protein 105 (RNG105) polyclonal antibodies were kindly provided by Dr. Shiina (National Institute for Basic Biology, Okazaki, Japan). Rabbit anti-Staufen polyclonal antibodies (AB5781), mouse monoclonal anti-FMRP antibodies (MAB2160), mouse monoclonal ANTI-FLAG M2 antibodies (F3165) and mouse monoclonal anti- Kinesin Heavy chain antibodies (MAB1614) were purchased from Merck KGaA (Darmstadt, Germany). Anti-mouse IgG and anti-rabbit IgG antibodies conjugated with AlexaFluor555 were purchased from Thermo Fisher Scientific (Waltham, MA). Anti-Digoxigenin-Rhodamine, Fab fragments were purchased from Merck. Peroxidase AffiniPure Goat Anti-Mouse IgG (H+L) was purchased from Jackson Immuno Research Laboratories, Inc. (West Grove, PA). Anti-DYKDDDDK tag, Monoclonal Antibodies, Peroxidase Conjugated were purchased from Wako.

Labeled RNA probes

The 3′ UTR of TBEV (nt 10277−11100), partial CDS for NS3 of TBEV (nt 5546−4599), luciferase (nt 31−930), Ca^{2+}/calmodulin-dependent protein kinase II α (CaMKIIα, nt 483−931), brain-derived neurotropic factor (BDNF, nt 2514−2859), and Arc (nt 2968−2354) were cloned into the pGEM-T (Easy) vector (Promega) [115]. After the cleavage of the plasmids by restriction enzyme, digoxigenin- (DIG-) and fluorescent- labeled RNA were transcribed by using the DIG RNA Labeling Kit (SP6/T7) (Roche) and Fluorescein RNA Labeling Mix (Roche), respectively.

Fluorescent in-situ hybridization (FISH) and IFA

Cells were fixed in 4% (w/v) paraformaldehyde for 15 min at 37°C and washed with 0.1 M glycine in PBS. The cells were permeabilized in 0.5% (v/v) Triton X-100 for 5 min at room temperature and were washed with PBS. The cells were post-fixed with 40% (v/v) formamide in 4 × saline sodium citrate buffer (0.6 M sodium chloride and 0.06 M trisodium citrate dehydrate) for 30 min at room temperature. After washing with PBS, the cells were treated with hybridize buffer (50% (v/v) formamid in 2 × saline sodium phosphate ethylenediaminetetraacetic acid (EDTA) buffer: 0.36 M sodium chloride, 0.02 M sodium phosphate buffer and 0.002 M EDTA) for 2 h at 45°C. The cells were hybridized overnight at 45°C with hybridization buffer containing 2 µg/mL of anti-sense fluorescein- or DIG- labeled RNA. The hybridized cells were incubated with hybridization buffer without labeled RNA for 1 h at 45°C and washed.

Following FISH, the cells were washed with PBS and blocked with 2% (w/v) bovine serum albumin. The cells were incubated at room temperature for 2 h with primary antibodies. After extensive washing, the cells were incubated with secondary antibodies conjugated with fluorescent dye and enclosed with a solution of Slowfade Gold antifade reagent with DAPI (Thermo Fisher Scientific). Fluorescent images were taken by using the LSM 700 confocal laser scanning microscopy (Zeiss). Images were processed with ZEN 2009 software (Zeiss), IMARIS

software (Bitplane AG, Zurich, Switzerland), or Image J [116].

Analysis of fluorescent signal in neurites

To analyze the fluorescent signals in the neurites of PC12 cells, Z-stack images of the cells stained with FISH and IFA were collected with the LSM 700 for 8.8 μm at intervals of 0.88 μm in depth. The three-dimensional images were reconstructed and analyzed with IMARIS software. Briefly, stained regions were assessed as voxels, and overlapping voxels of MAP2 and FISH signals in neurites were defined as the RNA signals in neurites. The measurements were conducted in five microscopic fields that were randomly selected from three biological replicates. Similar analysis was performed to analyze the localization of the RBPs in the neurites. Intensity line profiles of the viral proteins and the RBPs were analyzed with ZEN2009 software. To measure the fluorescent signals in the neurites of the primary neurons, neurites positive for the Arc, BDNF or CaMKIIα mRNA were randomly selected in five microscopic fields from three biological replicates, and the fluorescent signals in the area of interest (AOI) were measured with image J. The measurements were conducted in ten independent areas. Similar analysis was performed to measure the co-localized areas of FISH signal and RBPs in the neurites.

Analysis of binding of FMRP to TBEV genomic RNA

RNAs of TBEV wild type (wt) or the SL-2 loop C-U mutant were synthesized *in vitro* with MEGAscript SP6 Transcription Kit (Thermo Fisher Scientific). HEK293T cells (4.0×10^5 cells/wel) were seeded on a six-well plate and transfected with pCXSN-Flag-FMRP or pCXSN-Flag-FMRP (I304N) by using X-treameGENE HP Transfection Reagent. Following a 48 h of incubation, the cells were collected and treated with 250 μL/well of radioimmunoprecipitation assay buffer (50 mM Tris-HCl, 150 mM sodium chloride, 1% (v/v) NP-40, 0.5% (w/v) sodium deoxycholate, 0.1% (w/v) sodium dodecyl sulfate, and 1mM EDTA) containing protease and RNase inhibitor. The synthesized RNAs (1 μg) were added to the lysate,

and the mixture was pre-cleared with 5 μL of SureBeads Protein G magnetic beads (Bio-Rad Laboratories, Inc., Hercules, CA) for 30 min at 4°C. The lysate was then incubated with 5 μL of magnetic beads with 1 μL of anti-Flag antibody for 1 h at 4°C. Following three washes with PBS, the RNA bound to the beads was extracted from half of the beads with ISOGEN II (Nippon Gene Co., Ltd., Tokyo, Japan). The other half was used to perform Western blotting to detect FMRP with anti-FMRP antibodies, anti-mouse IgG antibodies conjugated with HRP and the Immobilon™ Western Chemiluminescent HRP Substrate (Merck). To detect TBEV RNA in the extracted RNAs, reverse transcription- (RT-) PCR was conducted with SuperScript III (Thermo Fisher Scientific) and Platinum Taq DNA Polymerase (Thermo Fisher Scientific) with TBEV-specific primers. Four biological replicates were performed for each experiment.

Luciferase activity of the RNA-expressing plasmids

HEK293T cells were transfected with plasmids expressing luciferase mRNA with or without flavivirus UTRs. After 48 h of incubation, cells were collected and luciferase activity was measured with luciferase assay system (promega). Three biological replicates were performed.

Detection of dendritic mRNAs in primary neuron by RT-PCR

Total RNA in primary neurons seeded on 12 well plate was collected by using ISOGEN II. To detect dendritic mRNAs, Beta-Actin mRNA and TBEV genomic RNA in the extracted RNAs, RT-PCR was conducted with SuperScript III and Platinum Taq DNA Polymerase using specific primers. Three biological replicates were performed for each experiment.

Animal model

Ten five-week-old female C57BL/6 mice (Japan SLC Inc.) were divided randomly into two groups and inoculated with 100 PFUs of virus (TBEV wt or SL-2 loop C-U) intracerebrally. Morbidity was defined as the appearance of 10% weight loss. Surviving mice were monitored for 14 days to obtain survival curves, mortality rates and body weights. The experiment was repeated

twice (total n = 10). No statistical method was used to estimate the sample size. There were no mice excluded from the analysis. The President of Hokkaido University approved all animal experiments after review by the Animal Care and Use Committee of Hokkaido University (approval no. 13025).

Levels of paralysis and neurological symptoms of the infected mice (n = 5) were evaluated every day as described previously [117]. Briefly, four tests (ledge test, hind limb clasping, gait, and kyphosis) were conducted and scored individually on a scale of 0−3; a score of 0 represented an absence of the relevant phenotype and a score of 3 represented the most severe manifestation. For the ledge test, the mouse was placed on the ledge of cage and the state of movement was observed. To evaluate hind limb clasping, the tail of the mouse was grasped near its base, the mouse was lifted, and the hind limb position was observed. To evaluate the mouse's gate, the mouse was placed on a flat surface and was observed from behind as it walked. The level of kyphosis was observed while the mouse walked after being placed on a flat surface. One mouse infected with TBEV wt and one mouse infected with SL-2 loop C-U were excluded from the analysis at 8 day post infection (d.p.i.) due to death.

Analysis of viral titer, viral sequence and histology of mice

The brains of the mice were collected at 3 and 6 d.p.i. (n = 3) for viral titer analysis. They were weighed and homogenized as 10% suspensions (w/v) in PBS with 10% FBS. The suspension was clarified by centrifugation at 12,000 rpm for 5 min at 4 °C and titrated by plaque forming assay in BHK-21 cells. Total RNAs of brains of the dead mice were extracted with ISOGEN II (Nippon Gene). Following amplification by RT-PCR with SuperScript III (Thermo Fisher Scientific) and Platinum Taq DNA Polymerase (Thermo Fisher Scientific) with TBEV-specific primers, SL-2 region was sequenced with 3130 genetic analyzer (Thermo Fisher Scientific). For histological analysis, the brains were collected from the infected mice at 3 and 6

d.p.i. (n = 3). Organs were fixed in 10% phosphate-buffered formalin (pH 7.2) and embedded in paraffin. Sections were stained with Carrazzi's hematoxylin and eosin. Histological changes in the brain (cerebral cortex, midbrain, hippocampus, cerebellum, and medulla oblongata) were observed under a microscope.

Prediction of the RNA secondary structure of 5′ UTRs of TBEV

The RNA secondary structures of the 5′ UTRs of TBEV (nt 1−240) were predicted with mfold Web Server provided by University At Albany [118]. The RNA secondary structures of the constructs with deletions or mutations in the 5′ UTR were confirmed with mfold prediction.

Phylogenetic analysis of flavivirus 5′ UTRs

The evolutionary history was inferred by using the Maximum Likelihood method based on the Tamura-Nei model [119]. The tree with the highest log likelihood (-1012.9710) is shown. The percentage of trees in which the associated taxa clustered together is shown next to the branches. Initial tree(s) for the heuristic search were obtained automatically by applying Neighbor-Join and BioNJ algorithms to a matrix of pairwise distances estimated using the Maximum Composite Likelihood approach, and then selecting the topology with superior log likelihood value. The tree is drawn to scale, with branch lengths measured in the number of substitutions per site. The analysis involved 15 nucleotide sequences of 5′ UTRs of flaviviruses and hepatitis C virus (TBEV Oshima5-10: AB062063.2, TBEV Sofjin-HO: AB062064.1, TBEV Hypr: U39292.1, TBEV Neudoerfl: U27495.1, LANV TP21: AF253419.1, OHFV Guriev: AB507800.1, KFDV P9605: JF416958.1, ZIKV MR766: LC002520.1, DENV2 16681: U87411.1, WNV NY99-6-LP: AB185914.2, JEV Nakayama: : EF571853.1, YFV Ivory Coast 1999: AY603338.1, CulexFlavivirus Tolyo: AB262759.2, AedesFlavivirus Narita-21: AB488408.1 and HCV JFH-1: AB047639.1). All positions containing gaps and missing data were eliminated. There were a total of 74 positions in the final dataset. Evolutionary analyses were conducted in MEGA7 [120].

Statistical analysis

Data are expressed as mean ± the standard errors. Following a one-way analysis of variance test, the Tukey−Kramer test was used to determine the statistical significance of differences in the mean values of the fluorescent signals in neurites (Fig. 13C, 14C, 16C, 16F & 21C), the fluorescent signals in the AOI (Fig. 23B) and the luciferase activity (Fig. 15). Following the F-test to analyze variances, the unpaired two-sided Student's or Welch's *t*-test was used to determine statistical significance between TBEV wt and SL-2 loop C-U mutant at each time point (Fig. 18B, 18C, 19B, 19C, 19D. 20B & 20D). The Kaplan−Meier survival curves and the log-rank test were used to evaluate the survival of the infected mice (Fig. 19A). Days until onset and average survival time were expressed as 95% confidence intervals. The statistical analysis was performed with SAS University Edition software (SAS Institute Inc., Cary, NC).

Results

5' UTR of TBEV is a cis-acting element important for RNA transport to neurites.

PC12 cells differentiate into neuronal phenotype and form neurites in the presence of neuronal growth factors. To examine whether the genomic RNA of TBEV is transported to neurites in differentiated PC12 cells, as observed in primary neurons [109,121], the PC12 cells were infected with TBEV. Accumulations of viral antigen and FISH signal for TBEV genomic RNA were observed in the neurites (Fig. 12A), as seen in the dendrites of the primary neurons.

A flavivirus replicon, a viral genomic RNA in which most of the CDS for the viral structural proteins was deleted, has been used for analysis of intracellular replication of the viral genome [122–124]. In this study, a plasmid expressing the TBEV replicon RNA (pCMV-TBEV REP) was used to analyze the viral factor involved in the transport of genomic RNA (Fig. 12B). Differentiated PC12 cells were transfected with the plasmid and the distribution of viral RNA was examined by FISH. Viral RNAs were observed in the neurites (Fig. 12C), indicating that viral structural proteins are not required for the transport of genomic RNA. I introduced a mutation into the catalytic site of the viral RdRp (pCMV-TBEV REP ΔGDD), which is essential for replication of flavivirus genome [124]. Viral genomic RNA was still detected in the neurites of cells transfected with the ΔGDD construct (Fig. 12C), indicating that the transport is independent of the process of genome replication including synthesis of the negative strand of the genomic RNA. Furthermore, mutation of the first initiation codon of the viral polyprotein (pCMV-TBEV REP ΔATG) did not alter the distribution of viral genomic RNA in the neurites (Fig. 12C). Overall, these results indicate that the transport of genomic RNA does not require expression of the viral proteins.

To analyze the RNA region required for transport, plasmids expressing RNA for a luciferase CDS fused with partial sequences of the TBEV were constructed (Fig. 13A). Expressed

RNA with TBEV UTRs was detected in neurites, but those with any of the CDS for the viral proteins, without the UTRs, were not (Fig. 13B & C), indicating that the UTRs of TBEV, but not CDS, were important for the transport of mRNA to neurites.

In chapter I, it was observed that the viral antigen accumulations in dendrites of cells infected with tick-borne flaviviruses, but less in those infected with mosquito-borne WNV [109]. I hypothesized that this difference could be caused by differences in the UTRs and constructed plasmids expressing luciferase mRNA with the UTRs of TBEV or WNV (Fig. 14A). The mRNAs expressed with the 5′ UTR of TBEV were localized to neurites, while those with the 5′ UTR of WNV were not, regardless of the 3′ UTR sequences (Fig. 14B & C). Complete deletion of the 3′ UTR drastically reduced the expression of the RNAs in reporter assay, indicating that the 3′ UTR was involved in the stability of the RNAs (Fig. 15). These data suggest that the 5′ UTR of TBEV contains a motif required for the transport of mRNA to neurites.

There are two stem-loop structures (SL-1, nt 4–103 and SL-2, nt 107–128) predicted in the 5′ UTR of TBEV [18] (Figs. 16A & 17A). A plasmid with deletion of SL-1 or SL-2 in the 5′ UTR was constructed to analyze the importance of these structures in transport (Fig. 16A). The mRNA with deletion of SL-1 was still detected in the neurites, while deletion of SL-2 abolished the localization (Fig. 16B & C). These data indicated that the SL-2 region of TBEV 5′ UTR is required for mRNA transport.

To further analyze the role of SL-2, we introduced mutations in the SL-2 region of pCMV-Luc (5′ TBEV/3′ TBEV). The mutations of SL-2 loop G-U and C-U were designed without affecting formation of the stem structure. The mutations of SL-2 stem were designed to dissociate the stem structure (Fig. 16D). After transfection of PC12 cells, the mutation of SL-2 loop G-U or SL-2 stem slightly decreased the signals in the neurites. However, the mRNAs with

the mutation was still detected in the neurites, and showed no significant difference from those of TBEV wild-type (wt). The mRNAs with the SL-2 loop C-U mutation were not detected in the neurites completely (Fig. 16E & F). These indicated that C at nt position 120 in SL-2 is the most important in the transport of mRNA to neurites.

Sequence of the 5′ UTRs were compared among flaviviruses. Phylogenetic tree of flavivirus 5′ UTR showed that tick-borne flaviviruses form a distinct cluster from that of mosquito-borne flaviviruses (Fig. 17B). Sequence alignment showed that the SL-2 sequences were completely conserved among tick-borne flaviviruses (Fig, 17C), but not among mosquito-borne flaviviruses.

Mutation-impeding genome transport to dendrites attenuated the neurological symptom of TBEV

To construct a mutant TBEV lacking the ability to transport the genome in dendrites, a C-to-U mutation at nt position 120 in the 5′ UTR was introduced into the infectious clone of TBEV. Viral genomic RNA was detected in the dendrites infected with TBEV wt, but the signal in dendrites was weak in SL-2 loop C-U-infected cells (Fig. 18A). The virus growth of SL-2 loop C-U was slightly lower until 48 h.p.i., but caught up that of TBEV wt at 72 h.p.i (Fig. 18B). Number of the viral antigen accumulation in the dendrites also decreased significantly in cells infected with SL-2 loop C-U (Fig. 18A & C), indicating that the C-U mutation of the SL-2 loop significantly decreased the transport of genomic RNA to dendrites.

To evaluate the effects of TBEV genome transport on the pathogenesis in mice, C57BL/6 mice were inoculated with TBEV wt or SL-2 loop C-U intracerebrally. No differences in morbidity or mortality were observed between the two groups (Table 2 and Fig. 19A). Slightly prolonged survival time (TBEV wt, 7.9 ± 0.46 d post-infection (d.p.i.); SL-2 loop C-U, 8.9 ± 0.68

d.p.i.; $p < 0.02$) and reduced weight loss at days 6 and 7 (Fig. 19B) were observed in the mice infected with SL-2 loop C-U. The percentage of mice showing severe neurological symptoms was reduced (TBEV wt, 70%; SL-2 loop C-U, 30%), and the level of cerebellar ataxia of infected mice was scored and was found to be significantly lower from 5 to 7 d.p.i. in mice infected with SL-2 loop C-U (Fig. 19C). The virus titer was lower in the brain infected with SL-2 loop C-U at 3 d.p.i., but caught up with TBEV wt at 6 d.p.i. (Fig. 19D). In the histological observation of the brain, shrunken and eosinophilic Purkinje cells were observed in both groups of mice (Fig. 19E). Perivascular cuffing and meningitis were rarely seen. No reversion or compensatory mutation in the 5′ UTR was found in the mice infected with SL-2 loop C-U. Thus, preventing the transport of the genome did not affect the lethality after viral multiplication, but attenuated the neurological symptoms of TBEV in mice.

Role of neuronal granules in viral genome transport

Neuronal granules have been shown to regulate the transport of mRNAs and local protein translation in neuronal dendrites [98,99]. I hypothesized that neuronal granules are involved in the transport of TBEV genomic RNA and local viral replication. Localization of viral proteins, viral RNA and RBPs in neuronal granules, such as FMRP, RNG105 and Staufen, was analyzed in primary neurons infected with TBEV wt or SL-2 loop C-U. The number of the viral antigen accumulations was significantly higher in the neurites with the neuronal granules compared with those without the neuronal granules (Fig. 20A & B). Viral RNA of TBEV wt was colocalized with RBPs in dendrites, but that of SL-2 loop C-U was not (Fig. 20C & D). These results suggested that TBEV genomic RNA was transported via the neuronal granule. However, their detailed localizations varied. FMRP colocalized with viral antigen and was recruited into the site of the viral antigen in the dendrites (Fig. 21A, B & D). Signals of FMRP in the neurites increased significantly in the neuron infected with TBEV wt (Fig. 21C). In contrast, RNG105 surrounded the accumulation of viral antigen, but did not completely colocalize with the viral protein. (Fig.

21D). Distribution of Staufen was not changed clearly by the TBEV infection (Fig. 21A, B & D)

To further analyze the interaction of the neuronal granule RBPs and viral genomic RNA, binding of FMRP to the genomic RNA of TBEV was examined. *In vitro* synthesized RNAs of the full-length TBEV genome were mixed with Flag-tagged FMRP expressed in HEK293T cells. RNAs that coimmunoprecipitated with FMRP were detected by RT-PCR. RNAs for TBEV wt coimmunoprecipitated with FMRP, while RNAs with C-to-U mutation at nt 120 in the SL-2 region showed decreased binding (Fig. 22A). A missense mutation (I304N) was identified in the second K homology domain of the *FMRP* gene of a fragile X syndrome patient and shown to be involved in altered RNA binding and transport [125,126]. This mutation was found to drastically reduce the binding of FMRP to TBEV genomic RNA (Fig. 22B). These results indicated that SL-2 region of TBEV 5′ UTR, important for the transport, is also critical for binding to an RBP of neuronal granule, FMRP. It was also shown that the transported TBEV genomic RNA altered the distribution of bound FMRP in neuronal granules.

To evaluate the effect of TBEV genome transport on neuronal function, the distribution and expression of host mRNAs for Arc, BDNF, and CaMKIIα were examined in primary neurons infected with TBEV wt or SL-2 loop C-U. The mRNA signals in dendrites, especially the mRNA of BDNF, decreased significantly in neurons infected with TBEV wt but not in those infected with SL-2 loop C-U (Fig. 23A & B). The expression of the mRNAs was reduced more by infection of TBEV wt than SL-2 Loop C-U (Fig. 23C). These results indicated that the transport of TBEV genomic RNA disturbed that of host dendritic mRNAs.

Discussion

The transport of TBEV genomic RNA occurred independently of viral proteins and differed from that of other neurotropic viruses. Dendritic and axonal transport of viral genomes has been reported in several neurotropic DNA and RNA viruses [78]. The genomic DNA of herpes simplex virus type 1 and 2 (*Herpesviridae*) undergo anterograde or retrograde transport through the binding of viral proteins with host motor proteins [81]. Virions of poliovirus (*Picornaviridae*) are known to be incorporated into synaptic vesicles during anterograde transport [127]. Complexes of nucleoprotein and genomic RNA of rabies virus (*Rhabdoviridae*) are transferred via retrograde processes [79]. The genomes of these viruses require their viral proteins for transport, while it was shown that the transport of TBEV genomic RNA in dendrites occurs independently of the viral proteins and is regulated by the UTR of the genomic RNA itself (Figs. 12-16). Besides, the viral genome of reported neurotropic viruses usually replicated in the neuronal cell body. However, transported TBEV genomes replicate locally in the dendrites, which has not been reported in other neurotropic viruses.

The 5′ UTR of TBEV was demonstrated to have a function in RNA transport, in addition to protein translation and genome replication. The UTRs of flavivirus are important for many functions in viral multiplication. The complementary sequences in the 5′ and 3′ UTRs cyclize the viral genome, which is essential for viral genome replication [3,18,122,128]. SL-1 in the 5′ UTR is thought to recruit the NS5 protein for genome replication [15,128]. The loop C-U mutation introduced to the recombinant TBEV overlapped with the cyclization sequences and therefore may affect genome cyclization, resulting in delayed viral growth and decreased neurological symptoms (Fig. 18 & 19). However, RNA with the TBEV 5′ UTR and WNV 3′ UTR, which could not cyclize the RNA, was efficiently transported to the neurite, indicating that transport was independent of the TBEV 3′ UTR and genome cyclization (Fig. 14). In addition, reporter assay

revealed that, regardless of the transport of the genome, the mutations introduced to 5′ UTR did not affect RNA stability or translation efficiency, but the deletion of 3′ UTR drastically reduced the stability (Fig. 15). These results suggest that genome transport via the SL-2 region is independent of other known functions of 5′ UTR, and that the TBEV 3′ UTR was not directly involved in the transport although it stabilized the RNA.

SL-2 in the 5′ UTR of TBEV genomic RNA was shown to be a unique viral *cis*-acting element important for the transport of mRNA. Mutant RNA that cannot form the stem structure (SL-2 stem) was still transported to dendrites (Fig. 16D–F). The mutation in the SL-2 loop region that reduced transport also resulted in reduced binding to an RBP in neuronal granules (Fig. 22). These results indicated that the transport signal may be regulated by the intact sequence of the SL-2 region via the binding to RBPs. Several studies have reported signals of transport and recognition by RBP(s) of some dendritic mRNAs, such as CaMKIIα [129], postsynaptic density protein 95 [130], and BDNF [131]. However, the consensus sequence or motif for mRNA transport has not been elucidated, and the SL-2 sequence does not contain sequences similar to known transport signals. The transport of TBEV genomic RNA reduced the transport of dendritic mRNA, especially BDNF mRNA (Fig. 23). The genomic RNA of TBEV and dendritic mRNA may share competing RNA sequences or structures required for transport. This information regarding the viral signal element will contribute to further understanding of the transport mechanism of dendritic mRNA which is important for neuronal functions.

RBPs, such as FMRP [106,112], Staufen [110], and RNG105 [111], are primary components of the neuronal granule and regulate RNA transport and local translation. It was shown that FMRP interacted with the genomic RNA of TBEV and accumulated at the site of local TBEV replication (Figs. 21 & 22), while Staufen and RNG105 did not. It is possible that this unusual localization of FMRP disrupted the local translation of host dendritic mRNAs bound to FMRP in dendrites,

resulting in the development of neurological disease.

The neurological symptoms of TBEV in mice were exacerbated by genome transport and local replication in dendrites. The defect of the transport of the TBEV genomic RNA did not affect the lethality following to viral encephalitis, but was involved in the attenuation of neurological symptoms (Fig. 23). Neurological symptoms caused by the RNA transport might be somehow independent of the lethality by encephalitis. Recent studies have shown that disruption of the transport and local translation of dendritic mRNAs is involved in many neurodegenerative disorders. In fragile X syndrome, mutations and silencing of the *FMRP* gene caused dysregulation of the local translation of the dendritic mRNAs, such as the metabotropic glutamate receptor, and CaMKIIα, resulting in abnormalities of morphology and dendritic function [112]. BDNF mRNA and its signaling pathway in dendrites has been shown to be involved in Alzheimer's disease [103,132]. In this study, it was shown that TBEV infection caused the unusual localization of FMRP in dendrites (Fig. 21) and that TBEV genomic RNA transport reduced the expression and transport of host dendritic mRNAs by neuronal granules (Fig. 23). It was reported that neuronal RNA granules and FMRP were involved in mRNA stability [133]. It is possible that TBEV genomic RNA disturbed binding of FMRP to dendritic mRNAs, and that the unbound RNAs were not transported by neuronal granule, resulting in their degradation. These data indicated that the disturbed transport of host dendritic mRNA by TBEV caused neuronal dysfunction, exacerbating the neurological symptoms in TBEV-infected mice.

The sequence of the SL-2 region is completely conserved among tick-borne flaviviruses, but not among mosquito-borne viruses (Fig. 17). In chapter I, it was shown that various tick-borne flaviviruses replicate locally in the dendrites [109]. In the transmission cycle of tick-borne flaviviruses, ticks get infected through blood suckling of viremic mammals or co-feeding of infected ticks. Viral infection and replication in the CNS of mammals are

considered non-essential processes for transmission [2,36]. A recent study showed that the UTR sequence that regulates the innate immune system was important for the epidemiological fitness of Dengue virus in a human epidemic [21]. It has also been suggested that the tick FMRP ortholog is involved in the tick RNA interference (RNAi) pathway [134]. Binding of the SL-2 to the tick FMRP or related protein might be important for tick-borne flaviviruses to evade RNAi pathway, resulting in conservation of the sequences.

In this chapter II, I revealed the mechanism of transport of TBEV genomic RNA in neuronal dendrites was revealed, and demonstrated the involvement of this transport in the development of neurological disease caused by TBEV infection [135]. I propose a model of viral replication and neuronal dysfunction in dendrites caused by TBEV infection (Fig. 24). The genomic RNA of TBEV is transported with RBPs in a neuronal granule. Transport of the viral RNA disturbed that of the host dendritic mRNAs and disrupts the distribution of the components of neuronal granules, such as FMRP. Local replication of the viral genomic RNA in dendrites causes degeneration of the dendrites as shown in the chapter 1 [109]. The transport and local replication of the viral RNA may result in neuronal dysfunction leading to the neurological symptoms observed with TBEV infection. My study demonstrated the hijacking of the neuronal granule system by a neuropathogenic virus for the transport of viral genomic RNA in dendrites for the first time. The description of this unique virus-host interaction will improve further understanding of the molecular mechanisms of viral replication and the pathogenicity of neurotropic viruses. It will also promote the study of neurodegenerative diseases caused by disruption of dendritic mRNA transport and could lead to the development of treatment options with virus-based vectors that can transport and express target genes locally in dendrites.

Table 2. Physical differences between mice infected with TBEV wt or SL-2 LoopC-U.

TBEV	wt	Sl-2 loop C-U
Morbidity †	100%	100%
Mortality	100%	100%
Onset of disease (d.p.i.) **	6.7 ± 0.42	7.9 ± 0.20
Survival time (d.p.i.) **	7.9 ± 0.46	8.9 ± 0.68
Severe neurological signs ‡	70%	30%

Five-week-old male C57BL/6 mice were inoculated with 100 plaque forming units of TBEV wt or SL-2 loop C-U intracerebrally ($n = 10$).

† Morbidity was defined as appearance of 10% weight loss.

‡ Severe neurologic sign was defined as appearance of spastic paralysis of hindlimbs and stooping position.

Statistical differences of onset of disease and survival time were assessed with the Student's *t*-test. **$p < 0.02$.

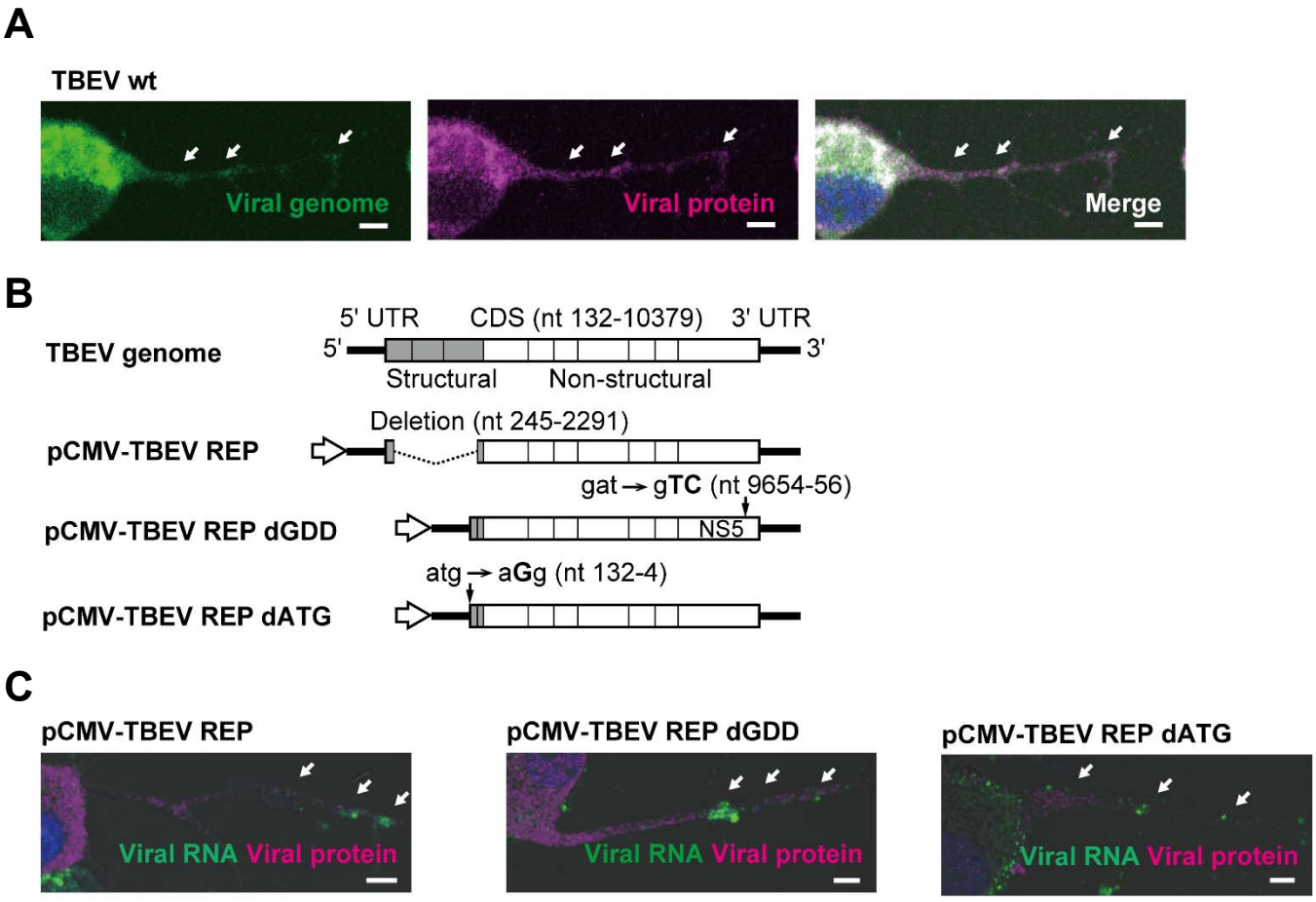

Fig. 12. Viral proteins were not required for the genomic RNA transport of TBEV.

(A) Differentiated PC12 cells were infected with TBEV wild-type (wt), and fixed at 48 h post-infection. The cells were stained with specific antibodies against viral proteins (magenta) and fluorescent RNA probe against viral genomic RNA (green). **(B)** Schematic diagram of the constructs expressing the TBEV replicon RNAs. Under the control of a CMV promoter (white arrows), a replicon of TBEV with deletion of the sequences for structural proteins was cloned into the RNA expression vector (pCMV-TBEV REP). Mutations of the catalytic site of the RNA-dependent RNA-polymerase (dGDD) and protein initiation codon (dATG) were introduced. **(C)** Differentiated PC12 cells were transfected with pCMV-TBEV REP, pCMV-TBEV REP dGDD, or pCMV-TBEV dATG. The transfected cells were fixed at 72 h post-transfection, and were stained with the fluorescent RNA probe against the genomic RNA of TBEV (green), antibodies against the NS3 protein (magenta) and DAPI (blue). White arrows indicate the FISH signal in neurites. Scale bars indicate 5 μm in length.

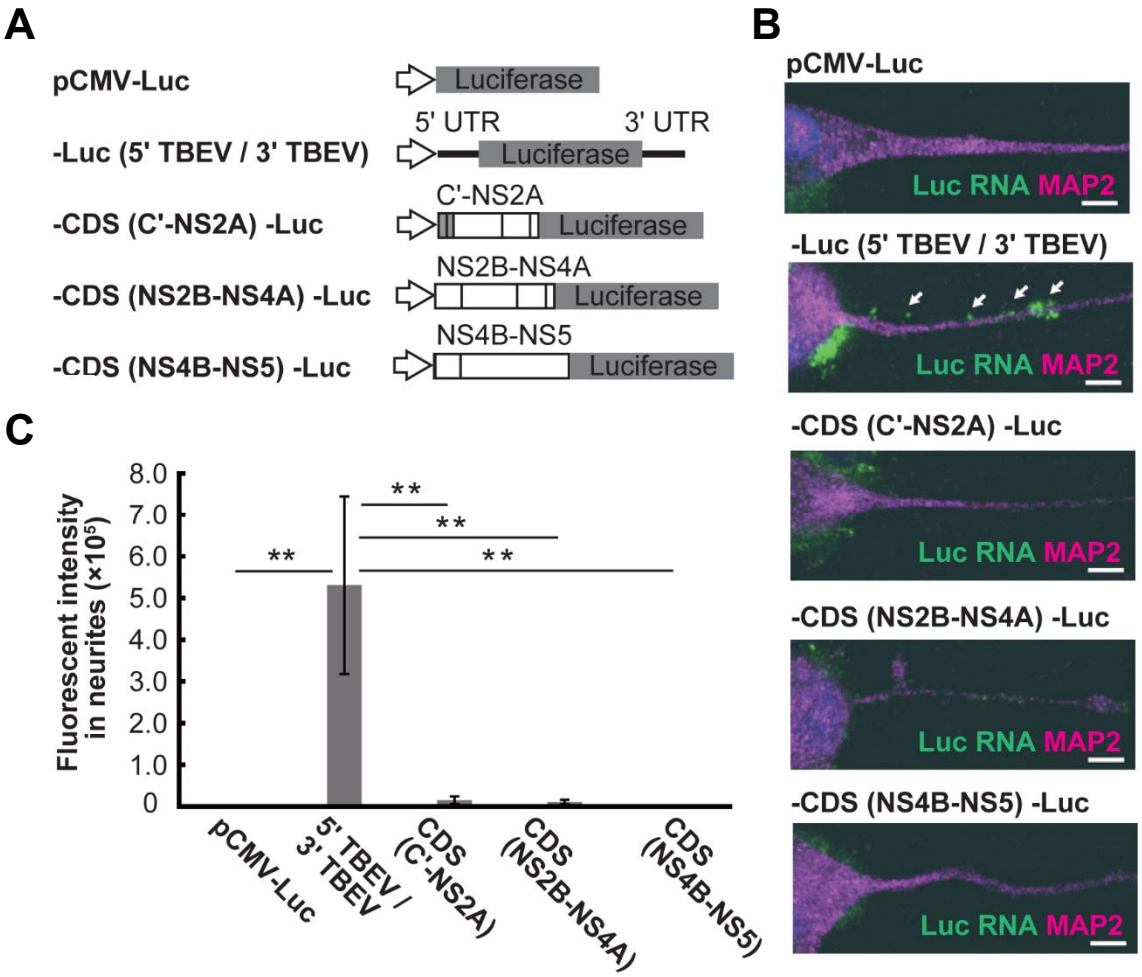

Fig. 13. UTRs of TBEV functions as a signal of RNA transport.

Differentiated PC12 cells were transfected with the plasmids expressing the RNA of luciferase with TBEV sequences. Following fixation, the cells were hybridized with a fluorescent RNA probe for the *luciferase* gene (green), and stained with DAPI (blue) and antibodies against MAP2 (magenta). FISH signal in the neurites was analyzed from the Z-stack images from five independent microscopic fields. **(A)** A CDS for *luciferase* (gray square) was cloned with or without the partial sequence for TBEV replicon RNA. **(B)** Fluorescence images and **(C)** fluorescence intensity in the PC12 neurites. Scale bars indicate 5 μm in length. White arrows indicate the FISH signal for luciferase RNA in the neurites. Error bars represent SEM; $^{**}p < 0.02$.

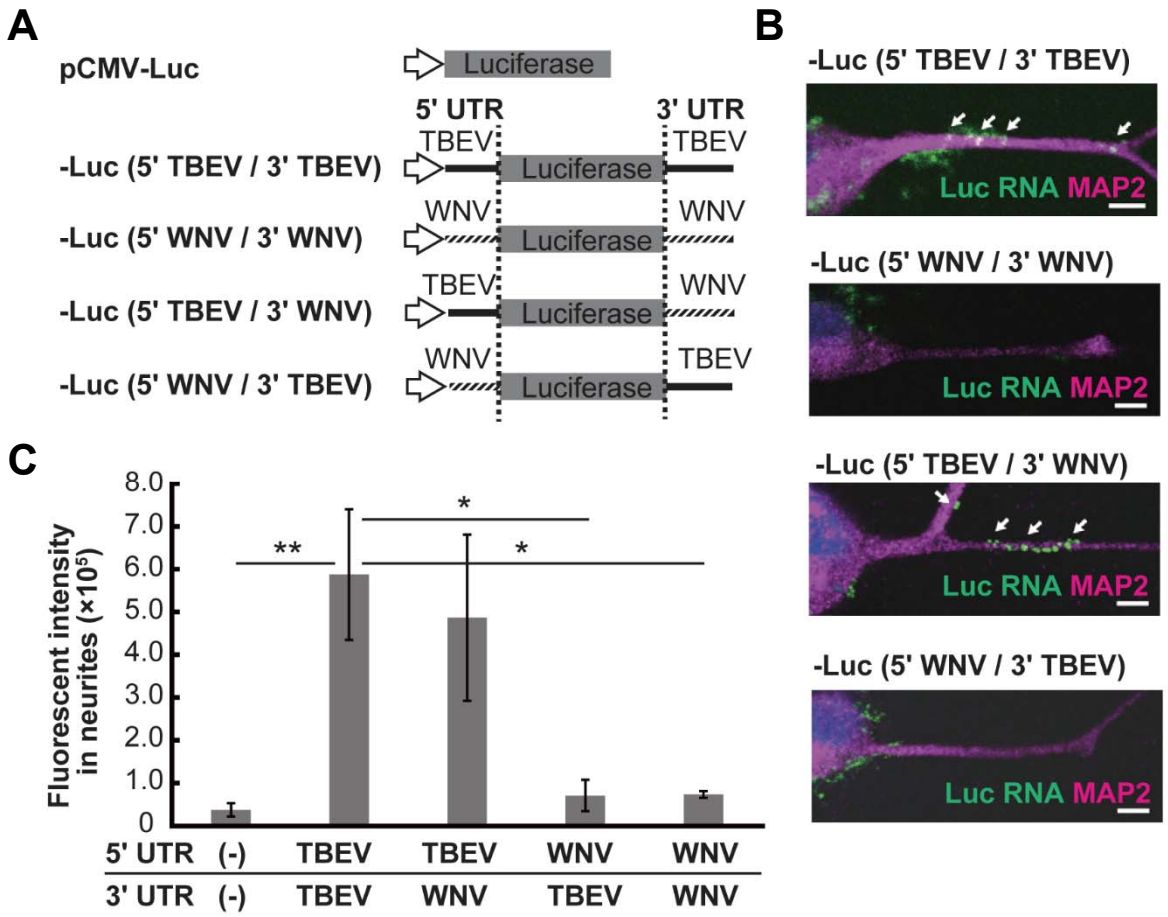

Fig. 14. 5' UTR of TBEV functions as a signal of transport, but that of WNV does not.

Differentiated PC12 cells were transfected with the plasmids expressing the RNA of luciferase with TBEV/West Nile virus (WNV) UTRs. Following fixation, the cells were hybridized with a fluorescent RNA probe for the *luciferase* gene (green), and stained with DAPI (blue) and antibodies against microtubule-associated protein 2 (MAP2; magenta). Fluorescent in-situ hybridization (FISH) signal in the neurites was analyzed from the Z-stack images from five independent microscopic fields. **(A)** A CDS for luciferase was cloned with/without the 5' and 3' UTRs of TBEV (black line) and WNV (striped line). **(B)** Fluorescence images and **(C)** fluorescence intensity in the PC12 neurites. Scale bars indicate 5 μm in length. White arrows indicate the FISH signal for luciferase RNA in the neurites. Error bars represent SEM; $^{**}p < 0.02$ and $^{*}p < 0.05$.

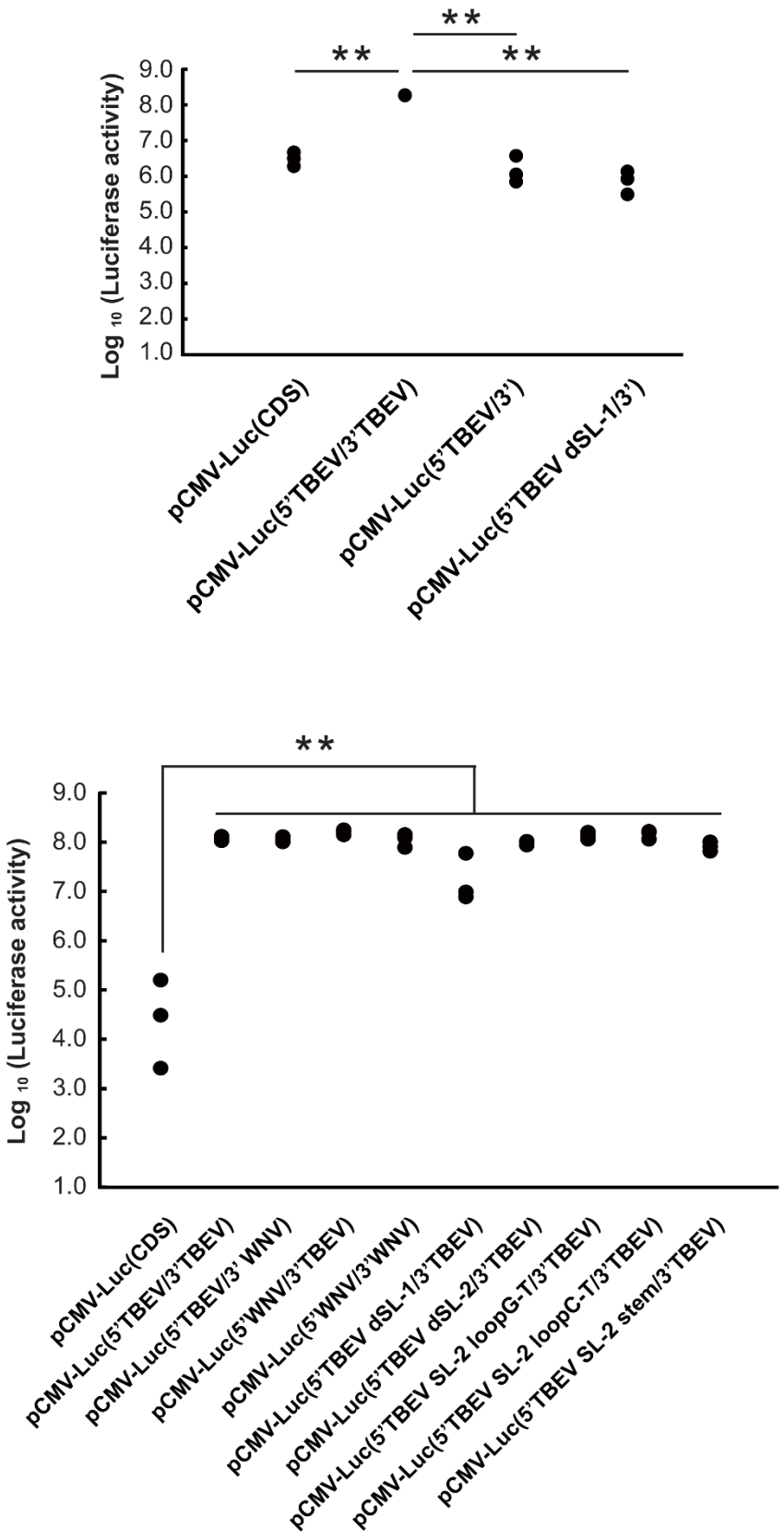

Fig. 15. Luciferase activity of the constructs expressing luciferase mRNA with or without flavivirus UTRs.

HEK293T cells were transfected with plasmids expressing luciferase mRNA with or without flavivirus UTRs. Following 48 h of incubation, cells were collected and luciferase activity was measured (n = 3).

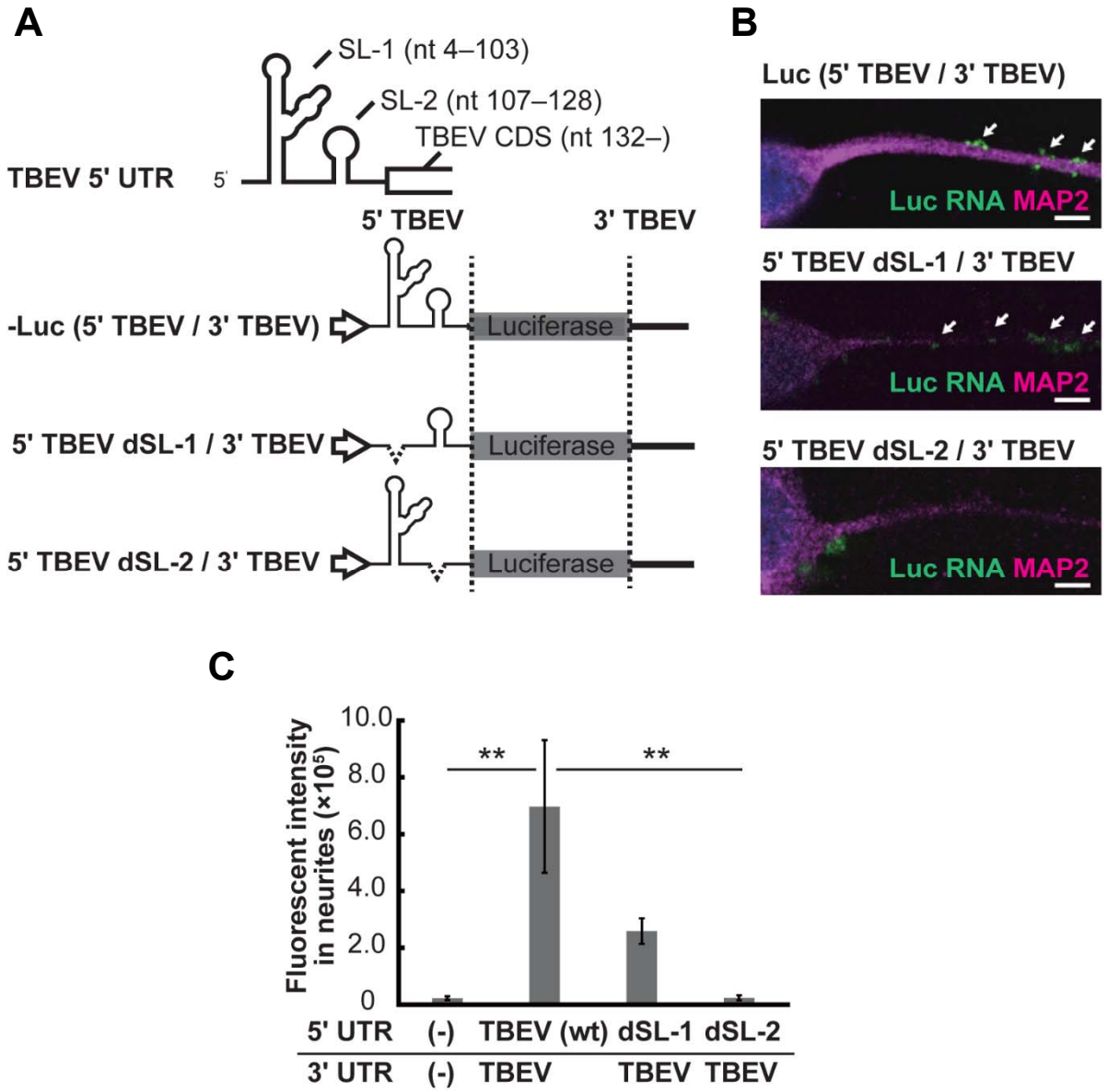

Fig. 16. Analysis of the roles of the stem loop structure of TBEV 5' UTR in genome transport.

Differentiated PC12 cells were transfected with the plasmids expressing the mRNA of luciferase with the UTRs of TBEV with deletion (A−C) or the mutation (D−F) of 5' UTR. Following fixation, the cells were hybridized with a fluorescent RNA probe for the *luciferase* gene (green), and stained with DAPI (blue) and antibodies against MAP2 protein (magenta). FISH signal in the neurites was analyzed from the Z-stack images from five independent microscopic fields. **(A)** Schematic diagram of the predicted RNA-secondary structure (upper) and the constructs expressing mRNA with a deletion (lower) are shown. The 5' UTR has a predicted branched SL-structures (SL-1) and single SL-structure (SL-2). The SL-1 or the SL-2 regions were deleted in pCMV-Luc (5' TBEV/3' TBEV). **(B, E)** Fluorescence images and **(C, F)** fluorescence intensity in the PC12 neurites. **(D)** Schematic diagram of the sequence and RNA secondary structure of the TBEV SL-2 and the constructs used to analyze the role of SL-2 in transport. G-to-U, C-to-U in loop, or four mutations in stem were introduced in pCMV (5' TBEV/3' TBEV). Scale bars indicate 5 μm in length. White arrows indicate the FISH signal for luciferase RNA in the neurites. Error bars represent SEM; $^{**}p < 0.02$ and $^{*}p < 0.05$.

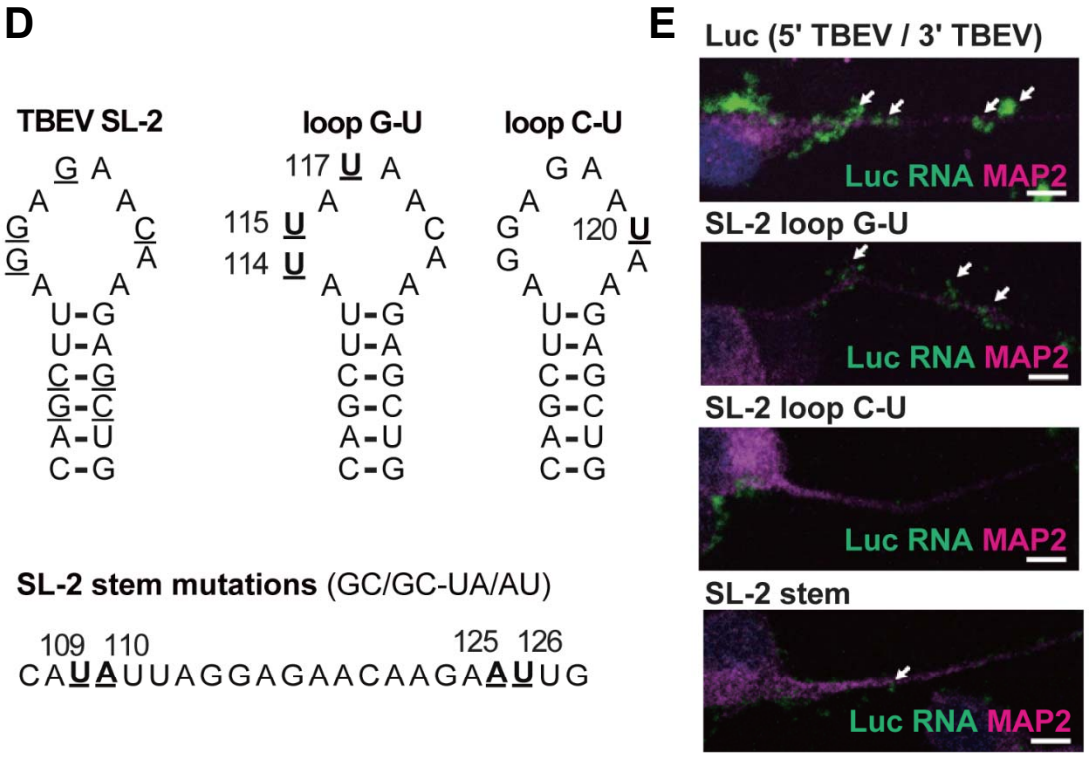
D
TBEV SL-2
loop G-U
loop C-U
SL-2 stem mutations (GC/GC-UA/AU)
109 110
CAUAUUAGGAGAACAAGAAUUG
125 126
E
Luc (5' TBEV / 3' TBEV)
Luc RNA MAP2
SL-2 loop G-U
Luc RNA MAP2
SL-2 loop C-U
Luc RNA MAP2
SL-2 stem
Luc RNA MAP2

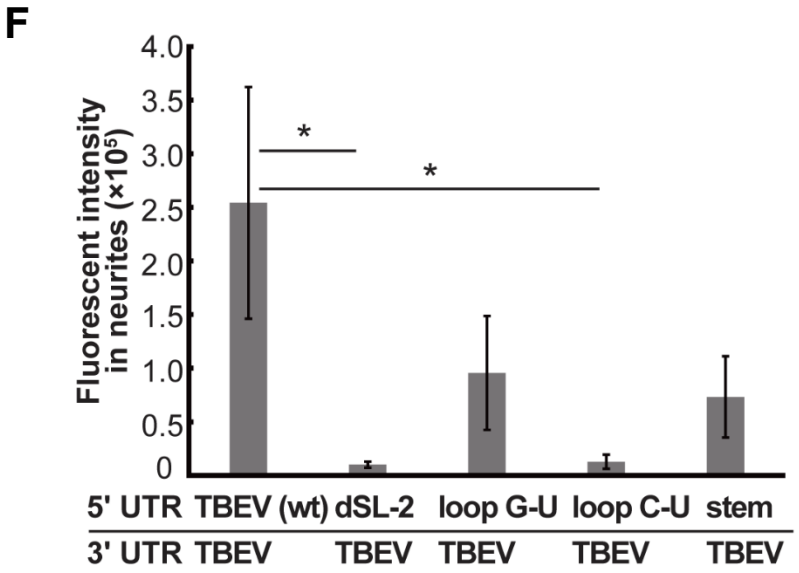
F
Fluorescent intensity in neurites (×10⁵)
4.0
3.5
3.0
2.5
2.0
1.5
1.0
0.5
0
*
*
5' UTR TBEV (wt) dSL-2 loop G-U loop C-U stem
3' UTR TBEV TBEV TBEV TBEV TBEV

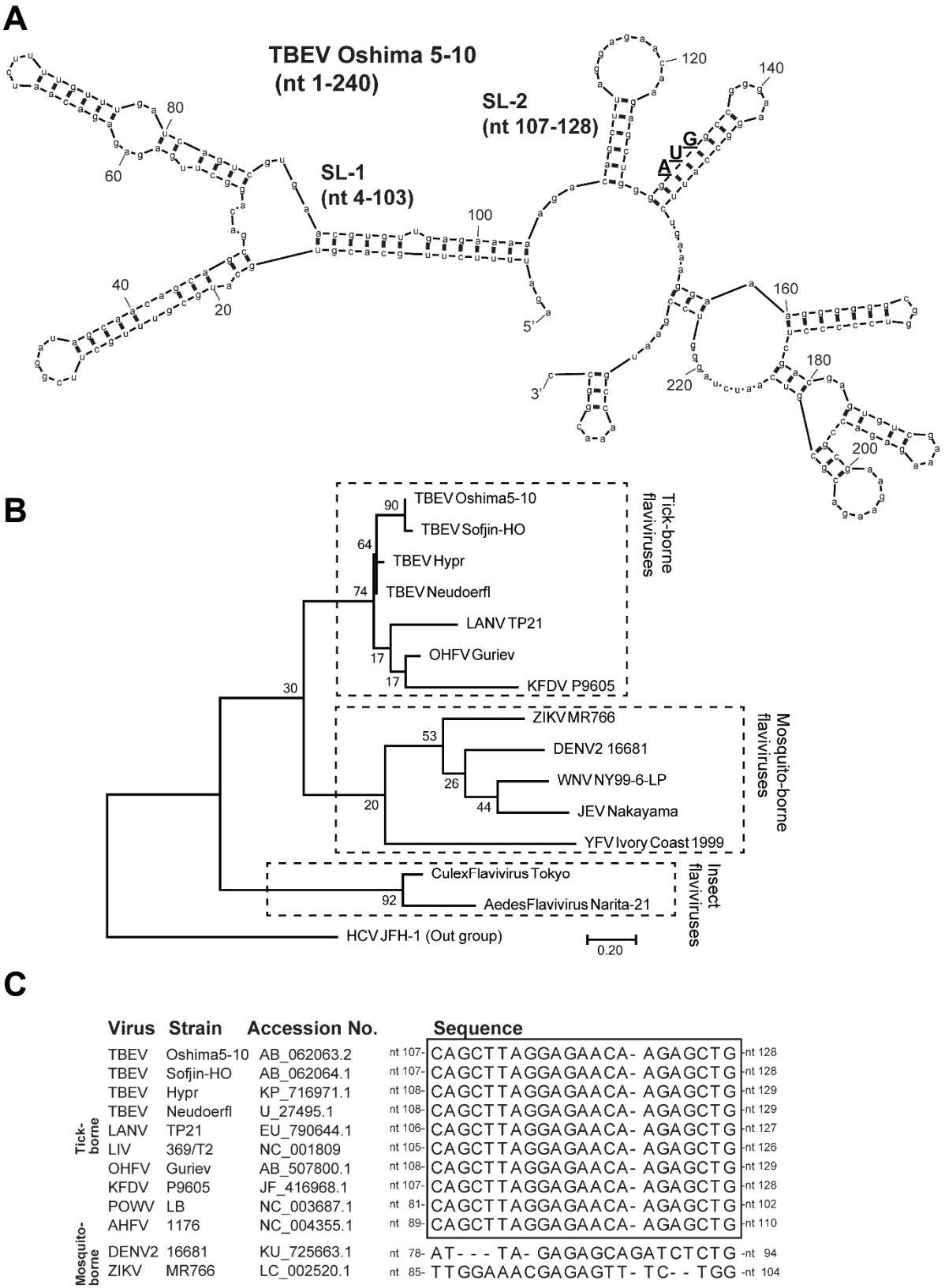

Fig. 17. Comparison of sequences of 5' UTRs among flaviviruses.

(A) RNA secondary structures of the TBEV Oshima 5-10 strain (nt 1−240) were predicted by mfold. Initiationcodons of the viral CDS are underlined and in bold. **(B)** Phylogenetic tree of the flaviviruses based on the 5' UTR sequences. Groups enclosed with dotted lines indicate tick-borne, mosquito-borne or insect flaviviruses. Scale bar indicates substitutions/site. **(C)** Alignment of the SL-2 sequences of tick-borne and mosquito-borne flaviviruses. LIV, Looping ill virus; KFDV, Kyasanur forest disease virus; HCV, hepatitis C virus; POWV, Powassan virus; AHFV, Alkhurma hemorrhagic fever virus.

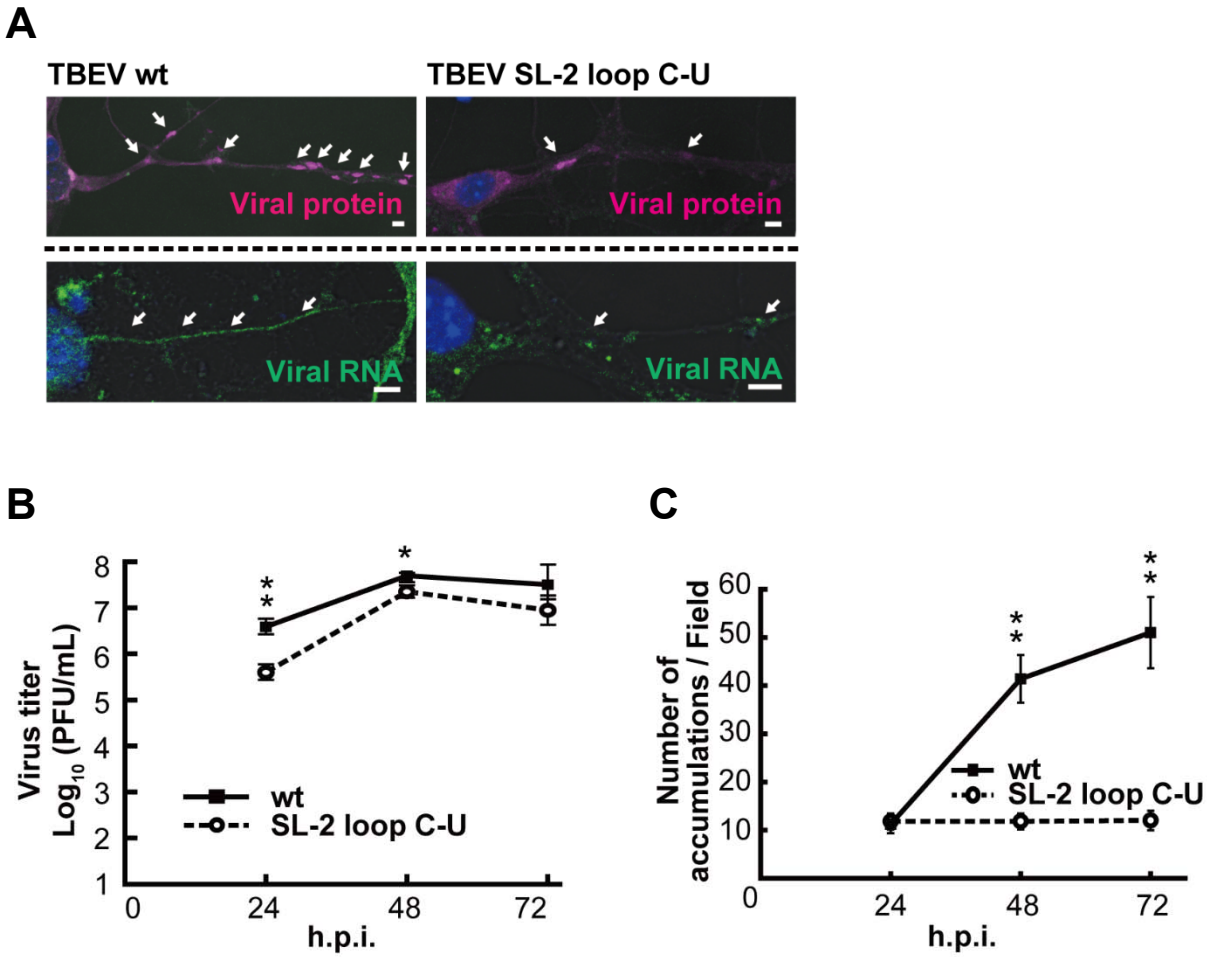

Fig. 18. Mutation in SL-2 impended genome transport of infectious virus.

Primary mouse neurons were infected with TBEV wild-type (wt; black squares with continuous lines) or SL-2 loop C-U (white circles with broken lines) at a multiplicity of infection (MOI) of 0.1. **(A)** The cells were fixed at 48 h.p.i. and the viral proteins and viral genomic RNAs were stained with IFA (upper panels, magenta) and FISH (lower panels, green), respectively. **(B)** Viral titer in the supernatant was measured by plaque forming assay. **(C)** Viral antigen accumulation was counted at 24, 48, or 72 h.p.i. in five independent microscopic fields. White scale bars indicate 5 μm in length. White arrows indicate viral antigen accumulation or the viral genome in dendrites. Error bars represent SEM; $^{**}p < 0.02$ and $^{*}p < 0.05$.

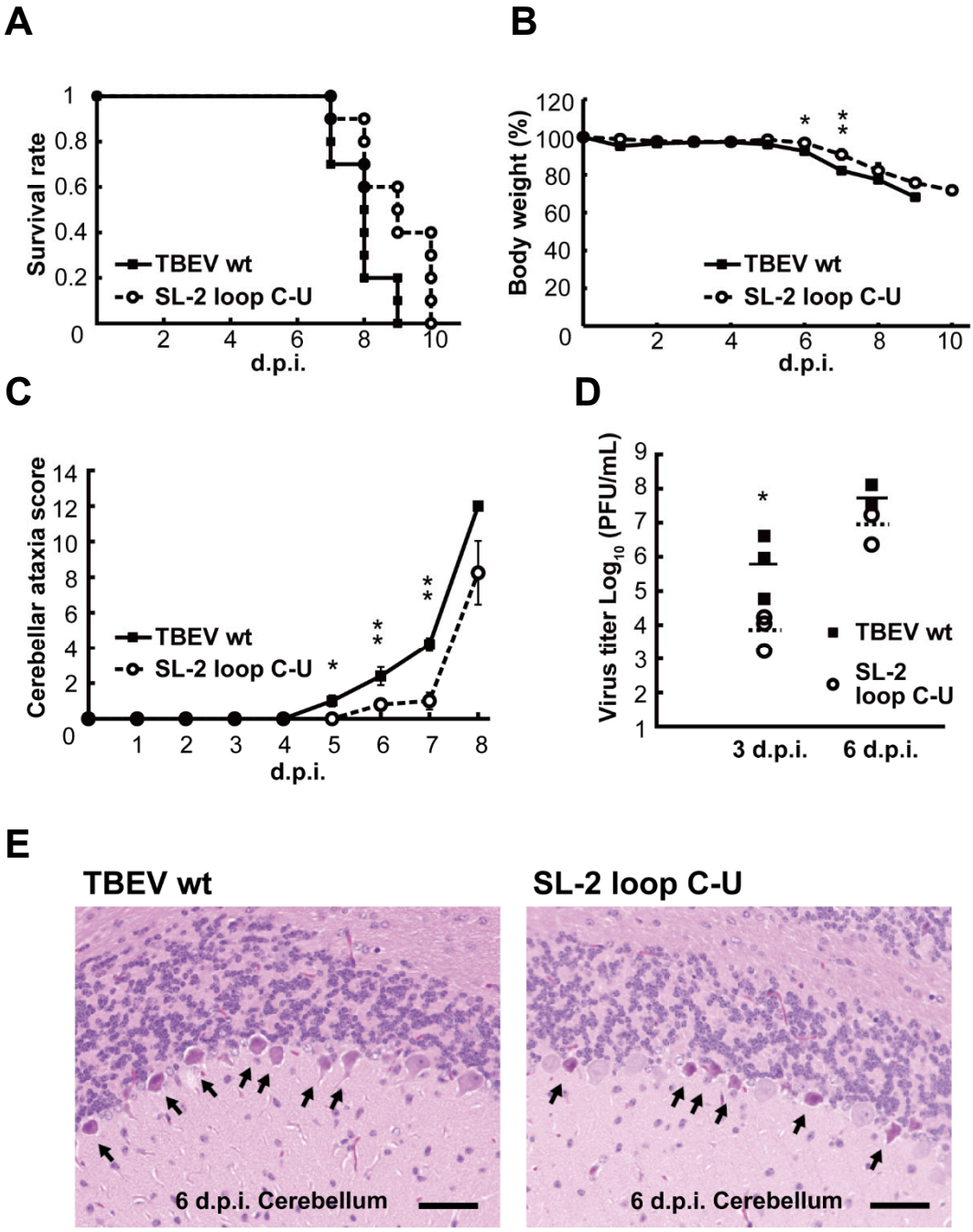

Fig. 19. Mutation impending genome transport to dendrites attenuated the neurological symptoms caused by TBEV infection.

Five-week-old male C57BL/6 mice were inoculated with 100 plaque forming units of TBEV wt or SL-2 loop C-U intracerebrally. **(A)** The Kaplan−Meier survival estimate was calculated (n = 10). **(B)** Body weight was measured during the infection (n = 10). **(C)** The neurological score of the mice (n = 5) was examined until 8 d.p.i. **(D)** The mice were sacrificed at 3 or 6 d.p.i. (n = 3), and the viral titer in the brain were analyzed. Continuous and broken lines indicate the average of viral titer in the brain infected with TBEV wt and SL-2 loop C-U, respectively. **(E)** Histology of the cerebellum infected with TBEV wt or SL-2 C-U at 4 d.p.i. Scale bars indicate 50 μm in length. Black arrows indicate an degenerated purkinje cells. Error bars represent SEM; $^{**}p < 0.02$ and $^{*}p < 0.05$.

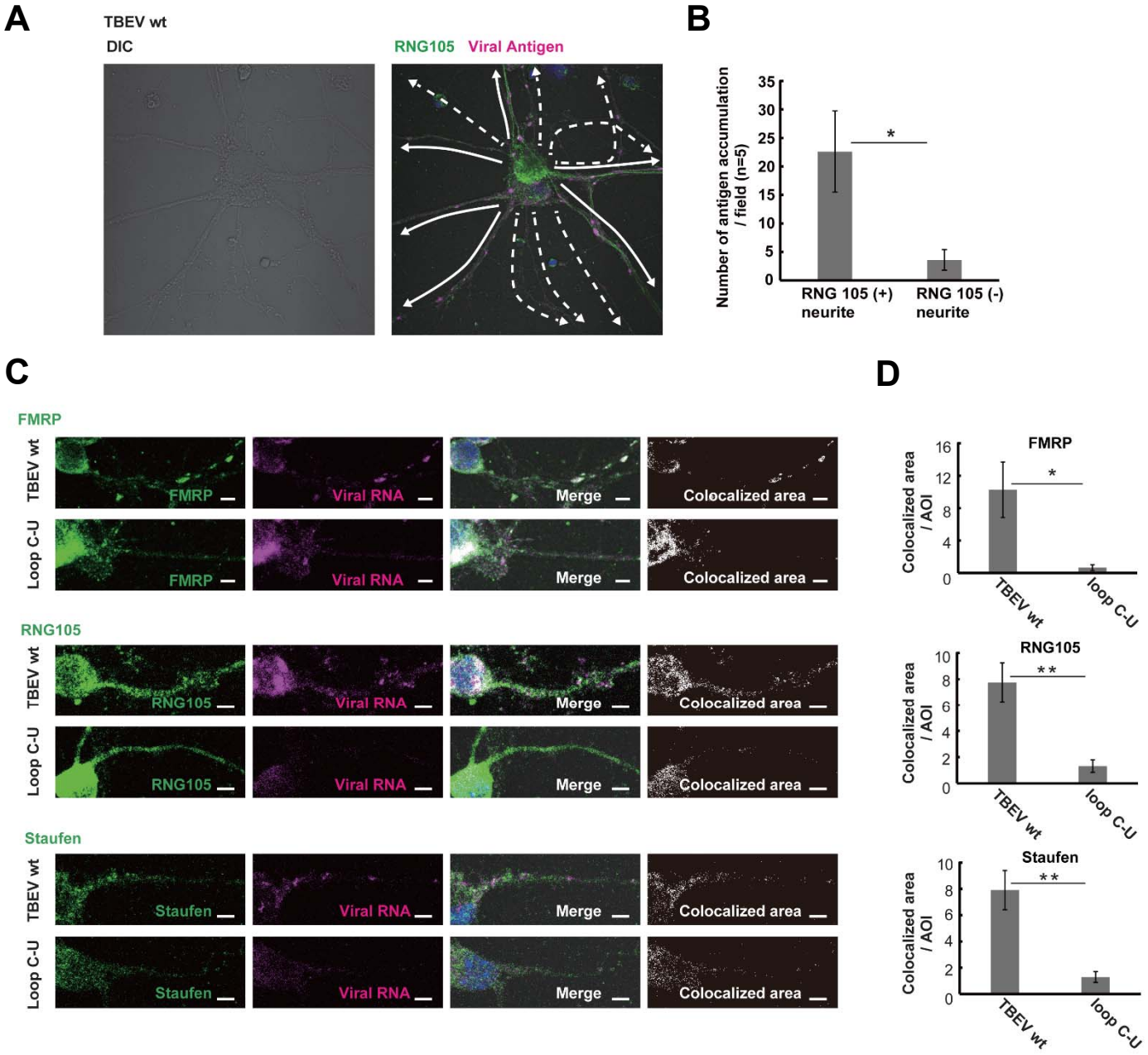

Fig. 20. Localization of the RBPs of neuronal granules and genomic RNA of TBEV in infected neuron.

(A-B) Primary mouse neurons were infected with TBEV wt at a multiplicity of infection of 0.1. and fixed at 48 h post-infection. The cells were stained with antibodies against RNG105 and antibodies against viral proteins (magenta). **(A)** The differential interference contrast microscope image (DIC, left) and fluorescent image of RNG105 and viral proteins are shown (right). White continuous and broken arrows show the paths of the RNG105-positive and negative neurites, respectively. **(B)** Antigen accumulations in RNG105 positive or negative neurites were counted in five microscopic fields independently. **(C-D)** Primary mouse neurons were infected with TBEV wt or SL-2 Loop C-U at a MOI of 0.1. Following fixation at 72 h.p.i., the cells were stained with antibodies against FMRP, RNG105 or Staufen (green) and fluorescent probes against viral RNA (magenta). **(C)** Fluorescent images of the neurons. Colocalized areas of RBPs and viral genomic RNA are shown in white (right panels). **(D)** Colocalized areas of RBPs and viral genomic RNA in dendrites were measured in ten AOI. Scale bars indicate 5 μm in length. Error bars represent SEM; $^{**}p < 0.02$ and $^{*}p < 0.05$.

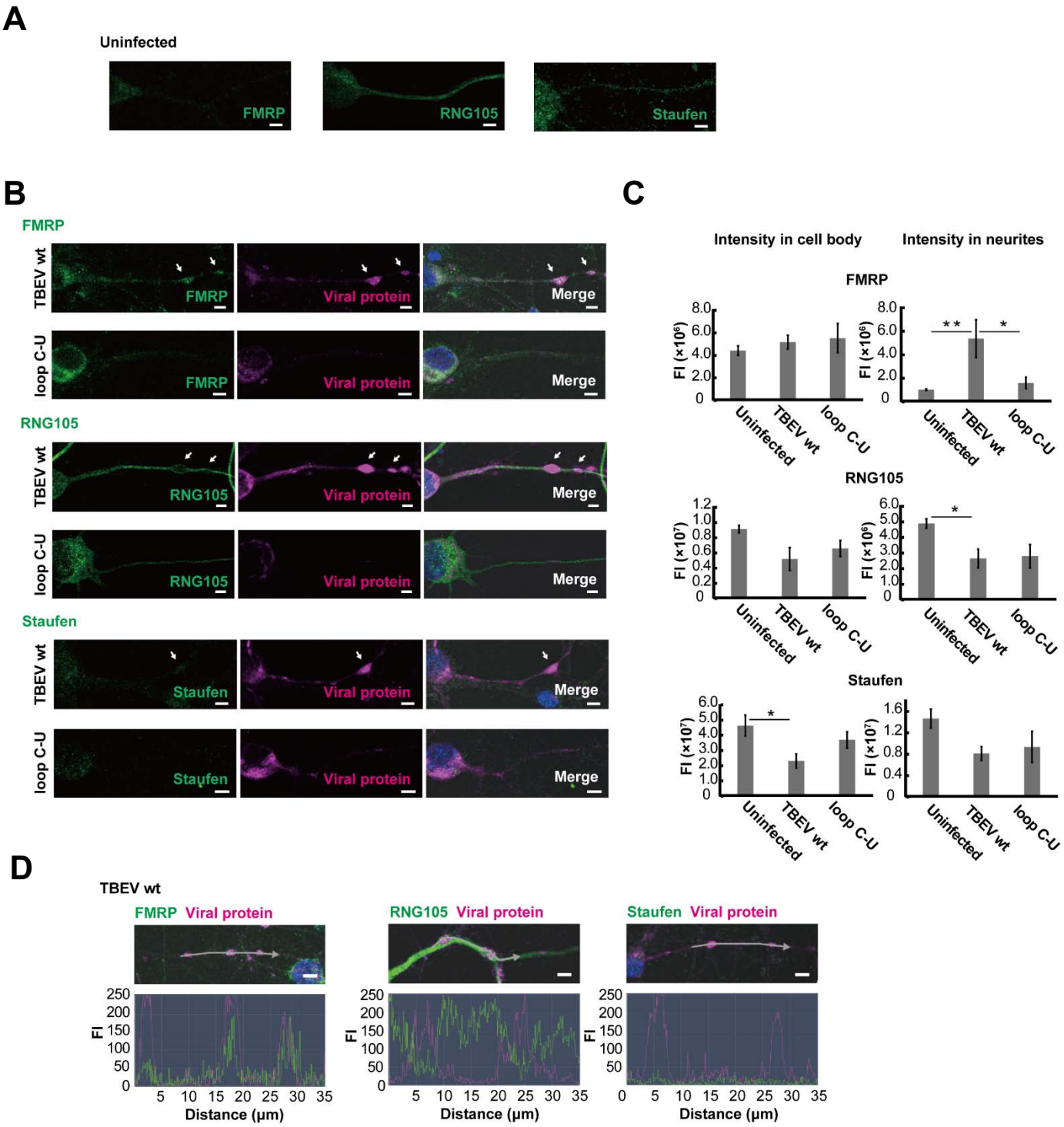

Fig. 21. TBEV infection accumulated FMRP in dendrites.

Primary mouse neurons were un infected or were infected with TBEV wt or SL-2 loop C-U at a multiplicity of infection of 0.1. and fixed at 48 h post-infection. The cells were stained with antibodies against fragile X mental retardation protein (FMRP), RNA granule protein 105 (RNG105), or Staufen (green), and antibodies against viral proteins (magenta). **(A)** Fluorescent images of the uninfected neurons **(B)** Fluorescent images of the infected neurons. White arrows indicate dendrites with viral antigen accumulations **(C)** The signals of RBPs in the cell body or neurites were analyzed in Z-Stack images of five microscopic fields. **(D)** Fluorescent Intensity (FI) line profile of the neurites infected with TBEV wt are defined with gray arrows. Scale bars indicate 5 μm in length. Error bars represent SEM; **p < 0.02 and *p < 0.05.

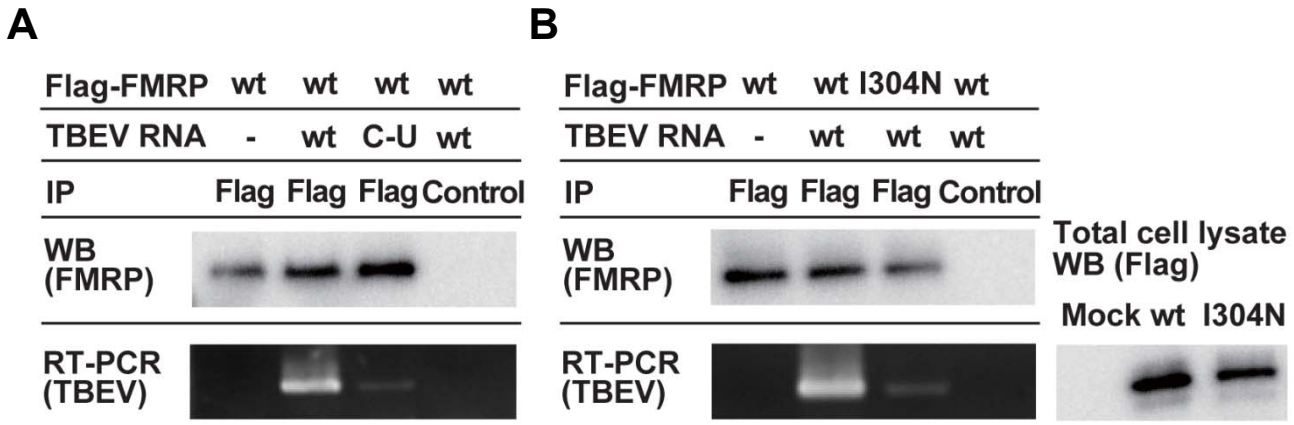

Fig. 22. Interaction between the RBP of neuronal granule and genomic RNA of TBEV.

Full-length RNAs of TBEV wt (wt) or of SL-2 loop C-U (C-U) (A) was mixed with cell lysate expressing Flag-FMRP wt (wt) or I304N (B). The mixture was immuneprecipitated (IP) with beads with anti-Flag antibody (Flag) or beads only (Control), and precipitated protein and RNA were detected by Western blotting (WB) and reverse transcription (RT-) PCR, respectively. Right panels show expression of the FMRP wt or I304N in total cell lysate.

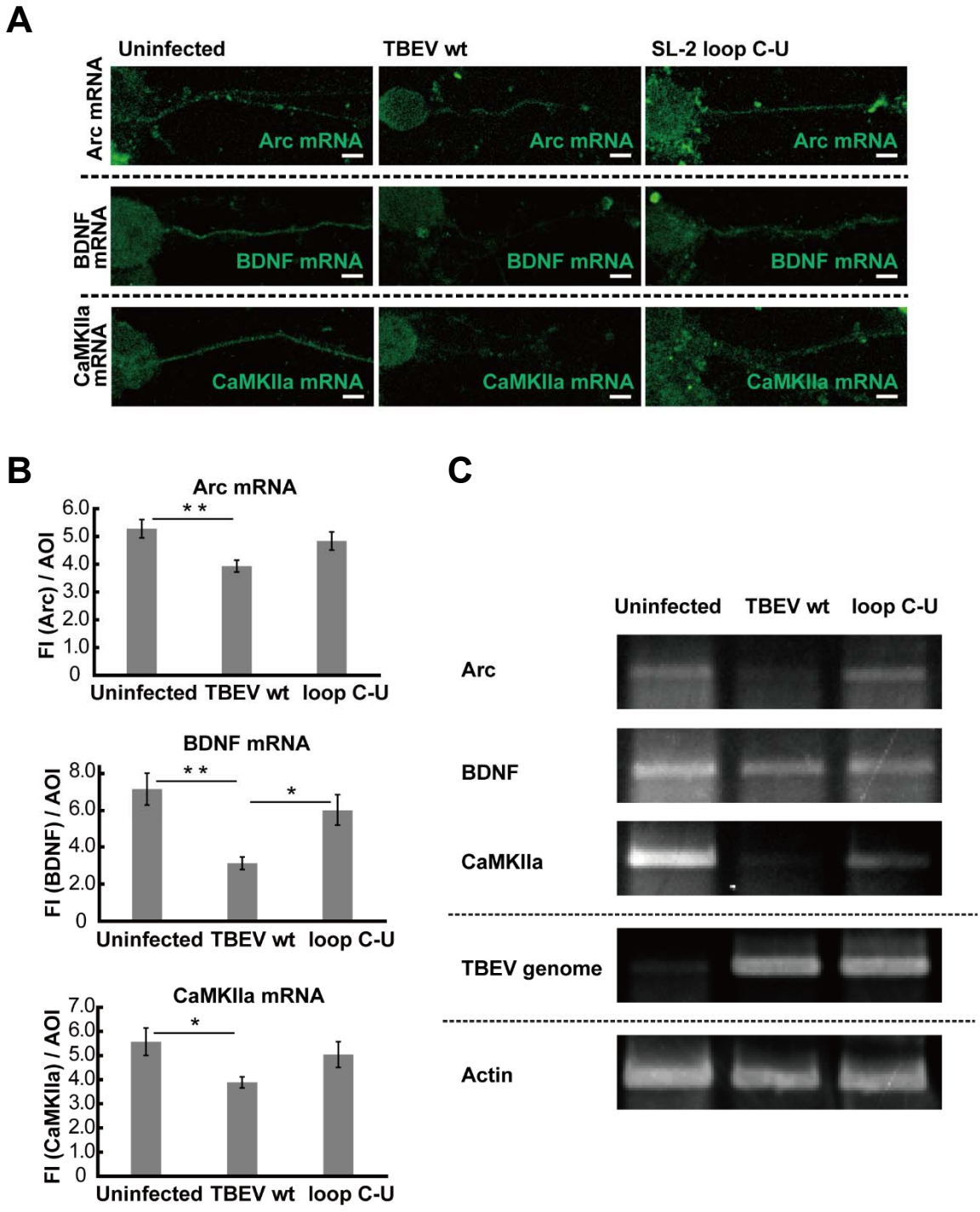

Fig. 23. TBEV infection and transport of viral RNA disrupted the localization of dendritic mRNAs.

Primary mouse neurons were infected with TBEV wt or SL-2 loop C-U at an MOI of 0.1. **(A)** The cells were fixed at 48 h.p.i. and mRNA for Arc, BDNF, or CaMKIIα was stained by FISH (green). Scale bars indicate 5 μm in length. **(B)** Fluorescent signal of the mRNA for Arc, BDNF, or CaMKIIα in dendrites were measured in ten AOI. **(C)** RNAs in neurons were detected by RT-PCR Error bars represent SEM; $^{**}p < 0.02$ and $^{*}p < 0.05$.

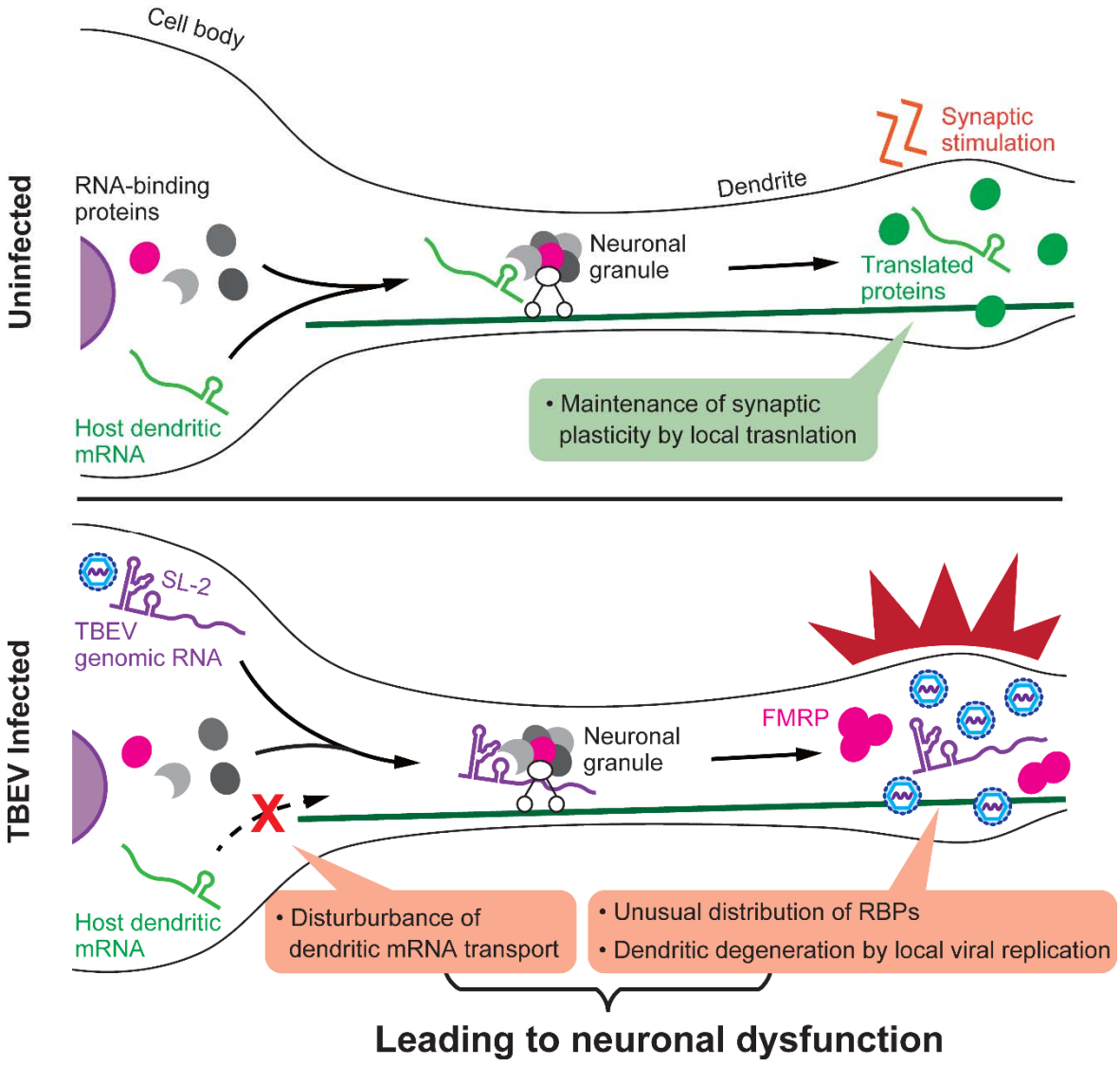

Fig. 24. Model of TBEV genomic RNA transport and dendritic dysfunction.

Dendritic mRNAs bound to RBPs of the neuronal granule are transported and locally translated in dendrites for maintenance of synaptic plasticity. In neurons infected with TBEV, viral genomic RNAs bind to RBPs (such as FMRP) via the SL-2 region, and are transported to dendrites. This transport disturbed the transport of dendritic mRNAs. The transported viral genomic RNAs alter RBP distribution, and, the local replication initiates the degeneration of dendrites, resulting in neuronal dysfunction.

Conclusion

Flaviviruses represent a significant threat to public health worldwide. Several flaviviruses cause severe neurological disease associated with high levels of mortality in humans and animals. However, no specific treatment has been developed due to the lack of information about the detailed pathogenic mechanisms.

In chapter I, I conducted the analysis of replication of encephalitic flaviviruses by using primary culture of mouse neuron. It was shown that mosquito and tick-borne flaviviruses replicated differently in primary neuronal cultures. During the infection of the tick-borne flaviviruses, viral antigens were detected in the cell body in early time points and then accumulated in the neuronal dendrites, while it was not observed by the infection of the mosquito-borne flaviviruses. The replication of viral genomic RNA was observed at the site of the accumulations in the dendrites infected with TBEV. TBEV infection was associated with ultrastructural alterations of membrane structures in the dendrites. These data indicated that TBEV replicated in neuronal dendrites locally. There is no previous report showing the replication of a neurotropic virus in infected dendrites. Because, dendrite is important for the formation of the neuronal circuit and control of synaptic plasticity, it was suggested that the degeneration of dendritic structure caused by the local viral replication affected neuronal disease by TBEV infection.

In chapter II, I further analyzed the molecular mechanism of genomic RNA transport of TBEV to dendrites involved in the local replication in dendrites. The 5′ UTR in the viral genomic RNA was identified as a critical viral factor for the transport to dendrites. The mutant TBEV with impaired genomic RNA transport caused a reduction in neurological symptoms in infected mice. The genomic RNA colocalized with components of neuronal granules which transports specific

host mRNAs in dendrites for neuronal functions, such as neurogenesis and the plasticity of the synaptic communication. The genomic RNA of TBEV interacted with FMRP, a component of the neuronal granule, via the 5′ UTR. Furthermore, the transport of TBEV genomic RNA disrupted that of host mRNAs in dendrites. These results indicated that TBEV used the neuronal granule system for the transport of viral genomic RNA. Recent researches showed that the mRNA transport in neuron was involved in many neurodegenerative diseases, such as Alzheimer's disease and fragile-X mental retardation syndrome. It was also suggested that the competitive inhibition of the neuronal granule system by TBEV infection caused neuronal dysfunction, exacerbating the neurological symptoms in the TBEV-infected mice. This is the first study which revealed hijacking of neuronal granule machinery by a neurotropic virus during the development of neurological disease.

These findings of the local viral replication and viral genome transport in dendrites encourage further study to understand the molecular mechanism of viral replication in CNS and the pathogenicity of neurotropic viruses. The findings of the unique virus-host interaction between viral genomic RNA and neuronal granule machinery will also promote the study of neurodegenerative diseases caused by disruption of dendritic mRNA transport. These findings also could lead to the development of treatment options with virus-based vectors that can transport and express target genes locally in dendrites.

Acknowledgement

I would like to thank my supervisors Professor Hiroaki Kariwa, Associate Professor Kentaro Yoshii and Assistant Professor Shintaro Kobayashi (Laboratory of Public Health, Faculty of Veterinary Medicine, Hokkaido University) for their persevering guidance. I would like to extent my graduate to Professor Hirofumi Sawa (Division of Molecular Pathobiology, Research Center for Zoonosis Control) and Lecturer Rie Hasebe (Laboratory of Veterinary Hygiene, Faculty of Veterinary Medicine) for their intellectual discussion and critical reading of this thesis. I would like to appreciate Associate Professor Osamu Ichii (Laboratory of Anatomy) and Assistant Professor Takeshi Yamasaki (Laboratory of Veterinary Hygiene) for advice and support of experiments. I would like to thank Professor Tatsuhiko Igarashi (Kyoto University) and Associate Professor Nobuyuki Shiina (National Institute for Basic Biology) for their kind offer of experimental materials.

I am grateful to the coordinator of the Program for Leading Graduate Schools, Hokkaido University, Professor Motohiro Horiuchi (Laboratory of Veterinary Hygiene) and the members of the Leading Office for their help with my school life. I would like to thank all the members and alumni of Laboratory of Public Health and excellent colleagues of this graduate school. It was great pleasure for me to study and work with you all. Finally, I am eternally grateful to my family for their encouragement and support of my school life.

My graduate school days and these Ph.D. works were financially supported by the Grant-in-Aid for Graduate Student, Program for Leading Graduate Schools, Hokkaido University (2014, Adopted person: Minato Hirano) and the Research Fellowship for Young Scientists, JSPS (2015-2018, Project number: 15J00686). I greatly appreciate their supports for my works and hope that future generations will be helped as well.

References

1. Schmaljohn, A. L. & McClain, D. *Alphaviruses (Togaviridae) and Flaviviruses (Flaviviridae). Medical Microbiology* (University of Texas Medical Branch at Galveston, 1996).

2. Gould, E. & Solomon, T. Pathogenic flaviviruses. *Lancet* **371,** 500–509 (2008).

3. Lindenbach, B. D. & Rice, C. M. Flaviviridae: The Viruses and Their Replication. *Fields Virol.* 1101–1151 (2007). doi:10.1016/0038-092X(88)90131-4

4. Mackenzie, J. S., Gubler, D. J. & Petersen, L. R. Emerging flaviviruses: the spread and resurgence of Japanese encephalitis, West Nile and dengue viruses. *Nat. Med.* **10,** S98–S109 (2004).

5. Mackenzie, J. S. & Williams, D. T. The zoonotic flaviviruses of southern, south-eastern and eastern Asia, and Australasia: the potential for emergent viruses. *Zoonoses Public Health* **56,** 338–56 (2009).

6. Rovida, F. *et al.* West Nile Virus Outbreak in the Lombardy Region, Northern Italy, Summer 2013. *Vector-Borne Zoonotic Dis.* **15,** 278–283 (2015).

7. Zhang, F.-C. *et al. Severe dengue outbreak in Yunnan, China, 2013. International Journal of Infectious Diseases* **27,** (2014).

8. Balogh, Z. *et al.* Tick-borne encephalitis outbreak in Hungary due to consumption of raw goat milk. *J. Virol. Methods* **163,** 481–5 (2010).

9. Haddow, A. D. *et al.* Genetic characterization of Zika virus strains: geographic expansion of the Asian lineage. *PLoS Negl. Trop. Dis.* **6,** e1477 (2012).

10. Grobbelaar, A. A. *et al.* Resurgence of Yellow Fever in Angola, 2015-2016. *Emerg. Infect. Dis.* **22,** 1854–5 (2016).

11. Lanciotti, R. S. Origin of the West Nile Virus Responsible for an Outbreak of Encephalitis in the Northeastern United States. *Science (80-.).* **286,** 2333–2337 (1999).

12. Kuhn, R. J. *et al.* Structure of Dengue VirusImplications for Flavivirus Organization, Maturation, and Fusion. *Cell* **108,** 717–725 (2002).

13. Chambers, T. Flavivirus Genome Organization, Expression, And Replication. *Annu. Rev. Microbiol.* **44,** 649–688 (1990).

14. Methylation status of intracellular dengue type 2 40 S RNA. *Virology* **96,** 159–165 (1979).

15. Filomatori, C. V. *et al.* A 5’ RNA element promotes dengue virus RNA synthesis on a circular genome. *Genes Dev.* **20,** 2238–2249 (2006).

16. Polacek, C., Friebe, P. & Harris, E. Poly(A)-binding protein binds to the non-polyadenylated 3’ untranslated region of dengue virus and modulates translation efficiency. *J. Gen. Virol.* **90,** 687–692 (2009).

17. Alvarez, D. E., Filomatori, C. V. & Gamarnik, A. V. Functional analysis of dengue virus cyclization sequences located at the 5′ and 3′UTRs. *Virology* **375,** 223–235 (2008).

18. Kofler, R. M., Hoenninger, V. M., Thurner, C. & Mandl, C. W. Functional analysis of the tick-borne encephalitis virus cyclization elements indicates major differences between mosquito-borne and tick-borne flaviviruses. *J. Virol.* **80,** 4099–113 (2006).

19. Pijlman, G. P. *et al.* A Highly Structured, Nuclease-Resistant, Noncoding RNA Produced by Flaviviruses Is Required for Pathogenicity. *Cell Host Microbe* **4,** 579–591 (2008).

20. Pompon, J. & Garcia-Blanco, M. A. RNA: Jack of All Trades and Master of All. *Cell* **160,** 579–580 (2015).

21. Manokaran, G. *et al.* Dengue subgenomic RNA binds TRIM25 to inhibit interferon expression for epidemiological fitness. *Science (80-.).* **350,** (2015).

22. Stiasny, K., Brandler, S., Kössl, C. & Heinz, F. X. Probing the flavivirus membrane fusion mechanism by using monoclonal antibodies. *J. Virol.* **81,** 11526–31 (2007).

23. Konishi, E. & Mason, P. W. Proper maturation of the Japanese encephalitis virus envelope glycoprotein requires cosynthesis with the premembrane protein. *J. Virol.* **67,** 1672–5 (1993).

24. Stadler, K., Allison, S. L., Schalich, J. & Heinz, F. X. Proteolytic activation of tick-borne encephalitis virus by furin. *J. Virol.* **71,** 8475–81 (1997).

25. Ma, L., Jones, C. T., Groesch, T. D., Kuhn, R. J. & Post, C. B. Solution structure of dengue virus capsid protein reveals another fold. *Proc. Natl. Acad. Sci. U. S. A.* **101,** 3414–9 (2004).

26. Westaway, E. G., Mackenzie, J. M., Kenney, M. T., Jones, M. K. & Khromykh, A. A. Ultrastructure of Kunjin virus-infected cells : colocalization of NS1 and NS3 with double-stranded RNA , and of NS2B with NS3 , in virus-induced membrane structures . Ultrastructure of Kunjin Virus-Infected Cells : Colocalization of NS1 and NS3 with Doubl. (1997).

27. Anwar, A. *et al.* The Kinase Inhibitor SFV785 Dislocates Dengue Virus Envelope Protein from the Replication Complex and Blocks Virus Assembly. *PLoS One* **6,** e23246 (2011).

28. Welsch, S. *et al.* Composition and Three-Dimensional Architecture of the Dengue Virus Replication and Assembly Sites. *Cell Host Microbe* **5,** 365–375 (2009).

29. Li, H., Clum, S., You, S., Ebner, K. E. & Padmanabhan, R. The serine protease and RNA-stimulated nucleoside triphosphatase and RNA helicase functional domains of dengue virus type 2 NS3 converge within a region of 20 amino acids. *J. Virol.* **73,** 3108–16 (1999).

30. Egloff, M.-P., Benarroch, D., Selisko, B., Romette, J.-L. & Canard, B. An RNA cap (nucleoside-2'-O-)-methyltransferase in the flavivirus RNA polymerase NS5: crystal structure and functional characterization. *EMBO J.* **21,** 2757–68 (2002).

31. Thiel, H.-J., Behrens, S.-E. & Steffens, S. The RNA-dependent RNA polymerases of different members of the family Flaviviridae exhibit similar properties in vitro. *J. Gen. Virol.* **80,** 2583–2590 (1999).

32. Mackenzie, J. M. & Westaway, E. G. Assembly and Maturation of the Flavivirus Kunjin Virus Appear To Occur in the Rough Endoplasmic Reticulum and along the Secretory Pathway , Respectively †. **75,** 10787–10799 (2001).

33. Kuno, G., Chang, G. J., Tsuchiya, K. R., Karabatsos, N. & Cropp, C. B. Phylogeny of the genus Flavivirus. *J. Virol.* **72,** 73–83 (1998).

34. de Micco, P. *et al.* Phylogeny of the genus Flavivirus using complete coding sequences of arthropod-borne viruses and viruses with no known vector. *J. Gen. Virol.* **81,** 781–790 (2000).

35. Blitvich, B. J. & Firth, A. E. Insect-specific flaviviruses: a systematic review of their discovery, host range, mode of transmission, superinfection exclusion potential and genomic organization. *Viruses* **7,** 1927–59 (2015).

36. Lindquist, L. & Vapalahti, O. Tick-borne encephalitis. *Lancet* **371,** 1861–71 (2008).

37. Wolfe, N. D., Dunavan, C. P. & Diamond, J. Origins of major human infectious diseases. doi:10.1038/nature05775

38. McMichael, A. J., Woodruff, R. E. & Hales, S. Climate change and human health: present and future risks. *Lancet (London, England)* **367,** 859–69 (2006).

39. Estrada-Peña, A., Ayllón, N. & de la Fuente, J. Impact of climate trends on tick-borne pathogen transmission. *Front. Physiol.* **3,** 64 (2012).

40. Nash, D. *et al.* The Outbreak of West Nile Virus Infection in the New York City Area in 1999. *N. Engl. J. Med.* **344,** 1807–1814 (2001).

41. Komar, N. *et al.* Experimental Infection of North American Birds with the New York 1999 Strain of West Nile Virus. *Emerg. Infect. Dis.* **9,** 311–322 (2003).

42. Konishi, E., Kitai, Y., Nishimura, K. & Harada, S. Follow-up survey of Japanese encephalitis virus infection

in Kumamoto Prefecture, South-West Japan: status during 2009-2011. *Jpn. J. Infect. Dis.* **65,** 448–50 (2012).

43. Kutsuna, S. *et al.* Autochthonous Dengue Fever, Tokyo, Japan, 2014. *Emerg. Infect. Dis.* **21,** 517–520 (2015).

44. Takashima, I. *et al.* A case of tick-borne encephalitis in Japan and isolation of the the virus. *J. Clin. Microbiol.* **35,** 1943–7 (1997).

45. Yoshii, K., Kojima, R. & Nishiura, H. Unrecognized Subclinical Infection with Tickborne Encephalitis Virus, Japan. *Emerg. Infect. Dis.* **23,** 1753–1754 (2017).

46. Yoshii, K., Song, J. Y., Park, S.-B., Yang, J. & Schmitt, H.-J. Tick-borne encephalitis in Japan, Republic of Korea and China. *Emerg. Microbes Infect. 2017 69* **6,** emi201769 (2017).

47. Takeda, T., Ito, T., Osada, M., Takahashi, K. & Takashima, I. Isolation of tick-borne encephalitis virus from wild rodents and a seroepizootiologic survey in Hokkaido, Japan. *Am. J. Trop. Med. Hyg.* **60,** 287–91 (1999).

48. Yoshii, K. *et al.* Epizootiological study of tick-borne encephalitis virus infection in Japan. *J. Vet. Med. Sci.* **73,** 409–12 (2011).

49. Sejvar, J. J. *et al.* Neurologic Manifestations and Outcome of West Nile Virus Infection. *JAMA* **290,** 511 (2003).

50. Anastasiadou, A., Kakoulidis, I., Butel, D., Kehagia, E. & Papa, A. Follow-up study of Greek patients with West Nile virus neuroinvasive disease. *Int. J. Infect. Dis.* **17,** e494–e497 (2013).

51. Solomon, T. *et al.* Poliomyelitis-like illness due to Japanese encephalitis virus. *Lancet* **351,** 1094–1097 (1998).

52. Ooi, M. H. *et al.* The Epidemiology, Clinical Features, and Long-Term Prognosis of Japanese Encephalitis in Central Sarawak, Malaysia, 1997–2005. *Clin. Infect. Dis.* **47,** 458–468 (2008).

53. Czupryna, P. *et al.* Tick-borne encephalitis in Poland in years 1993-2008 - epidemiology and clinical presentation. A retrospective study of 687 patients. *Eur. J. Neurol.* **18,** 673–679 (2011).

54. Kaiser, R. The clinical and epidemiological profile of tick-borne encephalitis in southern Germany 1994-98: a prospective study of 656 patients. *Brain* 2067–78 (1999).

55. Mickiene, A. *et al.* Tickborne encephalitis in an area of high endemicity in lithuania: disease severity and long-term prognosis. *Clin. Infect. Dis.* **35,** 650–8 (2002).

56. Kimura, T., Sasaki, M., Okumura, M., Kim, E. & Sawa, H. Flavivirus Encephalitis. *Vet. Pathol.* **47,** 806–818 (2010).

57. Hayasaka, D. *et al.* Mortality following peripheral infection with tick-borne encephalitis virus results from a combination of central nervous system pathology, systemic inflammatory and stress responses. *Virology* **390,** 139–50 (2009).

58. Nagata, N. *et al.* The Pathogenesis of 3 Neurotropic Flaviviruses in a Mouse Model Depends on the Route of Neuroinvasion After Viremia. *J. Neuropathol. Exp. Neurol.* **74,** (2015).

59. Banker, G. A. & Cowan, W. M. Rat hippocampal neurons in dispersed cell culture. *Brain Res.* **126,** 397–42 (1977).

60. Ishihara, N. *et al.* Mitochondrial fission factor Drp1 is essential for embryonic development and synapse formation in mice. *Nat. Cell Biol.* **11,** 958–966 (2009).

61. Okabe, S. Fluorescence imaging of synapse formation and remodeling. *Microscopy* **62,** 51–62 (2013).

62. Lewis, P. & Lentz, T. L. Rabies virus entry into cultured rat hippocampal neurons. *J. Neurocytol.* **27,** 559–73 (1998).

63. Perkins, D., Pereira, E. F. R., Gober, M., Yarowsky, P. J. & Aurelian, L. The herpes simplex virus type 2 R1 protein kinase (ICP10 PK) blocks apoptosis in hippocampal neurons, involving activation of the MEK/MAPK survival pathway. *J. Virol.* **76,** 1435–49 (2002).

64. Chen, C.-J. *et al.* Glial activation involvement in neuronal death by Japanese encephalitis virus infection. *J. Gen. Virol.* **91,** 1028–1037 (2010).

65. Diniz, J. A. P. *et al.* West Nile virus infection of primary mouse neuronal and neuroglial cells: the role of astrocytes in chronic infection. *Am. J. Trop. Med. Hyg.* **75,** 691–6 (2006).

66. Biederer, T. & Scheiffele, P. Mixed-culture assays for analyzing neuronal synapse formation. *Nat. Protoc.* **2,** 670–676 (2007).

67. Viesselmann, C., Ballweg, J., Lumbard, D. & Dent, E. W. Nucleofection and Primary Culture of Embryonic Mouse Hippocampal and Cortical Neurons. *J. Vis. Exp.* (2011). doi:10.3791/2373

68. SILBER, L. A. & SOLOVIEV, V. D. Far Eastern tick-borne spring-summer (spring) encephalitis. *Am. Rev. Sov. Med.* 1–80 (1946).

69. Hayasaka, D. *et al.* Amino acid changes responsible for attenuation of virus neurovirulence in an infectious cDNA clone of the Oshima strain of Tick-borne encephalitis virus. *J. Gen. Virol.* **85,** 1007–1018 (2004).

70. Takano, A. *et al.* Construction of a replicon and an infectious cDNA clone of the Sofjin strain of the Far-Eastern subtype of tick-borne encephalitis virus. *Arch. Virol.* **156,** 1931–41 (2011).

71. Yoshii, K. *et al.* Construction of an infectious cDNA clone for Omsk hemorrhagic fever virus, and characterization of mutations in NS2A and NS5. *Virus Res.* **155,** 61–68 (2011).

72. Heinz, F. X. & Kunz, C. Homogeneity of the Structural Glycoprotein from European Isolates of Tick-borne Encephalitis Virus: Comparison with Other Flaviviruses. *J. Gen. Virol.* **57,** 263–274 (1981).

73. Yoshii, K. *et al.* Single point mutation in tick-borne encephalitis virus prM protein induces a reduction of virus particle secretion. *J. Gen. Virol.* **85,** 3049–3058 (2004).

74. Schönborn, J. *et al.* Monoclonal antibodies to double-stranded RNA as probes of RNA structure in crude nucleic acid extracts. *Nucleic Acids Res.* **19,** 2993–3000 (1991).

75. Hayasaka, D., Yoshii, K., Ueki, T., Iwasaki, T. & Takashima, I. Sub-genomic replicons of Tick-borne encephalitis virus. *Arch. Virol.* **149,** 1245–1256 (2004).

76. Yoshii, K. *et al.* Packaging the replicon RNA of the Far-Eastern subtype of tick-borne encephalitis virus into single-round infectious particles: development of a heterologous gene delivery system. *Vaccine* **23,** 3946–3956 (2005).

77. Růzek, D. *et al.* Morphological changes in human neural cells following tick-borne encephalitis virus infection. *J. Gen. Virol.* **90,** 1649–58 (2009).

78. Salinas, S., Schiavo, G. & Kremer, E. J. A hitchhiker's guide to the nervous system: the complex journey of viruses and toxins. *Nat. Rev. Microbiol.* **8,** 645–655 (2010).

79. Klingen, Y., Conzelmann, K.-K. & Finke, S. Double-labeled rabies virus: live tracking of enveloped virus transport. *J. Virol.* **82,** 237–45 (2008).

80. Zaichick, S. V *et al.* The Herpesvirus VP1/2 Protein Is an Effector of Dynein-Mediated Capsid Transport and Neuroinvasion. *Cell Host Microbe* **13,** 193–203 (2013).

81. Owen, D., Crump, C. & Graham, S. Tegument Assembly and Secondary Envelopment of Alphaherpesviruses. *Viruses* **7,** 5084–5114 (2015).

82. Matsuda, K. *et al.* In vitro demonstration of neural transmission of avian influenza A virus. *J. Gen. Virol.* **86,** 1131–9 (2005).

83. Khromykh, A. A., Varnavski, A. N. & Westaway, E. G. Encapsidation of the flavivirus kunjin replicon RNA by using a complementation system providing Kunjin virus structural proteins in trans. *J. Virol.* **72,** 5967–77 (1998).

84. Gehrke, R. *et al.* Incorporation of tick-borne encephalitis virus replicons into virus-like particles by a packaging cell line. *J. Virol.* **77,** 8924–33 (2003).

85. Yoshii, K., Goto, A., Kawakami, K., Kariwa, H. & Takashima, I. Construction and application of chimeric virus-like particles of tick-borne encephalitis virus and mosquito-borne Japanese encephalitis virus. *J. Gen. Virol.* **89,** 200–211 (2008).

86. Omalu, B. I., Shakir, A. A., Wang, G., Lipkin, W. I. & Wiley, C. A. Fatal Fulminant Pan-Meningo-Polioencephalitis Due to West Nile Virus. *Brain Pathol.* **13,** 465–472 (2006).

87. Desai, A., Shankar, S. K., Ravi, V., Chandramuki, A. & Gourie-Devi, M. Japanese encephalitis virus antigen in the human brain and its topographic distribution. *Acta Neuropathol.* **89,** 368–73 (1995).

88. Gelpi, E. *et al.* Visualization of Central European tick-borne encephalitis infection in fatal human cases. *J. Neuropathol. Exp. Neurol.* **64,** 506–12 (2005).

89. Baumann, N. & Pham-Dinh, D. Biology of oligodendrocyte and myelin in the mammalian central nervous system. *Physiol. Rev.* **81,** 871–927 (2001).

90. Hussmann, K. L., Samuel, M. A., Kim, K. S. & Michael, S. Differential Replication of Pathogenic and Nonpathogenic Strains of West Nile Virus within Astrocytes. (2012). doi:10.1128/JVI.02577-12

91. Cho, H. *et al.* Differential innate immune response programs in neuronal subtypes determine susceptibility to infection in the brain by positive-stranded RNA viruses. *Nat. Med.* 1–8 (2013). doi:10.1038/nm.3108

92. Ramírez, O. A. & Couve, A. The endoplasmic reticulum and protein trafficking in dendrites and axons. *Trends Cell Biol.* **21,** 219–227 (2011).

93. Ori-McKenney, K. M., Jan, L. Y. & Jan, Y.-N. Golgi Outposts Shape Dendrite Morphology by Functioning as Sites of Acentrosomal Microtubule Nucleation in Neurons. *Neuron* **76,** 921–930 (2012).

94. Pierce, J. P., Mayer, T. & McCarthy, J. B. Evidence for a satellite secretory pathway in neuronal dendritic spines. *Curr. Biol.* **11,** 351–5 (2001).

95. McCarthy, B. J. & Milner, T. A. Dendritic ribosomes suggest local protein synthesis during estrous synaptogenesis. *Neuroreport* **14,** 1357–1360 (2003).

96. Li, X.-Q., Sarmento, L. & Fu, Z. F. Degeneration of neuronal processes after infection with pathogenic, but not attenuated, rabies viruses. *J. Virol.* **79,** 10063–8 (2005).

97. Offerdahl, D. K., Dorward, D. W., Hansen, B. T. & Bloom, M. E. A three-dimensional comparison of tick-borne flavivirus infection in mammalian and tick cell lines. *PLoS One* **7,** e47912 (2012).

98. Doyle, M. & Kiebler, M. a. Mechanisms of dendritic mRNA transport and its role in synaptic tagging. *EMBO J.* **30,** 3540–52 (2011).

99. Bramham, C. R. & Wells, D. G. Dendritic mRNA: transport, translation and function. *Nat. Rev. Neurosci.* **8,** 776–789 (2007).

100. Kiebler, M. A. & DesGroseillers, L. Molecular insights into mRNA transport and local translation in the mammalian nervous system. *Neuron* **25,** 19–28 (2000).

101. Hirokawa, N. & Takemura, R. Molecular motors and mechanisms of directional transport in neurons. *Nat. Rev. Neurosci.* **6,** 201–14 (2005).

102. Kanai, Y., Dohmae, N. & Hirokawa, N. Kinesin Transports RNA: Isolation and Characterization of an RNA-Transporting Granule. *Neuron* **43,** 513–525 (2004).

103. Mus, E., Hof, P. R. & Tiedge, H. Dendritic BC200 RNA in aging and in Alzheimer's disease. *Proc. Natl. Acad. Sci.* **104,** 10679–10684 (2007).

104. Crawford, D. C., Acuña, J. M. & Sherman, S. L. FMR1 and the fragile X syndrome: Human genome epidemiology review. *Genet. Med.* **3,** 359–371 (2001).

105. Maezawa, I. & Jin, L. W. Rett Syndrome Microglia Damage Dendrites and Synapses by the Elevated Release of Glutamate. *J. Neurosci.* **30,** 5346–5356 (2010).

106. Dictenberg, J. B., Swanger, S. A., Antar, L. N., Singer, R. H. & Bassell, G. J. A Direct Role for FMRP in Activity-Dependent Dendritic mRNA Transport Links Filopodial-Spine Morphogenesis to Fragile X Syndrome. *Dev. Cell* **14,** 926–939 (2008).

107. Ellencrona, K., Syed, A. & Johansson, M. Flavivirus NS5 associates with host-cell proteins zonula occludens-1 (ZO-1) and regulating synaptic membrane exocytosis-2 (RIMS2) via an internal PDZ binding mechanism. *Biol. Chem.* **390,** 319–23 (2009).

108. Roche, J. P., Packard, M. C., Moeckel-Cole, S. & Budnik, V. Regulation of synaptic plasticity and synaptic vesicle dynamics by the PDZ protein Scribble. *J. Neurosci.* **22,** 6471–9 (2002).

109. Hirano, M. *et al.* Tick-borne flaviviruses alter membrane structure and replicate in dendrites of primary mouse neuronal cultures. *J. Gen. Virol.* **95,** 849–861 (2014).

110. Lebeau, G. *et al.* Staufen1 regulation of protein synthesis-dependent long-term potentiation and synaptic function in hippocampal pyramidal cells. *Mol. Cell. Biol.* **28,** 2896–907 (2008).

111. Shiina, N., Yamaguchi, K. & Tokunaga, M. RNG105 Deficiency Impairs the Dendritic Localization of mRNAs for Na+/K+ ATPase Subunit Isoforms and Leads to the Degeneration of Neuronal Networks. *J. Neurosci.* **30,** 12816–12830 (2010).

112. Kao, D.-I., Aldridge, G. M., Weiler, I. J. & Greenough, W. T. Altered mRNA transport, docking, and protein

translation in neurons lacking fragile X mental retardation protein. *Proc. Natl. Acad. Sci.* **107,** 15601–15606 (2010).

113. Ohashi, R. *et al.* Comprehensive behavioral analysis of RNG105 (Caprin1) heterozygous mice: Reduced social interaction and attenuated response to novelty. *Sci. Rep.* **6,** 20775 (2016).

114. Phongphaew, W. *et al.* Valosin-containing protein (VCP/p97) plays a role in the replication of West Nile virus. *Virus Res.* **228,** 114–123 (2017).

115. Blichenberg, A. *et al.* Identification of a cis-acting dendritic targeting element in the mRNA encoding the alpha subunit of Ca2+/calmodulin-dependent protein kinase II. *Eur. J. Neurosci.* **13,** 1881–8 (2001).

116. Schneider, C. A., Rasband, W. S. & Eliceiri, K. W. NIH Image to ImageJ: 25 years of image analysis. *Nat. Methods* **9,** 671–675 (2012).

117. Guyenet, S. J. *et al.* A Simple Composite Phenotype Scoring System for Evaluating Mouse Models of Cerebellar Ataxia. *J. Vis. Exp.* e1787–e1787 (2010). doi:10.3791/1787

118. Zuker, M. Mfold web server for nucleic acid folding and hybridization prediction. *Nucleic Acids Res.* **31,** 3406–15 (2003).

119. Tamura, K. & Nei, M. Estimation of the number of nucleotide substitutions in the control region of mitochondrial DNA in humans and chimpanzees. *Mol. Biol. Evol.* **10,** 512–26 (1993).

120. Kumar, S., Stecher, G. & Tamura, K. MEGA7: Molecular Evolutionary Genetics Analysis Version 7.0 for Bigger Datasets. *Mol. Biol. Evol.* **33,** 1870–1874 (2016).

121. Bílý, T. *et al.* Electron Tomography Analysis of Tick-Borne Encephalitis Virus Infection in Human Neurons. *Sci. Rep.* **5,** 10745 (2015).

122. Friedrich, S. *et al.* AUF1 p45 Promotes West Nile Virus Replication by an RNA Chaperone Activity That Supports Cyclization of the Viral Genome. *J. Virol.* **88,** 11586–11599 (2014).

123. Westaway, E. G., Mackenzie, J. M. & Khromykh, A. A. Kunjin RNA replication and applications of Kunjin replicons. *Adv. Virus Res.* **59,** 99–140 (2003).

124. Khromykh, A. A., Kenney, M. T. & Westaway, E. G. trans-Complementation of flavivirus RNA polymerase gene NS5 by using Kunjin virus replicon-expressing BHK cells. *J. Virol.* **72,** 7270–9 (1998).

125. Schrier, M. *et al.* Transport kinetics of FMRP containing the I304N mutation of severe fragile X syndrome in neurites of living rat PC12 cells. *Exp. Neurol.* **189,** 343–353 (2004).

126. Ascano, M. *et al.* FMRP targets distinct mRNA sequence elements to regulate protein expression. *Nature*

492, 382–386 (2012).

127. Ohka, S. *et al.* Receptor-dependent and -independent axonal retrograde transport of poliovirus in motor neurons. *J. Virol.* **83,** 4995–5004 (2009).

128. Liu, Z.-Y. *et al.* Viral RNA switch mediates the dynamic control of flavivirus replicase recruitment by genome cyclization. *Elife* **5,** 39926–39937 (2016).

129. Mori, Y., Imaizumi, K., Katayama, T., Yoneda, T. & Tohyama, M. Two cis-acting elements in the 3' untranslated region of alpha-CaMKII regulate its dendritic targeting. *Nat. Neurosci.* **3,** 1079–84 (2000).

130. Subramanian, M. *et al.* G-quadruplex RNA structure as a signal for neurite mRNA targeting. *EMBO Rep.* **12,** 697–704 (2011).

131. Chiaruttini, C. *et al.* Dendritic trafficking of BDNF mRNA is mediated by translin and blocked by the G196A (Val66Met) mutation. *Proc. Natl. Acad. Sci. U. S. A.* **106,** 16481–6 (2009).

132. Tapia-Arancibia, L., Aliaga, E., Silhol, M. & Arancibia, S. New insights into brain BDNF function in normal aging and Alzheimer disease. *Brain Res. Rev.* **59,** 201–220 (2008).

133. De Rubeis, S. & Bagni, C. Fragile X mental retardation protein control of neuronal mRNA metabolism: Insights into mRNA stability. *Mol. Cell. Neurosci.* **43,** 43–50 (2010).

134. Kurscheid, S. *et al.* Evidence of a tick RNAi pathway by comparative genomics and reverse genetics screen of targets with known loss-of-function phenotypes in Drosophila. *BMC Mol. Biol.* **10,** 26 (2009).

135. Hirano, M. *et al.* Dendritic transport of tick-borne flavivirus RNA by neuronal granules affects development of neurological disease. *Proc. Natl. Acad. Sci.* **114,** 9960–9965 (2017).

Summary in Japanese

研究の背景

フラビウイルスによるアルボウイルス感染症は、その広い分布域、感染制御の難しさ故に、世界的に重要視される人獣共通感染症の 1 つである。中でも、脳炎フラビウイルス (ウエストナイルウイルス、日本脳炎ウイルス、ダニ媒介性脳炎ウイルス：TBEV）によって引き起こされる神経疾患は、その高い致死率、後遺症発生率故に、罹患者の生活の質を大きく損なう重大な疾病である。これらのウイルスの引き起こす病変はすべて非化膿性脳炎と一括りにされるが、その神経症状には、ダニ媒介性脳炎において知覚異常が顕著に現れるなどウイルスごとに差異があることが知られている。しかし、これらの差を引き起こすウイルスの神経病原性発現機序の詳細は殆ど明らかになっていない。本研究では TBEV を中心とする脳炎フラビウイルスの神経細胞内複製および病原性発現機構の解明を試みた。

第一章　　脳炎フラビウイルスの神経細胞内複製機構の比較解析

脳組織を生体から分離し *in vitro* にて培養を行うことが可能な初代培養技術は、これまで広く行われてきたマウスモデルを用いた解析と比較して、細胞内レベルでの変化をより詳細に観察可能である。第一章では、脳炎フラビウイルスの神経病原性発現機序の解明を目的とし、マウス初代培養神経細胞における神経向性フラビウイルスの比較解析を行った。

ウイルス抗原と細胞内小器官マーカーを用いた間接蛍光抗体法により、感染神経細胞内におけるウイルス抗原分布解析を行った結果、蚊媒介性ウイルス（日本脳炎ウイルス、ウエストナイルウイルス）とダニ媒介性ウイルス（TBEV）の間にウイルス抗原分布の差異が在ることが示された。感染後 12-24 時間においては、全てのウイルスでウイルス抗原は細胞質を中心として観察されたが、TBEV の感染では感染後 24-48 時間において、樹状突起上に結節状のウイルス抗原の集積が形成された。この性質はダニ媒介性フラビウイルス間でよく保存されていた。時間経過によるウイルス抗原分布の変化は、ウイルス構成要素 (タンパク質およびゲノム）の細胞質から樹状突起への移動を示唆していた。

細胞内小器官マーカーの染色により、この TBEV の抗原集積は樹状突起微小管近傍の ER に存在す

ることが示された。微小管重合阻害薬での処理により、樹状突起上への抗原分布は消失し、抗原集積への微小管の関与を示していた。また、ウイルス因子特異的抗体を用いた解析により、TBEV の構造タンパク質、非構造タンパク質、ウイルスゲノム複製時に産生される 2 本鎖 RNA の全てが樹状突起上の抗原集積部位に存在することが示された。ウイルスゲノムの構造タンパク質領域をゲノムから欠損させた単回感染性ウイルス様粒子の感染においても、同様のウイルス抗原集積は観察された。したがって、TBEV の神経細胞の感染時には、ウイルスゲノム RNA はゲノム RNA 単体もしくは非構造タンパク質との複合体の形で樹状突起へと輸送され、輸送されたウイルスゲノム RNA は樹状突起上にて局所的なウイルス複製を行い、抗原集積を形成していることが明らかになった。感染細胞の電子顕微鏡観察により、TBEV の複製は神経突起上にウイルス粒子を含む層状の特異な膜構造を形成することが明らかになった。

これらの実験結果により第一章では、ダニ媒介性フラビウイルスは神経細胞の樹状突起上へとウイルスゲノムを輸送した上で局所複製を行い、膜構造の変性を引き起こしていることが明らかになった。このような特異な性質は他の神経向性ウイルスにおいても報告が無く、ダニ媒介性脳炎ウイルスの重篤な神経症状に関与することが示唆された。

第二章　　TBEV の神経細胞内ゲノム RNA 輸送機構および神経病態への影響の解析

神経細胞は特定の RNA を樹状突起へと輸送し、局所的なタンパク質生産を行う神経顆粒と呼ばれる機構を持つことが知られている。第二章では、樹状突起でのウイルス複製を可能とするウイルスゲノム RNA 輸送のメカニズムの解明と TBEV 神経病態への影響の探索を目的とし解析を行った。

神経細胞モデルである PC12 細胞と RNA 発現系を用いて、樹状突起へのウイルスゲノム輸送を担うウイルス因子について解析を行った。結果、この輸送にウイルスタンパク質の発現は不要であり、ゲノム RNA 依存性に行われていることが示された。また、ウイルスゲノムの 5′非翻訳領域（5′ UTR）中の SL-2 領域がウイルス側の責任因子として同定された。リバースジェネティクス法により特定された領域への変異導入を行い、ゲノム輸送能が欠損した変異ウイルスを作出した。輸送能欠損ウイルスをマウスモデルに脳内接種した際には、野生型ウイルスと比較しマウスに生じた神経症状の有意な減弱が観察された。ウイルスゲノム輸送およびそれに伴った樹状突起におけるウイルス複製は、TBEV

の神経症状へと関与することが示された。

輸送の宿主因子として神経細胞内 RNA 輸送機構である神経顆粒に着目し解析を行った。樹状突起において神経顆粒を構成する複数のタンパク質（FMRP、RNG105、Staufen）とウイルスゲノム RNA の共局在が認められた。また、この中でも FMRP はウイルス感染時に樹状突起上のウイルス複製部位に異常蓄積していた。免疫沈降法を用いた実験により、FMRP の RNA 結合ドメインと TBEV ゲノムの SL-2 領域に相互作用が認められた。神経顆粒は神経細胞において樹状突起 mRNA と呼ばれる様々な RNA を輸送することが知られている。ウイルス感染神経細胞において樹状突起 mRNA（Arc、BDNF、CaMKIIa）の分布を観察したところ、樹状突起における減少が認められた。ウイルスゲノムの輸送は生理的な RNA 輸送を阻害することが示された。

これらの実験結果により第二章では、TBEV はウイルスゲノム 5′UTR 中の SL-2 領域と FMRP の相互作用により RNA 輸送機構である神経顆粒を乗っ取ってゲノムを輸送し、神経機能阻害を引き起こしているという新規の病態モデルが示された。神経細胞内におけるウイルスゲノム輸送はポリオウイルスなど様々なウイルスで観察されているが、それらはウイルスタンパク質依存性でありウイルスゲノム依存性のものはこれまで報告にない。TBEV は、極めてユニークな機構を用いて神経細胞内において複製を行っており、ダニ媒介性脳炎の強い神経症状へと影響していることが示された。

まとめと今後への展望

本研究により、TBEV の神経顆粒を利用した神経細胞内複製・病原性発現機構が提唱された。この機構は輸送に伴った樹状突起 mRNA 輸送の阻害および局所複製による膜構造変性により、TBEV の神経症状の発現に寄与していると考えられる。神経顆粒はアルツハイマー病など様々な神経変性疾患へと関与することから、本研究はウイルス性疾患のみならず、広く神経変性疾患の病態解明に寄与すると考えられる。また、本研究で得られた知見を応用することで、樹状突起へと外来 RNA を輸送することが可能な新規ウイルスベクターの開発が期待される。そして、このようなベクターを利用することで、樹状突起 mRNA 輸送異常に起因する神経変性疾患への新規の治療戦略の開発へと繋がることが期待される。